BIOMIMETIC POLYDIMETHYLSILOXANE CELL SUBSTRATE DESIGN FOR ENHANCED *IN VITRO* CELLULAR BEHAVIOR

by

Meftune Özgen Öztürk Öncel

B.S., in Chemical Engineering, Hacettepe University, 2011

M.S., in Biomedical Engineering, Boğaziçi University, 2014

Submitted to the Institute of Biomedical Engineering

in partial fulfillment of the requirements

for the degree of

Doctor

of

Philosophy

Boğaziçi University

2021

BIOMIMETIC POLYDIMETHYLSILOXANE CELL SUBSTRATE DESIGN FOR ENHANCED *IN VITRO* CELLULAR BEHAVIOR

APPROVED BY:

Assoc. Prof. Dr. Bora Garipcan .....
(Thesis Advisor)

Assoc. Prof. Dr. Duygu Ege .....

Assoc. Prof. Dr. Sedat Odabaş .....

Prof. Dr. Lokman Uzun .....

Assist. Prof. Dr. Banu İyisan .....

DATE OF APPROVAL: 01.02.2021

ACKNOWLEDGMENTS

Throughout my Ph.D. studies, I have received a great deal of encouragement and support.

I would first like to express my very sincere thanks to my advisor Assoc. Prof. Dr. Bora Garipcan, for his consistent support, tolerance, guidance and motivation. I truly appreciate his insightful feedback, which has always stimulated me to bring my studies into a higher level.

I would like to thank to my thesis progress committee members, Assoc. Prof. Dr. Duygu Ege and Assoc Prof. Dr. Sedat Odabaş, for their thoughtful comments and invaluable suggestions to improve the quality of my thesis work. I would like to express my gratitude to my other thesis committee members, Prof. Dr. Lokman Uzun and Assist. Prof. Dr. Banu İyisan for allocating time to review my thesis, their contributions and thoughtful comments. I would also like to thank Prof. Dr. Deniz Hür for his support in self-assembled monolayer synthesis.

I would like to acknowledge my friends and colleagues for their patient support, motivation and wonderful collaboration. They have been a family to me.

Finally, I would like to thank to my sister, my parents, my aunt, my grandfather and my husband. I am forever grateful for their understanding, encouragement and wise counsel.

This Ph.D. work was supported by TUBITAK (Grant No. 112T564 and 113T026), German Federal Ministry of Science and Education and Cologne Fortune (Grant No: 01DL14001) and Bogazici University Research Fund (Grant No: 6701 and 11501).

ACADEMIC ETHICS AND INTEGRITY STATEMENT

I, Meftune Özgen Öztürk Öncel, hereby certify that I am aware of the Academic Ethics and Integrity Policy issued by the Council of Higher Education (YÖK) and I fully acknowledge all the consequences due to its violation by plagiarism or any other way.

Name :

Signature:

Date:

ABSTRACT

BIOMIMETIC POLYDIMETHYLSILOXANE CELL SUBSTRATE DESIGN FOR ENHANCED *IN VITRO* CELLULAR BEHAVIOR

Recent developments in cell-based therapies and toxicological investigations reveal the need for well-designed, stable and flexible cell substrates. Mimicking the natural cellular microenvironment by altering cell substrate properties (stiffness, topography and chemical/biochemical composition) can significantly affect cell-substrate interfacial characteristics and potentially influence cellular behavior. Hence, the main objective of this thesis is to design biomimetic Polydimethylsiloxane (PDMS) cell substrates to enhance *in vitro* behavior of target cell types. In the first study, simple and one-step surface modification of PDMS is successfully accomplished by the preparation of amino acid (histidine, His; and leucine, Leu) conjugated self-assembled monolayers (SAMs) for enhanced osteoblast proliferation, morphology, alkaline phosphatase activity and mineralization. In the second study, PDMS substrates with healthy myocardium-like stiffness are produced and modified with conventional [(3-aminopropyl)triethoxysilane, APTES; octadecyltrimethoxysilane, OTS] and amino acid (His, Leu) conjugated SAMs. Comparative effects of these substrates are investigated on induced pluripotent stem cell (iPSC) behavior and their differentiation into cardiomyocytes. The last study is developed by using PDMS with a cornea-friendly stiffness, corneal endothelial cell (CEC) microenvironment-mimetic white rose petal topography patterning and collagen IV or hyaluronic acid modification for enhanced CEC proliferation, morphology and increased phenotypic marker expression. All these biomimetic approaches demonstrate successful platforms to improve cell substrate properties of PDMS, rendering very promising tools for cell-based therapies, microfluidics, drug screening and organ-on-chip platforms.

Keywords: Polydimethylsiloxane, Biomimetic, Self-assembled monolayer, Osteoblasts, Induced pluripotent stem cells, Cardiomyocyte differentiation, Corneal endothelial cells.

ÖZET

IN VITRO HÜCRE DAVRANIŞLARININ GELİŞTİRİLMESİ AMAÇLI BİYOMİMETİK POLİDİMETİLSİLOKSAN HÜCRE SUBSTRATI TASARIMI

Hücre-temelli tedaviler ve toksikolojik araştırmalar, iyi tasarlanmış, kararlı ve ayarlanabilir özellikli hücre substratı gereksinimini ortaya koymaktadır. Hücrelerin doğal mikroçevrelerinin fiziksel, topografik, kimyasal/biyokimyasal özelliklerinin taklit edilmesi, hücre-substrat arayüzeyi özelliklerini etkileyerek, hücre tepkilerini değiştirebilir. Bu sebeple, bu tezin temel amacı, belirli tipteki hücrelerin *in vitro*daki davranışlarını iyileştirmek için biyomimetik Polidimetilsiloksan (PDMS) substratların tasarlanmasıdır. İlk çalışmada, osteoblastların çoğalma, morfoloji, alkalen fosfataz aktivitesi ve mineralizasyonunu iyileştirmek amaçlanarak, amino asit (histidin, His; lözin, Leu) konjüge kendiliğinden düzenlenen monokatmanlar (KDM) sentenlenmiş; PDMS substratların bu KDMler ile kolay ve tek basamaklı yüzey modifikasyonu sağlanmıştır. İkinci çalışmada, PDMS substratlar sağlıklı miyokardiyum sertliğine yakın sertlikte hazırlanarak, geleneksel (aminopropiltrietoksisilan, APTES; oktadesiltrimetoksisilan, OTS) ve amino asit (His, Leu) konjüge KDMler ile modifiye edilmiştir. Bu yüzeylerin indüklenmiş pluripotent kök hücre davranışına ve kardiyomiyositlere farklılaşmasına etkileri incelenmiştir. Son çalışma, korneaya uyumlu sertlikteki PDMS substratların, kornea endotel hücre (KEH) mikroçevresi-taklidi beyaz gül taç yaprağı topografisi desenleme ile kolajen IV veya hiyalüronik asit modifikasyonları ile elde edilen yüzeylerdeki iyileştirilmiş KEH çoğalması, morfolojisi ve artan fenotipik belirteç gösterimleri üzerine geliştirilmiştir. Tüm bu sunulan yaklaşımlar, PDMSin hücre substratı özelliklerini geliştirerek; hücre-temelli tedavilerde, mikroakışkan tasarımlarında, ilaç araştırmalarında ve çip üzeri organ platformlarında ümit veren araçlar haline getirmiştir.

Anahtar Sözcükler: Polidimetilsiloksan, Biyomimetik, Kendiliğinden düzenlenen monokatmanlar, Osteoblastlar, İndüklenmiş pluripotent kök hücreler, Kardiyomiyosit farklılaşması, Kornea endoteli hücreleri.

TABLE OF CONTENTS

ACKNOWLEDGMENTS . . . iii
ACADEMIC ETHICS AND INTEGRITY STATEMENT . . . iv
ABSTRACT . . . v
ÖZET . . . vi
LIST OF FIGURES . . . x
LIST OF TABLES . . . xvi
LIST OF SYMBOLS . . . xvii
LIST OF ABBREVIATIONS . . . xviii
1. INTRODUCTION . . . 1
1.1 Motivation . . . 1
1.2 Objectives and Outline of the Thesis . . . 3
2. BACKGROUND . . . 7
2.1 Cell Microenvironment . . . 7
2.1.1 Extracellular Matrix . . . 8
2.1.2 Cell-cell interactions . . . 9
2.1.3 Signaling Factors . . . 10
2.1.4 Physical Environment . . . 10
2.2 Cell Substrates as Artificial Cell Microenvironments . . . 12
2.2.1 Surface Chemistry . . . 13
2.2.2 Surface Topography . . . 14
2.2.3 Surface Wettability . . . 15
2.2.4 Substrate Stiffness . . . 16
2.3 Cell Substrate Design for Specific Cell Types . . . 17
2.3.1 Osteoblasts . . . 17
2.3.2 Cardiomyocytes . . . 18
2.3.3 Corneal Endothelial Cells . . . 20
3. CELL SUBSTRATE DESIGN FOR IMPROVED OSTEOBLAST BEHAVIOR 23
3.1 Synthesis and Characterization of Amino Acid Conjugated SAMs . . . 23
3.2 Preparation and Characterization of PDMS Substrates . . . 24

3.3 *In vitro* Human Osteoblastic Cell Culture 26
3.3.1 Cell Proliferation Assay 27
3.3.2 Morphological Staining 27
3.3.3 Alkaline Phosphatase Activity Investigation 28
3.3.4 Mineralization Staining 28
3.4 Statistical Analysis 28
3.5 Results 29
3.5.1 Characterization of Amino Acid Conjugated SAMs 29
3.5.2 Characterization of Modified PDMS Substrates 30
3.5.3 Osteoblastic Behavior on PDMS Substrates 35
3.6 Discussion 39
4. CELL SUBSTRATE DESIGN FOR THE DIFFERENTIATION OF INDUCED PLURIPOTENT STEM CELLS INTO CARDIOMYOCYTES 45
4.1 Preparation and Characterization of PDMS Substrates with Healthy Myocardium-like Stiffness 45
4.2 Surface Chemical Modification and Characterization 46
4.3 Induced Pluripotent Stem Cell Culture 47
4.3.1 iPSCs Viability 47
4.3.2 Morphological Investigation 48
4.4 Cardiomyocyte Differentiation of iPSCs 48
4.4.1 Western Blot Analysis 49
4.4.2 Immunocytochemistry 49
4.4.3 Immunofluorescence Staining 50
4.5 Statistical Analysis 50
4.6 Results 50
4.6.1 Nanoindentation Analysis 50
4.6.2 Characterization of Amino Acid-SAMs Modified PDMS 51
4.6.2.1 XPS Analysis 51
4.6.2.2 WCA Analysis 53
4.6.3 iPSC Response to PDMS Substrates 53
4.6.4 Differentiation of iPSC into Cardiomyocytes on PDMS Substrates 56
4.7 Discussion 61

5. CELL SUBSTRATE DESIGN FOR ENHANCED CORNEAL ENDOTHELIAL CELL RESPONSE 66
5.1 Preparation and Characterization of PDMS Substrates 66
5.2 Corneal Endothelial Cell Culture 68
5.2.1 Cell Proliferation Assay 68
5.2.2 Morphological Staining 69
5.2.3 Immunocytochemistry 69
5.2.4 Western Blot Analysis 69
5.3 Statistical Analysis 70
5.4 Results 70
5.4.1 Topographical Investigation of Patterned PDMS Substrates . . 70
5.4.2 Nanoindentation Analysis 72
5.4.3 Characterization of Surface Chemical Modification 73
5.4.3.1 WCA Measurements 74
5.4.3.2 XPS Analysis 74
5.4.3.3 Immunofluorescence Staining 75
5.4.4 CEC Behavior on PDMS Substrates 75
5.5 Discussion 79
6. CONCLUSION 83
REFERENCES 84

LIST OF FIGURES

Figure 2.1	Schematic representation of fundamental cell microenvironment components: neighboring cells or cell-cell interactions, soluble signaling factors, ECM and physical environment [1].	7
Figure 2.2	Different organizations of ECM with their main components [2].	8
Figure 2.3	Graphical illustration of mechanotransduction (matrix metalloproteinase, MMPs; tissue inhibitor metalloproteinases, TIMPs) and cellular responses to intracellular signaling. Red arrows show cellular feedbacks; ECM receptors are indicated in purple and various biophysical signals are depicted by green [3].	11
Figure 2.4	Figure 2.4. Schematic representation of various cell substrate properties effecting cellular behavior [4].	12
Figure 2.5	Different surface chemical modification techniques to enhance cell-substrate surface interactions [5].	14
Figure 2.6	Corneal epithelial cells on (a) patterned and (b) smooth silicon oxide cell substrates. (c) Change in the direction of cell alignment from parallel to perpendicular on nano-sized grooves patterned surfaces [6, 7, 8].	15
Figure 2.7	Elasticity of cell type specific ECM and some examples of biomaterials with corresponding elasticity [9].	17
Figure 2.8	Generation of IPSCs from fibroblast cells [10].	19
Figure 3.1	The synthesis procedure of His-SAM and Leu-SAM.	23
Figure 3.2	Schematic illustration of PDMS modification. (A) Optimization of His-SAM modification (1-20 mM, 2h and 10 mM, 1-24h), and (B) modification of PDMS surface with His-SAM or Leu-SAM (10 mM, 24h).	25
Figure 3.3	(a) PDMS coated QCM sensor crystal (b) in the flow cell of QCM unit (c) and closed system of flow cell.	26
Figure 3.4	Surface zeta potentials (surface charges) of SNPs and His-SAM functionalized SNPs at pH = 5.0, 7.4 and 9.0.	30

Figure 3.5 (a) High-resolution N1s spectra and (b) WCA measurements of PDMS modified with increasing concentrations (1-20 mM) of His-SAM. 31

Figure 3.6 (a) High-resolution N1s spectra and (b) WCA measurements for His-SAM modification of PDMS with increasing dipping time (1-24 h). 32

Figure 3.7 (a) XPS wide scan spectra and (b) WCA measurements of native, Leu-SAM modified, and His-SAM modified PDMS substrates. 33

Figure 3.8 MB and EY dye adsorption capacity of His-SAM modified PDMS at various pHs. 34

Figure 3.9 Stability of His-SAM modification under 2 mL/min flow for 0.5 and 4 h. (a) XPS wide scan spectra showing the specific O1s, N1s, C1s, Si2s and Si2p peaks of His-SAM modified PDMS before and after continuous flow. (b) WCAs of His-SAM modified PDMS before and after exposure to flow (No significant differences were observed between groups). 35

Figure 3.10 Reduced Alamar Blue percentages showing the relative hFOB cell proliferation on native, Leu-SAM, and His-SAM modified PDMS with positive control of TCP over 7 days. Data were given as means ± SD and n = 7. All groups were statistically significant respect to native PDMS, each day (****$p < 0.0001$; except for Leu-SAM on Day 1, ***$p < 0.001$), *$p < 0.05$, **$p = 0.01$. 36

Figure 3.11 Fluorescence images of Alexa Fluor 488-phalloidin (green) and DAPI (blue) stained hFOBs on native, Leu-SAM, and His-SAM modified PDMS substrates and TCP. Scale bar = 100 μm. 37

Figure 3.12 ALP activity (U/L) of hFOB cells on native, Leu-SAM and His-SAM modified PDMS with positive control of TCP at different incubation times. Data were given as means ± SD and n = 5. Statistical significance values were calculated for each day, $^{*}p < 0.05$, $^{**}p < 0.01$, and $^{****}p < 0.0001$ (All groups were statistically significant relative to native PDMS with $^{****}p < 0.0001$, each day, except for Leu-SAM on Day 3, $^{**}p < 0.01$). 38

Figure 3.13 Alizarin red staining of hFOB cells on native, Leu-SAM, and His-SAM modified PDMS with positive control of TCP at different incubation times. Scale bar = 200 μm. 39

Figure 4.1 Modification procedure of PDMS substrates with conventional and amino acid conjugated SAMs. 46

Figure 4.2 Young modulus values of PDMS with increasing pre-polymer & cross-linker ratios. 51

Figure 4.3 Characterization of native and SAMs modified PDMS with XPS (a) survey spectra, (b) high resolution C1s and (c) N1s spectra. 52

Figure 4.4 Characterization of native and SAMs modified PDMS with WCA measurements. The data are given as the mean ± SD. $^{****}p < 0.0001$ for all comparisons between samples, except for $^{**}p < 0.01$ between PDMS-O and PDMS-L; no significant differences were found between PDMS-A and PDMS-H. 53

Figure 4.5 iPSC behavior 48 h after seeding on 50:1 PDMS-conv and PDMS-ext. (a) Optical microscopy images (10X) of cells on PDMS-conv and, (b) PDMS-ext. (c) Relative optical densities of iPSCs on TCP and PDMS substrates. The data are given as the mean ± SD. $^{****}p < 0.0001$ for all comparisons. 54

Figure 4.6 iPSC viability on native and SAM modified PDMS surfaces. Qualitative investigation of different PDMS surfaces' toxicity on cells by using acridine orange (green) and propidium iodide (red) staining (Scale bar = 100 μm). 55

Figure 4.7 iPSC viability on native and SAMs modified PDMS surfaces. Quantification of iPSC viability on native and modified PDMS surfaces with MTT assay according to the relative optical densities (**p < 0.01, **** and # indicate p < 0.0001 when compared to all other groups). 55

Figure 4.8 SEM images of iPSCs on native and SAM modified PDMS surfaces over 48 h (Scale bar = 50 μm). 56

Figure 4.9 Western blot analysis for the cardiac markers of (a) α-actinin; (b) TPM, and (c) cTnT with the control of β-actin. The data are presented as the mean ± SD; *p < 0.05, **p < 0.01, ***p < 0.001, and # indicate significant differences when compared to native PDMS in (a); and PDMS-L in (b). 57

Figure 4.10 (a) Optical microscopy images of beating areas (in white) on TCP and various PDMS substrates (Scale bar = 200 μm). (b) Frequency and (c) areas of beating cardiomyocyes on the 12^th day of differentiation. The data are presented as the mean ± SD (n = 3); *p <0.05, **p < 0.01 and ***p < 0.001. 58

Figure 4.11 Immunostaining for the cardiac marker, cTnT (red) with DAPI (blue) counterstain for nuclei. (a) Cells on day 12 of differentiation on TCP and different PDMS surfaces (Scale bar = 100 μm). (b) Quantification of cTnT fluorescent intensity of staining on day 12 of differentiation. The data are presented as the mean ± SD (n = 3); ***p < 0.001, ****p < 0.0001 and ####p < 0.0001. #p indicates significant difference when compared to all other groups. 59

Figure 4.12 (a) Quantification of cTnT positive cells (%) and (b) area. The data are presented as the mean ± SD (n = 3); *p < 0.05, **p < 0.01, ***p < 0.001 and ****p < 0.0001. 60

Figure 4.13 cTnT (red) and F-actin (green) staining of cells differentiated for 12 days on gelatin coated TCP, PDMS-L and PDMS, respectively and re-plated on fibronectin-coated TCP (Scale bar = 50 μm). 61

Figure 5.1 Schematic procedure of rose petal topography mimicked PDMS substrate preparation. 66

Figure 5.2 Functionalization of PDMS substrates with COL 4 and HA. 67

Figure 5.3 SEM images of rose petal patterns on PDMS surfaces; (a) positive replicas of (i) fresh and (ii) dry red rose, (iii) fresh and (iv) dry white rose petal patterns; (b) surface topography measurements of fresh (i) white and (ii) red rose petal patterned PDMS; (c) fresh white rose patterned (i) mold and (ii) cell substrate. 71

Figure 5.4 SEM images of rose petal mimicked PDMS (a) mold (positive replicate) with marked area, (b) 1^{st} replicate, (c) 3^{rd} replicate, (d) 5^{th} replicate, (e) 7^{th} replicate and (f) 10^{th} replicate (Scale bar = 100 μm). 72

Figure 5.5 Nanoindentation measurements of varying PDMS pre-polymer and curing agent formulations (****p $<$ 0.0001). 73

Figure 5.6 WCA analysis of native PDMS and APTES, HA and COL 4 functionalized PDMS. The data are presented as the mean ± SD (n = 3); ****p $<$ 0.0001 for all comparisons, except ***p =0.0002 for PDMS-NH2 vs PDMS-HA and **p =0.0012 for PDMS-NH_2 vs PDMS C4. 73

Figure 5.7 (a) XPS survey spectra of native PDMS and APTES, HA and COL 4 functionalized PDMS. (b) High resolution C1s spectra of native PDMS, (c) PDMS-NH_2, (d) PDMS-HA and (e) PDMS-C4. 74

Figure 5.8 Immunofluorescent staining against anti-hyaluronic acid on (a) PDMS and (b) PDMS-HA; against anti-collagen IV on (c) PDMS and (d) PDMS-C4. Scale bar = 200 μm. 75

Figure 5.9 Reduced alamar blue (%) with relative CEC proliferation on (a) flat and (b) white rose patterned native PDMS, PDMS-HA, PDMS-C4 and TCP over 7 days and (c) CEC proliferation on flat and white rose patterned PDMS and COL 4 on day 7 (***p $<$ 0.001 and ****p $<$ 0.0001). 76

Figure 5.10 Actin cytoskeleton (green) and nuclei (blue) staining of CECs on PDMS substrates (Scale bar = 100 μm). 77

Figure 5.11 Immunofluorescent staining of CECs for Na^+/K^+ ATPase (red) and DAPI (blue). Scale bar = 100 μm). 78

Figure 5.12 Western blot analysis of CECs on PDMS-C4, PDMS-C4-R and TCP. Quantification of (a) Na^+/K^+ ATPase, (b) N-Cadherin and (c) Collagen IV markers relative to β-actin ($^*p < 0.05$ and $^{**}p < 0.01$). 78

LIST OF TABLES

Table 3.1 Surface elemental composition of native and SAMs modified PDMS substrates. 33

LIST OF SYMBOLS

Al-Kα	K-alpha X-rays of aluminum
eV	electrovolt
mg	milligram
MHz	Mega Hertz
ml	milliliter
mM	millimolar
mTorr	millitorr
N/m	Newton/meter
rpm	round per minute
sccm	standard cubic centimeters per minute
V	Volt
°C	degree Celsius
μg	microgram
μL	microliter
μm	micrometer

LIST OF ABBREVIATIONS

AA-SAM	Amino acid conjugated self-assembled monolayer
AFM	Atomic Force Microscopy
APTES	(3-aminopropyl)triethoxysilane
ANOVA	Analysis of Variance
BPM	beat per minute
BSA	Bovine Serum Albumin
Bt	Benzotriazol-1-yl
Cbz	carboxybenzyl
COL 4	Collagen type 4
cTnT	Cardiac Troponin-T
DMEM	Dulbecco's Modified Eagle Medium
ESC	Embryonic stem cells
EY	Eosin y disodium salt
HA	Hyaluronic Acid
His	Histidine
His-SAM	Histidine conjugated self-assembled monolayer
HRP	Horseradish peroxidase
iPSC	Induced Pluripotent Stem Cell
Leu	Leucine
Leu-SAM	Leucine conjugated self-assembled monolayer
MB	Methylene Blue
IMDM	Iscove's modified Dulbecco's medium
NMR	Nuclear Magnetic Resonance
OTS	Octadecyltrimethoxysilane
PBS	Phosphate Buffered Saline
PDMS	Polydimethylsiloxane
SD	Standard Deviation
SEM	Scanning Electron Microscopy

SNP	Silicon nanoparticles
THF	Tetrahydrofuran
TPM	Tropomyosin
WCA	Water Contact Angle
XPS	X-ray Photoelectron Spectroscopy

1. INTRODUCTION

1.1 Motivation

In their native microenvironment, cells are found embedded in their specialized extracellular matrix (ECM), which is a source of biochemical signals and also provides a mechanical support [11]. To control *in vitro* behavior and (for stem cells) differentiation of cells, biomaterial platforms with well-defined mechanical, topographical and chemical properties are required. The production of such materials with tunable design considerations has attracted much interest in the areas of cell-based therapies [12, 13, 14], drug investigation [15, 16] and *in vitro* disease modeling [17, 18].

Polydimethylsiloxane (PDMS) has been attracted much attention in the biomedical area for developing cell culture substrates [19, 20], medical implants [21, 22], organs-on-chips [23, 24], and microfluidic devices [25, 26]. Comparable biocompatibility, low-toxicity, high oxygen permeability, low cost, ease of fabrication, and adjustable mechanical, topographical and chemical properties are some of the superior characteristics of PDMS, provoking its extensive use as a biomaterial. The surface of native PDMS is highly hydrophobic and does not have any cues for cell attachment [27]; revealing the need for its surface modification. Simple techniques like oxygen plasma [28], coating the surface with ECM molecules [29, 30] and complex chemistries like glutaraldehyde [31, 32] or EDC coupling [33], have been used for surface modification. However, these methods are either only stable for a very short while, or may result in the occurrence of cytotoxic residuals. Thus, there is a high demand for PDMS with enhanced surface properties and increased stability to provide a convenient environment for specific cell functions.

Among many different surface modification methods for enhanced cell interaction purposes, self-assembled monolayers (SAMs) provide superior advantages with their well-defined, stable and tunable surface chemistry on various types of substrates

[34] and easy preparation without any need of expensive and high-level equipment [35, 36]. SAMs modified surfaces have been reported for diverse applications, including drug delivery [37], biosensors [38], biomolecule immobilization [39], non-specific protein adsorption [40], in addition to their use in synthetic cell culture environments [41]. Since functional groups of SAMs, like -OH, -CH_3, -SH or -COOH, are found naturally in biological environment, the modification of cell substrates with SAMs plays a major role in regulating protein adsorption and cell behavior [42, 35]. Furthermore, SAMs are highly organized structures and they tune the wettability properties of surfaces depending on their functional groups [36]. Wettability is one of the most important characteristics of a cell substrate [43]. In this thesis, these given advantages of SAMs were increased by the incorporation of hydrophilic and hydrophobic amino acids to SAMs. Essential amino acids are known to stimulate bone formation by enhancing alkaline phosphatase activity and collagen synthesis [44]. Hence, the first study of this thesis offers stable, practical and biomimetic PDMS substrate surfaces with varying wettability. By designing these amino acid incorporated SAMs, the main aim was to enhance osteoblast cell-biomaterial interactions and regulate biological signals, as extracellular matrix-like surfaces have the tendency of providing better cell culture environments.

Induced pluripotent stem cells (iPSCs), which are obtained by the transduction of somatic cells with defined factors, have the ability to differentiate into many cell types, including cardiomyocytes, adipocytes and neurons [10]. Their indefinite *in vitro* proliferative capacity, ethical relevance and patient- or disease-specific applicability make iPSCs attractive sources for cell studies [45, 46]. Cardiomyocytes, differentiated from induced pluripotent stem cells (iPSCs), have the potential to produce patient- and disease-specific pharmacological and toxicological platforms, in addition to their cardiac cell therapy applications. Several studies show the sensitivity of stem cells to matrix stiffness [47, 48, 49]. Mimicking the natural healthy myocardium extracellular matrix (ECM) properties by altering the cell substrate properties, such as stiffness and chemical/biochemical composition can significantly affect cell-substrate interfacial characteristics and potentially influence cellular behavior and differentiation of iPSCs to cardiomyocytes. Within this motivation, a systematic and biomimetic approach,

which was based on the preparation of PDMS substrates having the similar stiffness as healthy heart tissue and a well-defined surface chemistry obtained by conventional and amino acid (histidine and leucine) conjugated self-assembled monolayers (SAMs) was proposed in the second study of the thesis.

Corneal endothelial cells (CECs) have low proliferation capacity *in vivo* and the decrease in the cell density causes serious visual problems up to blindness. Since all current treatment options for the corneal dysfunction are related to transplantable donor corneas, which are highly limited, there is a substantial demand for alternative approaches, like obtaining desired functional cell densities *in vitro* by using bioengineered cell substrates. As the microenvironment of cells and the interaction in between them regulate cellular behavior, properties of Descemet's membrane and corneal extracellular matrix (ECM) have been considered in designing biomaterials [50, 49, 51]. Hence, in the third study of the thesis, PDMS cell substrates were prepared in a cornea-friendly stiffness range and modified with two of the important ECM components of cornea: Collagen type IV (COL 4) and Hyaluronic Acid (HA). Additionally, we took the advantage of naturally occurring patterns - rose petals (negative reliefs), to control cell substrate topographies. Topographical features of white rose petals were similar to corneal endothelium due to hexagonal cell shapes and physiologically relevant cell density ($\approx$ 2000 cells/mm^2).

In this thesis, we have not only enhanced cell-substrate characteristics of PDMS, but also offered promising, facile and biomimetic approaches, which can be used in various *in vitro* cell culture studies, toxicological applications and as well as microfluidic systems.

1.2 Objectives and Outline of the Thesis

Various treatments approaches like cell based therapies, or therapeutic and toxicological investigations like in lab-on-a-chips or microfluidic systems reveal the need of well-designed cell substrates [52, 53, 54]. A successful cell substrate should be non-

toxic and biocompatible, in addition to provide a supportive platform with natural microenvironment-like mechanical and biochemical properties to enhance cellular viability, proliferation and functionality. PDMS has been a widely used polymer in biomaterial fabrication for cell culture substrates [19, 20] or lab-on-a-chip designs [25, 24] and microfluidics [55], due to its non-toxic nature with adjustable mechanical and surface properties. Prior to any cellular interactions, PDMS surface chemistry needs to be altered via plasma treatments, protein coating or modifications, as PDMS does not have any chemical cues for cell binding. Still, these techniques are either last for a very limited time or have very complicated experimental procedures. In addition to the need of both facile and effective surface modification technique, a combination of improved surface chemistry with natural cell microenvironment-like mechanical and topographical features would enhance *in vitro* cellular behavior. Therefore, the main purpose of my Ph.D. research was to develop PDMS substrates with improved biocompatibility, surface biochemistry, mechanical and topographical properties for enhanced interactions at the cell-substrate interface. The outline of the thesis with the main objectives are presented as in the following:

1. Indicating the motivation and the evaluation of the literature related to the thesis studies

    - Main motivations behind the thesis are given in the Chapter 1.
    - Enabling these motivations, a comprehensive literature review with background information on the important parameters of tissue type specific cell substrate design strategies are presented in Chapter 2.

    My Ph.D. thesis is a combination of three different studies with three different tissue types, in which PDMS is used as a cell substrate material for all of them.

2. Development of a facile and one-step surface chemical modification approach for PDMS to enhance in vitro osteoblastic behavior is presented in Chapter 3. The following findings are established in this chapter:

    - Synthesis and characterization of hydrophilic and hydrophobic amino acid conjugated self-assembled monolayers (SAMs).

- Investigation and characterization of optimum modification conditions with SAMs for 10:1 prepolymer to curing agent ratio of PDMS.
- Evaluating the *in vitro* osteoblast response in means of proliferation, morphology and maturation on PDMS substrates.

3. The effect of both healthy myocardium-like substrate stiffness and improved surface chemistry through conventional and amino acid conjugated SAMs on the behavior and cardiac differentiation of iPSCs are analyzed in Chapter 4. In the context of the chapter, following are investigated:

    - The optimum PDMS formulation to mimic the stiffness of healthy cardiac microenvironment.
    - An extended approach for 50:1 prepolymer curing agent ratio of PDMS to increase the thermodynamic stability of substrates.
    - A suitable surface modification protocol with conventional and amino acid conjugated SAMs.
    - Impact of PDMS cell substrates with healthy myocardium-like stiffness and comparative surface modification with SAMs on iPSC viability, attachment and cardiac differentiation.

4. In Chapter 5, a biomimetic approach is developed to improve cell substrate properties of PDMS for corneal endothelial cell applications, suggesting a substrate design with a cornea friendly stiffness, surface chemistry and white rose topography mimetic surface patterning. Main objectives of this chapter are:

    - Investigation of CEC microenvironment-like patterns from red and white rose petal relief topographies. Both of these rose petal topographies exhibit CEC shape-like hexagonal patterns. Size, depth and density of patterns are examined and compared with natural CEC microenvironment.
    - Production of PDMS substrates within a cornea-friendly stiffness range.
    - Functionalization of PDMS substrates with two of the important CEC ECM components: COL 4 and HA.

- Examining the effects of PDMS substrate mechanical, topographical and chemical properties on CEC proliferation, morphology and functional marker expression.

2. BACKGROUND

2.1 Cell Microenvironment

The fate of cellular processes has been found to be regulated by cell type specific microenvironment and accordingly the microenvironment concept is needed to be well understood prior to any study with cells; including drug testing, disease modeling and cell substrate design [56, 57]. Numerous advanced studies on *in vivo* cellular behavior have confirmed that cells can feel their own microenvironment and highly sensitive to the changes around. Thus, the structure and ingredients of this specialized habitat and interactions with cells are fundamental aspects of biomaterials for cell based therapies and regenerative medicine.

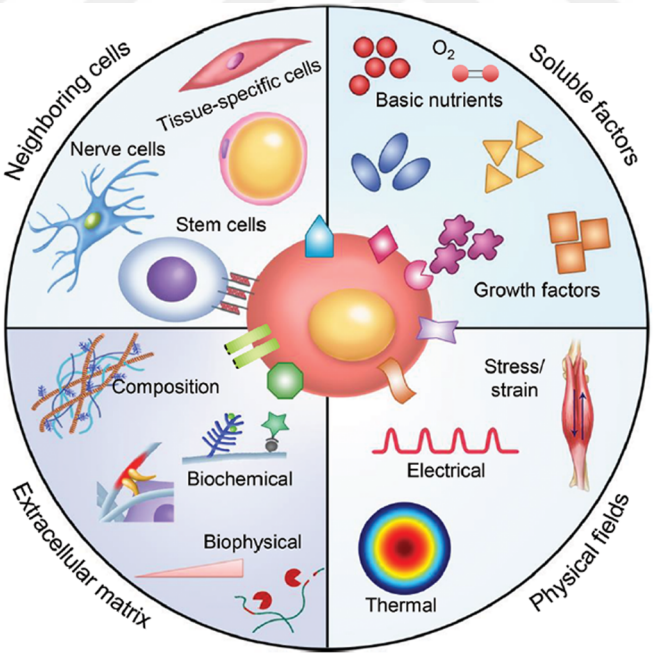

Figure 2.1 Schematic representation of fundamental cell microenvironment components: neighboring cells or cell-cell interactions, soluble signaling factors, ECM and physical environment [1].

Cell microenvironment is a complex and dynamic system, which is composed of extracellular matrix (ECM), soluble signaling factors (growth factors, morphogenic factors, cytokines, peptides, etc.), physicochemical environment (mechanical proper-

ties, topographical cues pH, O_2 tension, etc.) and cell-cell interactions (or neighboring cells). These four key parameters act as a support to cells and modulate their behavior synergistically (Figure 2.1).

2.1.1 Extracellular Matrix

ECM is a biological substance, secreted by the residing cells. It comprises mostly water and the remaining is a network of cell type specific macromolecules, like collagens, glycosaminoglycans and proteoglycans. The ECM of cells can be organized in two ways, depending on the ingredients and localization. The first one is the basement membrane, which is a thin layer and consists of mainly collagen type IV, laminins and proteoglycans; whereas the second organization is the interstitial matrix (Figure 2.2). The interstitial matrix provides a structural support around cells and mostly composed of type I collagen and fibronectin. The ECM is a natural scaffold to cells and it also helps to maintain cell homeostasis, in addition to the modulation of cellular behavior, including cellular growth, apoptosis, proliferation, migration and differentiation for stem cells [58, 59].

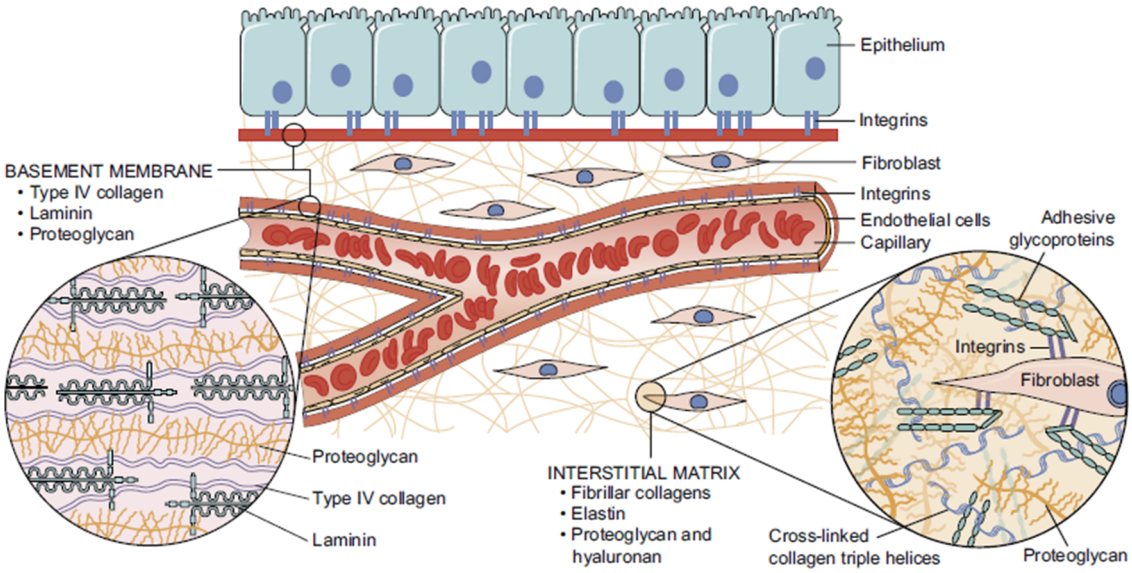

Figure 2.2 Different organizations of ECM with their main components [2].

Depending on the tissue type, several proteins are found in the ECM, including collagen, elastin and fibronectin [60]. Among all, collagens are the most abundant ones

in humans. Collagens are synthesized as procollagens, self-assembled and matured in the extracellular space. Collagens are structural proteins and fibril forms of collagens can resist compression even at high mechanical loads. Unlike collagen, elastin provides shape recovery in stretching tissues via passive recoiling. On the other hand, fibronectin and laminin are known as adhesive proteins, which allow cell attachment and migration. Several GAGs, like hyaluronic acid, chondroitin sulfate and heparin, affect ECM viscoelasticity to provide shear stiffness. Furthermore, they help the maintenance of homeostasis [61].

Cell-ECM interactions are regulated by direct and indirect mechanisms [62]. Direct mechanism occurs when ECM proteins interact with integrins, which are receptors on cellular surfaces. Integrins activate intracellular signaling pathways by providing a linkage between matrix and cell cytoskeleton. On the other hand, indirect mechanism arises from growth factors. Altogether, ECM characteristics and communication with cells direct important cell functions, like migration, growth and differentiation for stem cells [63, 64, 65].

One of the major challenges in biomaterial design is to mimic natural structure and functions of ECM, since its composition varies with time and cell type. Still a well-understood form and features of ECM would be highly supportive to engineer cell substrates.

2.1.2 Cell-cell interactions

In their natural environment, cells interact with same or different types of cells. Interactions between cells have demonstrated to be crucial for the modulation of cell responses and ingrowth [66]. The regulation of cell-cell interactions is performed by calcium dependent hemophilic adhesion molecules, cadherins [58, 67]. Cell-cell communications can occur via direct contact through gap junctions or autocrine, paracrine and endocrine signaling pathways. These specific interactions are essential to maintain barrier functions and one of the most influential mechanisms on stem cell differentiation

and tissue development [59].

2.1.3 Signaling Factors

Numerous small soluble factors, such as glucose, O_2, amino acids are found in the local aqueous microenvironment of cells. Changes in the concentration of all these basic nutrients effect cellular behavior, like the impact of oxygen concentration on pluripotency maintenance [68, 69], cardiomyocyte proliferation [70] and angiogenic responses of tumor cells [71]. Signaling molecules, like enzymes, growth factors, morphogenic factors, cytokines and hormons, are also essential components of cell microenvironment. Among them, growth factors are highly studied and necessary for the development. Growth factors are specific to cell type and their local concentration are modulated in time and space, which result in critical changes in cell responses [72]. Bone morphogenic proteins (BMPs), vascular endothelial growth factors (VEGFs) and transforming growth factors (TGFs) are specific examples to this family and they take part in the regulation of cell proliferation, growth and differentiation, which are essential for important events like tissue development, wound healing or fibrosis [1].

2.1.4 Physical Environment

Physical environment, including mechanical properties, topographical features, electrical, magnetic and thermal fields can also be sensed by cells and according to the changes in these fields cells alter their behavior (Figure 2.3). In addition to soluble signals, cell-ECM and cell-cell interactions, cells can feel and generate responses to these insoluble signals via integrin-regulated adhesions. The process of sensing biophysical environment and transduction of them into intracellular signals is termed mechanotransduction [73, 74].

Tissues possess a wide range of matrix stiffness, depending on their type. For instance bone is a very rigid tissue to provide a mechanical support for human body,

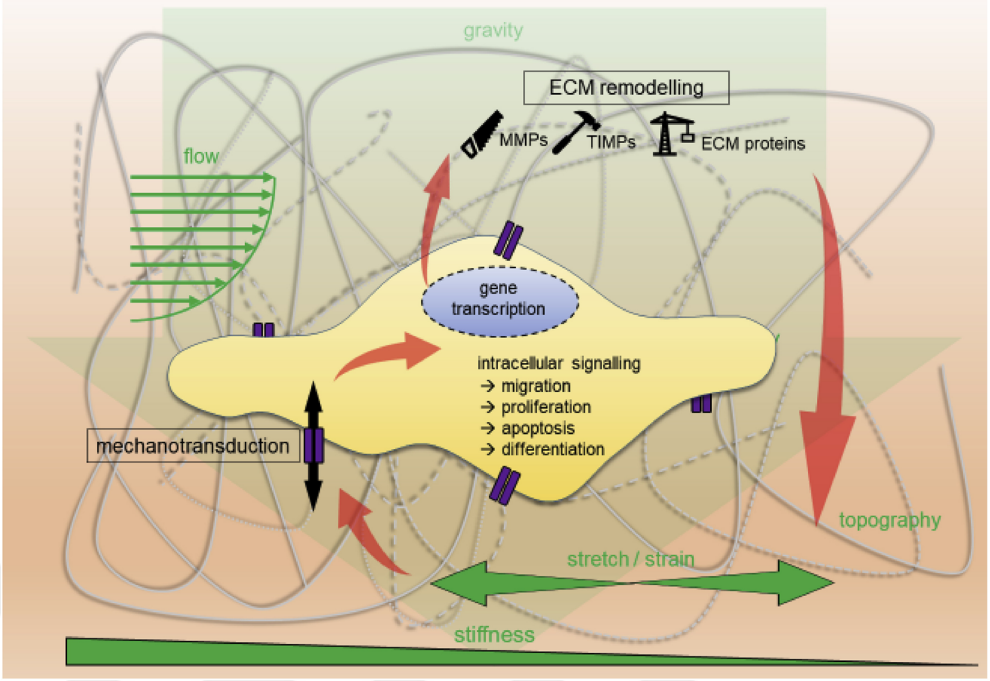

Figure 2.3 Graphical illustration of mechanotransduction (matrix metalloproteinase, MMPs; tissue inhibitor metalloproteinases, TIMPs) and cellular responses to intracellular signaling. Red arrows show cellular feedbacks; ECM receptors are indicated in purple and various biophysical signals are depicted by green [3].

whereas muscles or adipose tissues are relatively very soft ones. These variations between matrix stiffness help stem cells to differentiate into specific cell types and thus mechanical properties of microenvironment is very important during human development. Conversely, changes in mature tissue's matrix stiffness lead to dysfunction [9]. In addition to mechanical properties of ECM, internal (such as contractile forces) and external (stretching, compressive forces or shear stress) forces also have influence on stem cell differentiation, like the application of shear stress to embryonic stem cells induce them to differentiate vascular endothelial cells [75].

Cell shape and ECM topographical features are another modulators of cell behavior and growth [76]. Lineage specific cell shapes are optimized acccording to their functions, such as neurons possess long axons to be able to send signals to distant receivers [74]. During cellular physiological processes, cells do not only interact with each other, but also with porous ECM networks and fibrillar protein-proteoglycan structures. These micro and nanoscale arthitectures induce integrins to form focal adhesions, which are dynamic cell adhesion structures. These linkages activate signaling

pathways and regulate cell cytoskeletal organization. Thus, integrin mediated focal adhesion signaling influence cellular behavior, in forms of migration, proliferation or differentiation [77].

2.2 Cell Substrates as Artificial Cell Microenvironments

Cell substrates are materials on which cells adhere and culture *in vitro* for a variety of applications. With advances in biomaterials science, numerious cell substrates have been developed, including polymers, ceramics and metals. In the process of substrate design, interaction at the substrate-cell interface is essential to obtain desired *in vitro* cellular functions, such as adhesion, growth and differentiation. As discussed in Section 2.1, cells can feel and respond to their microenvironment. Therefore, in order to produce cell substrates to control over cell fate and functionality, characteristics of chosen cell type's microenvironment should be well studied and mechanical, topographical and chemical properties of substrate surfaces are needed to be adjusted accordingly (Figure 2.4) .

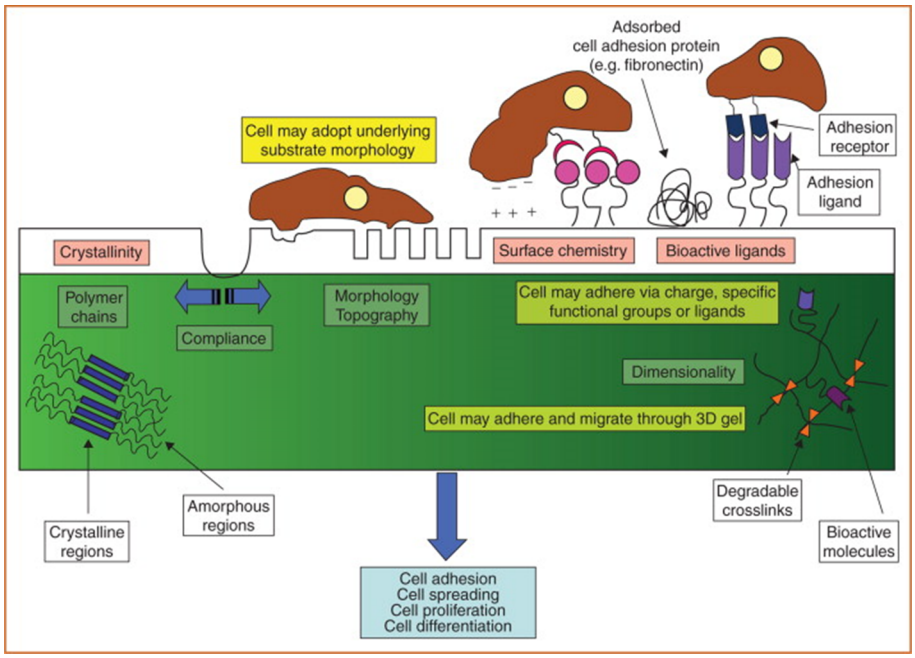

Figure 2.4 Figure 2.4. Schematic representation of various cell substrate properties effecting cellular behavior [4].

2.2.1 Surface Chemistry

Interactions at the interface between biomaterial surface and cell are fundamental to direct various cellular functions, like adhesion, viability, growth and differentiation. In order to produce cell substrates to control over desired cell behaviour *in vitro*, alteration in the chemical properties of substrates has been a widely employed approach. Depending on the type of the material to be used and the interested cell line, various surface chemistry related techniques have been developed. Chemical modification approaches are summarized in Figure 2.5 [5]. Among them, plasma treatment is a relatively simple technique [78]. Similarly, coating substrate surfaces with ECM macromolecules (physical adsorption), such as proteins, GAGs and polysaccharides, or growth factors, which are generally governed by van der Waals forces, are also easy to apply methods to increase the biocompatibility of substrates prior to cell culture [30, 58]. However, both of these techniques are stable for a short period of time. Instead, a more complicated covalent modification would provide long-term stability for cellular applications [79]. One example to covalent modification is the application of a mediator linker, 1-ethyl-3-(3-dimethylaminopropyl)carbodiimide/ N-hydroxysuccinimide (EDC-NHS) for the immobilization of biological molecules to substrates [80, 81]. For instance, Sangsanoh et al., modified scaffolds with laminin by using EDC-NHS as a crosslinker to improve cell adhesion and proliferation [82]. Introduction of functional groups, such as -OH, -CH_3, -COOH and -NH_2 to substrate surfaces through self assembled monolayers (SAMs) is an another promising strategy to form highly organized covalent attachment for enhanced cellular behavior, since these functional groups are already found in their natural environment [83, 84]. For example, amino (-NH_2) groups incorporated SAMs modified surfaces showed promotive effect on osteogenic differentiation [83], while methyl (-CH3) groups supported chondrogenesis of stem cells [85]. Furthermore, surface wettability properties can also be easily tuned, depending on the functional groups of SAMs [42, 35].

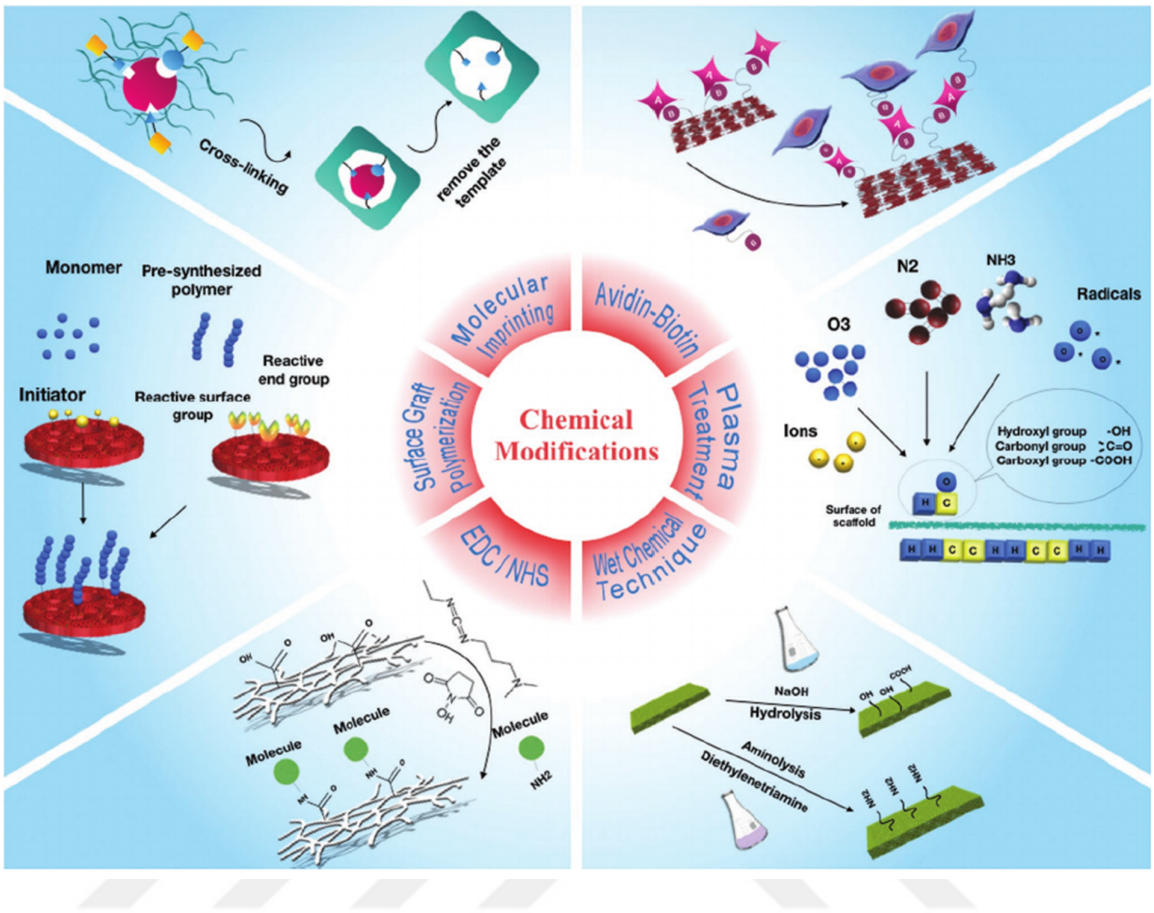

Figure 2.5 Different surface chemical modification techniques to enhance cell-substrate surface interactions [5].

2.2.2 Surface Topography

Cells in the human body are found in direct contact with various micro and nanotopographical cues of their surroundings and these biophysical signals coming from ECM components guide cellular adhesion, migration and other specific functions [86]. With this inspiring motivation, cell substrate's surface topography has engineered and these patterned surfaces resulted significant effects on cell behavior. Various patterning approaches have been develeoped, such as grooves, fibers, rods, wells, pillars and pits, to mimic natural microenvironment of cells for the *in vitro* control of their functions, through the crosstalk between substrate and cell cytoskeleton [87]. A few examples of cell responses to various substrate topographies are given in Figure 2.6. Corneal epithelial cells culture on patterns of grooves lead cells to elongate in the direction of these features, whereas their alignment was also influenced by the depth of grooves

[6, 7]. Same type of cells on nano-sized grooves showed perpendicular alignment to the grooves [8].

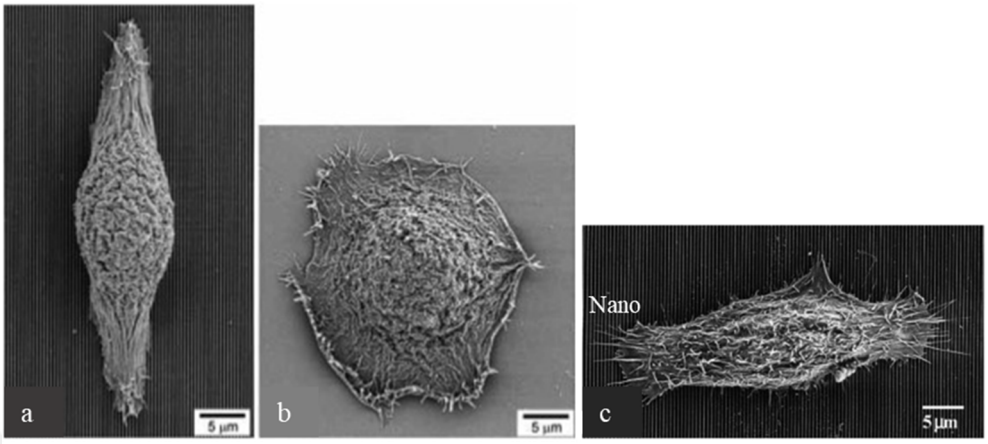

Figure 2.6 Corneal epithelial cells on (a) patterned and (b) smooth silicon oxide cell substrates. (c) Change in the direction of cell alignment from parallel to perpendicular on nano-sized grooves patterned surfaces [6, 7, 8].

Surface patterns on substrates have also confirmed to enhance adhesion and differentiation of stem cells [88]. Lv et al. showed that 70 nm-diameter-nanotubes improved osteogenic differentiation of MSCs [89], whereas smaller diameters (30 nm) did not enhance differentiation [90]. In another study, effects of well-polished smooth surfaces and TiO2 nanorods on MSC were investigated. Cells on nanorods tended to differentiate into osteoblasts, while smooth surfaces induced proliferation of MSCs [91, 88].

2.2.3 Surface Wettability

Surface wettability is a dynamic interfacial process and determined by surface topographical features and chemical composition [92]. It is defined as the ability of any surface to be wetted, when a drop of liquid is applied and characterized by water contact angle analysis. Generally, water is used as a liquid and a surface with a water contact angle (WCA) greater than 80° is considered to be hydrophobic, whereas the surface is hydrophilic, if WCA is lower [93]. Substrate hydrophobicity is a critical factor in many biological processes, including ECM macromolecules' adsorption, protein conformations as well as cell-material interactions [94]. For example, osteoblasts

prefer to adhere hydrophilic surfaces [95], although highly hydrophilic surfaces inhibit binding of adhesion-related proteins, like fibronectin, collagen or laminin [96]. Ayala et al. demonstrated the effect of surface wettability on the cytoskeleton of MSC and accordingly on adhesion. They tuned hydophobicity of substrates by changing the amont of -CH_2 groups [97]. In addition to surface chemical alterations, topographical features can effect wettability properties of surfaces. Yang et al. showed that addition of nanotopographical features to silicon substrates can enhance surface hydrophilicity and these patterned substrates effect ovarian cell behavior [98].

2.2.4 Substrate Stiffness

In vivo, stiffness of cell microenvironment varies from 100 Pa (brain) to 100 GPa (bone), depending on the tissue type [99]. Earlier studies demonstrated impacts of microenvironment stiffness on essential cellular behavior, such as proliferation, migration and differentiation [100]. Cells in the human body have the ability to "feel" the elastic modulus of their surroundings and respond to them by regulating their endogenous cytoskeleton. Focal adhesions are the sites, where these mechanical signals are sensed. Signals are transmitted through ECM-integrin-cytoskeleton and fundamental functions of cells are modulated via integrin-regulated adhesion signaling [74, 101]. Since cells are mechanosensitive and mechanoresponsive, cell substrates must be designed within the stiffness value range of original tissue's microenvironment to obtain strong adhesion of cells to substrates and desired cellular functionalities.

Figure 2.7 shows elasticity values of a few tissue types with some compatible biomaterial suggestions [9]. Engler et al. investigated the effect of substrate stiffness on the differentiation of MSCs, where soft substrate (mimicking brain tissue) directed neurogenic, musle mimetic substrate stiffness to myogenic and stiffest ones provided osteogenic differentiation of these stem cells [50]. In another study, this influence was demonstrated through the stem cell behavior on soft PDMS substrates (1.5 and 15 kPa) and they found that these soft substrates resulted some alterations in MSCs, where they displayed similar phenotypic features with pluripotent stem cells (PSCs)

[102]. Kim et al. observed the effect of scaffold mechanical properties on the cardiac differentiation of cardiosphere-derived cells (CDCs). They prepared scaffolds by blending N-Isopropylacrylamide with polyurethane to obtain a wide range of tensile moduli (between 48 and 461 kPa). Among these various scaffolds, the one with a modulus of 48 kPa was found to promote cardiac differentiation of CDCs, confirming the impact of ECM properties on cardiac differentiation [103].

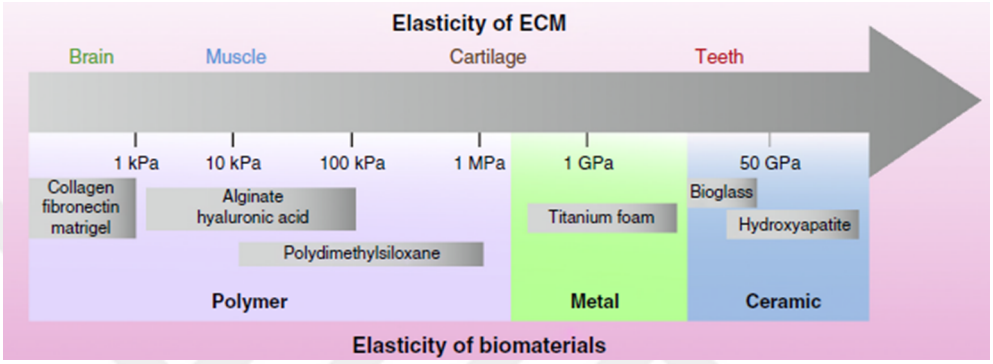

Figure 2.7 Elasticity of cell type specific ECM and some examples of biomaterials with corresponding elasticity [9].

2.3 Cell Substrate Design for Specific Cell Types

2.3.1 Osteoblasts

Bone tissue's ECM is mainly composed of collagen type. The remaining are macromolecules, like fibronectin, osteonectin and osteocalcin, and inorganic minerals including hydroxyapatite. All these macromolecules provide a stiff mechanical support to cells, in addition to the maintenance of osteoblast-specific phenotype [104]. Bone tissue-related pathological diseases, trauma or cancer have been worldwide issues, among aging population. Studies in biomaterials design and regenerative medicine have offered alternative solutions to this area by combining osteoconductive cell substrates and specific cell types, including osteoblasts and stem cells [105]. Cell substrates for bone regeneration should provide osteoblast microenvironment-like mechanical, chemical and topographical features to obtain well-controlled cell adhesion, growth and functionality.

Various types of biomaterials, changing from metals and polymers to ceramics have been used as cell substrates for *in vitro* osteoblast culture [106]. Many natural polymers, including chitosan, collagen or gelatin, have been selected for the production of substrates, due to their biocompatible nature. For instance, graphene oxide coated alginate scaffolds showed good cytocompatibility, in addition to their promotive effects osteogenic differentiation of adipose derived stem cells [107]. However, relatively low mechanical strength of natural materials direct scientists into synthetic materials [108]. To improve the cell-substrate interactions, synthetic materials' biological properties are required to be enhanced and consequently, different surface alteration methods have been developed. Among them, plasma activation technique is a relatively simple one. According to the results of Xing et al., plasma treated and strontium-doped phosphate coated titanium promoted osteogenic differentiation of bone marrow derived stem cells [109]. Furthermore, modification of substrate surfaces with functional groups, like -NH_2 and -OH are found to result osteogenic induction of MC3T3-E1 cells [110]. Similarly, differentiation of MSCs into osteoblasts were promoted by -NH_2 and -SH functional groups modified surfaces [83].

2.3.2 Cardiomyocytes

The heart is a highly organized tissue, which supports blood circulation through the body with rhythmic contractions. Rhythmic contractions in myocardium are controlled by generation of organized electrical stimuli. Heart is composed of cardiomyocytes, pace maker cells, Purkinje cells, vasculature and connective tissue [111].

Heart failure is a worldwide progressive disorder, which can be initiated from myocardial infarction (MI), sustained hypertension, severe arrhythmia, viral infection or a genetic disease. Among these, myocardial infarction, which generally resulted from coronary artery occlusion and ischemia, is clearly the major cause of death in the world. MI and other causes of heart failure are associated with the gradual decrease of cardiomyocytes [111]. Nowadays, cardiac transplantation is the only treatment for the patients with cardiomyocyte loss-related diseases [112]. Hence, recent cell therapy

approaches could influence the fate determination of cardiac stem cells and induce cardiac regeneration. To do that various cell sources, such as stem cells, progenitor cells, isolated autologous or allogenic cells, have been used with different cell substrate designs. Among them, iPSCs have been promising cell sources, due to their ethical relevance, patient and/or disease specific applicability and most importantly, their differentiation capacity into many cell types [113]. In the earliest research on IPSCs, adult mouse fibroblasts were introduced with the genes encoding transcription factors, called Oct3/4, Sox2, Klf4 and c-Myc by retroviruses (Figure 2.8). The transcription factors Oct3 and Sox2 are responsible from the pluripotency preservation whereas Klf4 and c-Myc enables Oct4 and Sox2 to connect the target by changing the chromatin structure [10].

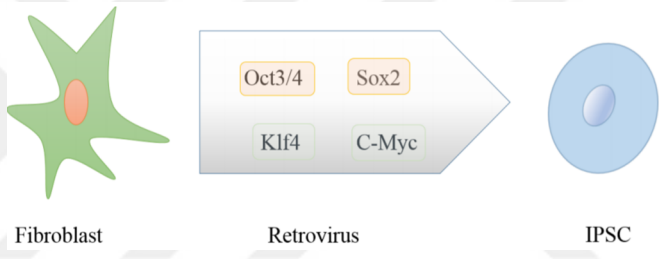

Figure 2.8 Generation of IPSCs from fibroblast cells [10].

Several studies related to myocardium show the sensitivity of stem cells to matrix stiffness, as discussed in the previous parts. For example, Breitbach et al. demonstrate this effect by mesenchymal stem cell (MSC) injection into a fibrotic scar, which is formed following a myocardial infarction. As this scar is a relatively hard tissue ($\approx$ 35-70 kPa [47]) it directs MSCs towards myocardial calcifications [48]. Furthermore, embryonic cardiomyocytes plated onto stiff (34 kPa) polyacrylamide gels (mimicking a post-infarct scar) or very soft (1 kPa) gels either stopped beating shortly after being plated or decreased in beating frequency, whereas an optimal elasticity facilitated a maximum cardiac work resulting from a cell-matrix strain match [49].

Xie et al., designed a study by using different pre-polymer cross-linker concentrations of PDMS, varying from 5:1 (1 MPa) to 45:1 (46 kPa) and investigated the influence of elasticity on myocardial cells and cardiac fibroblasts [114]. In a microflu-

idics study by Fu et al., PDMS-based biochips were fabricated for cardiac differentiation and ESC pluripotency maintenance. Optimum parameters for fabrication were investigated using 5:1, 10:1, 20:1 and 40:1 pre-polymer cross-linker ratios of PDMS substrates modified with polydopamine in combination with gelatin coating. Their results showed an enhanced ESC behavior and cardiac differentiation due to the surface chemical alteration. Additionally, they investigated the optimal stiffness for cardiac differentiation, which was determined as a ratio of 40:1 among all other formulations [115]. In another study by the same group, identical pre-polymer cross-linker concentrations of PDMS were used with iPSCs and they reported that 40:1 PDMS was the best for the cardiac differentiation of iPSCs, similar to their previous study with ESC [19]. Moreover, a PDMS formulation with a lower cross-linker amount, 60:1 was found to increase the cardiomyogenic differentiation of adult cardiac side population progenitor cells, whereas 30:1 PDMS, which was given as fibrotic myocardium, resulted in an increased proliferation capacity of the same type of cells [116].

2.3.3 Corneal Endothelial Cells

Corneal endothelial cells (CECs) are polygonal-shaped cells and forming monolayer on the posterior surface of the cornea. These cells are specialized for the active pumping of fluids across the cornea to retain its transparency [117]. In young adults, CEC density is $\approx$ 3000-3500 cells/mm^2, whereas this number decreases throughout lifetime due to the mitotically inactive nature of CECs [118, 119]. Trauma, aging, diseases and intraocular surgical procedures accelerate the decay of CEC density. When cell density drops below a critical level ($\approx$ 500 cells/mm^2), endothelial dysfunction occurs, causing the cornea to lose its optical clarity which leads to impaired vision and subsequently to blindness [51, 120]. Currently, corneal transplantation or corneal grafts, including full-thickness and selective endothelial keratoplasty are the only treatments for restoring corneal endothelium function [121]. Although these methods are successful, immune reaction and rejection of tissues, in addition to worldwide shortage of transplantable donor corneas hinder their wide-use [122]. Thus, there is a high demand for alternative therapies to repair, replace or regenerate corneal endothelium to

overcome CEC loss related visual impairment.

Recent studies on cell-based therapy have provided new opportunities to corneal endothelium replacement by using cell transplantation following an *in vitro* expansion of cells on specific biomaterials [123, 119, 124, 125]. However, functional expansion of CECs is still a challenge, in addition to their limited potential for *in vitro* proliferation [126, 127]. Thus, production of biomaterial platforms for the expansion of CECs in culture environment while preserving their functionalities has been a promising approach. Various natural cell substrates were developed for this purpose, including collagen/hyaluronic acid/chitosan [128], chitosan/ polycaprolactone [129, 124], cross-linked hyaluronan [130], cross-linked collagen/ gelatin/ hyaluronic acid [131] and decellularized cornea layers [132], but poor mechanical properties and high degradation rates lead to the of synthetic materials [133, 127]. On the other hand, synthetic materials lack cell binding cites and therefore they require surface modifications, prior to cell culture.

In native environment, CECs are in direct contact with underlying Descemet's membrane, which is mainly composed of Collagen type IV (COL 4) and VIII (COL 8) [134]. As the microenvironment of cells and the interaction in between them regulate cellular behavior, properties of Descemet's membrane and corneal extracellular matrix (ECM) have been considered in designing new biomaterials [51]. Palchesko et al. focused on the chemical and mechanical properties of corneal ECM and prepared polydimethylsiloxane (PDMS) substrates with Descemet's membrane-like mechanical properties. After coating with several ECM proteins, they reported that 50 kPa PDMS with COL 4 coating resulted a significant increase in CEC proliferation, in addition to improved expression of phenotypic markers [51]. Teo et al. developed various micro and nanoscale geometrical surface patterns (pillars and wells) on PDMS substrates inspired by topographical features of Descemet's membrane. Among them, the nanopillar surface topography was found to be the most suitable pattern to obtain CEC culture with typical cell shape and better functionality [135]. In a similar study, patterned tissue culture polystyrene (TCPS) was confirmed to significantly improve CEC expansion and CEC-related protein expression [126]. A more recent work described the

effect of PDMS with Descemet-like surface topography to initiate the differentiation of mesenchymal stem cells (MSC) into corneal endothelial-like cells [136]. Although these studies are inspired by the microenvironment of corneal endothelium, they focused only on one or two important parameters of ECM characteristics. However, combined effects of mechanical, topographical and biochemical properties of cell microenvironment regulate cell behavior *in vivo* and, thus, a holistic approach is required when designing cell substrates to obtain desired *in vitro* cell response [58].

3. CELL SUBSTRATE DESIGN FOR IMPROVED OSTEOBLAST BEHAVIOR

3.1 Synthesis and Characterization of Amino Acid Conjugated SAMs

His-SAM and Leu-SAM synthesis procedure is based on the activation of carboxylic acid groups (-COOH) of carboxybenzyl (Cbz)-protected L-His-OH and L-Leu-OH using benzotriazole chemistry [137, 138]. The intermediate products Cbz-L-Leu-Bt and Cbz-L-His-Bt were subsequently reacted with (3-aminopropyl)triethoxysilane (APTES) in tetrahydrofuran (THF) in the presence of Et3N as a base to synthesize Cbz-L-Leu-SAM and Cbz-L-His-SAM, respectively. These intermediates were deprotected under catalytic hydrogenation to give final products L-Leu-SAM and L-His-SAM (Figure 3.1). ^{1}H NMR. (Bruker, 500 MHz) was used for the characterization of His-SAM and Leu-SAM.

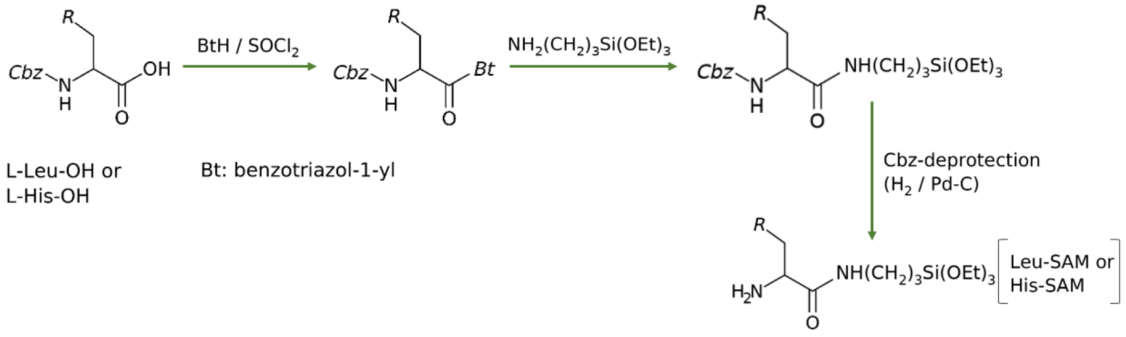

Figure 3.1 The synthesis procedure of His-SAM and Leu-SAM.

pH responsibility of His-SAM was investigated via zeta potential analysis and cationic methylene blue (MB) - anionic eosin y disodium salt (EY) adsorption at different pH conditions (pH = 5.0, 7.4 and 9.0). His-SAM functionalized silica nanoparticles (SNPs, kindly supplied from Dr. Bengi Ozgun Ozturk, Hacettepe University, Ankara,

Turkey) with an average size of 50-60 nm were used in the zeta potential measurements. For this purpose, 20 mg SNPs were added to 1 mL of SAMs solutions in absolute ethanol (10 mM) and surface modification was carried out overnight with continuous stirring. Subsequently, functionalized SNPs were washed thoroughly with ethanol (3 x 1 mL) and DI water (3 x 1 mL) while SNPs were centrifuged at 15,000 rpm and dispersed in the next washing solvent at each step. The pH dependent surface charges of SNPs were determined via zeta potential analyzer (Malvern Instruments, Zetasizer Nano ZSP) at pH= 5.0, 7.4 and 9.0.

The adsorption of MB (A4084, AppliChem) and EY (E4382, Sigma-Aldrich) was evaluated by dipping His-SAM modified PDMS into 5 mg/L aqueous solution of these dyes at various pH [139]. After 24 h, supernatant solutions were collected and measured by using a spectrophotometer (BIO-RAD iMark) to calculate the adsorption capacity and relative surface charge of His-SAM modified PDMS [140, 141].

3.2 Preparation and Characterization of PDMS Substrates

PDMS substrates were prepared by mixing 10:1 (w/w) ratio of prepolymer and curing agent (Sylgard 184, Dow Corning), followed by degassing under vacuum for 30 min. PDMS mixture was then spin-coated onto glass coverslips (18 mm diameter) at 2000 rpm for 5 s (CEE 200X, Brewer Science) to obtain thin and flat substrates. Curing was performed at 60°C for 24 h [142]. After the curing process, substrates were sonicated for 10 min in absolute ethanol and distilled water, respectively, and dried under N_2 stream.

Prior to modification with His-SAM and Leu-SAM, PDMS substrates were exposed to oxygen plasma for 1 min, at 200 mTorr and under 50 sccm oxygen flow (PM-100, March Plasma Systems) to produce reactive hydroxyl groups on surfaces without any alteration on the surface topography [143]. Surface modification conditions were optimized by using His-SAM as a model. Activated PDMS substrates were immersed into His-SAM in ethanol, having different concentrations in the range of 1-20

mM at room temperature for two hours, followed by using a fixed concentration and varying dipping time in the range of 1-24 h. Leu-SAM modification was performed under optimized conditions. Following the functionalization, solutions were removed, and substrates were rinsed with absolute ethanol and distilled water three times. SAM modification procedure of PDMS was schematized in Figure 3.2.

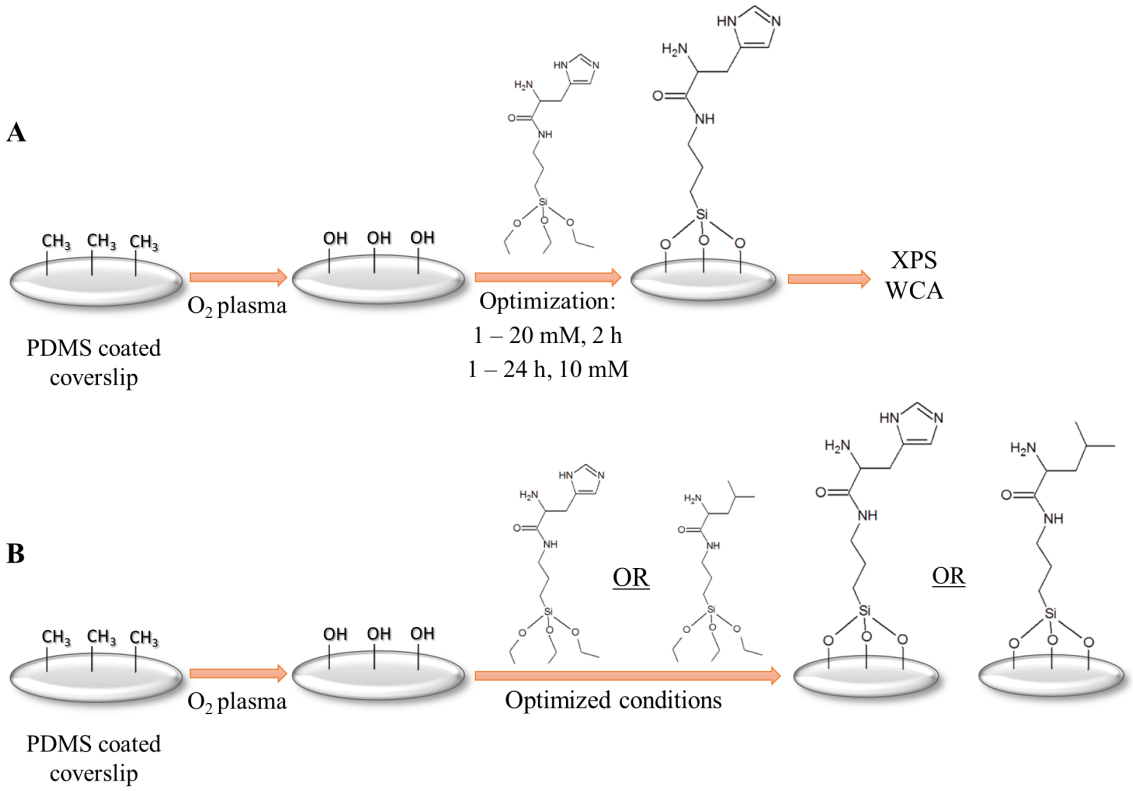

Figure 3.2 Schematic illustration of PDMS modification. (A) Optimization of His-SAM modification (1-20 mM, 2h and 10 mM, 1-24h), and (B) modification of PDMS surface with His-SAM or Leu-SAM (10 mM, 24h).

Surfaces of PDMS substrates were characterized in terms of functionality and wettability with XPS and WCA, respectively. Modification of PDMS substrates with His-SAM and Leu-SAM was verified chemically by using and XPS with Al-Kα source gun (Thermo Scientific). Wide scans were recorded in the binding energy range of 1350-0 eV with 150 eV pass energy. Wettability of surfaces before and after modifications was investigated by using sessile drop water contact angle analysis (CAM-100, KSV Instruments). Measurements were carried out at room temperature by introducing 2

μL of distilled water droplets to the surfaces while recording the images for 10 s. For each experimental group, three random areas of five samples were measured.

The stability of PDMS surface modification through SAMs was evaluated under constant flow. His-SAM was selected as a model for this purpose and surfaces of Quartz Crystal Microbalance (QCM, QCM200, Stanford Research Systems) sensor crystals (Maxtek) were coated with PDMS, as shown in Figure 3.3(a), and modified with His-SAM by using the optimized procedure (10 mM His-SAM concentration and 24 h dipping time).

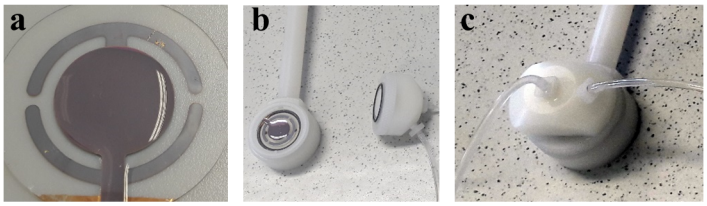

Figure 3.3 (a) PDMS coated QCM sensor crystal (b) in the flow cell of QCM unit (c) and closed system of flow cell.

The flow cell part of QCM [Figure 3.3 (b and c)] was used to apply a constant 2 mL/min DI H_2O flow for 0.5 or 4 h through His-SAM modified PDMS with a tubing system and a peristaltic pump (Watson-Marlow Sci-Q 300, Fisher Scientific). Surface chemical functionality and wettability properties of His-SAM modified PDMS were investigated before and after flow application by using the same steps given above with XPS and WCA analysis, respectively.

3.3 *In vitro* Human Osteoblastic Cell Culture

Human fetal osteoblast cells (hFOB 1.19, ATCC CRL-11372) were used to investigate the effects of PDMS substrates with different surface chemistries. Cells were maintained and expanded in DMEM/F-12 (Sigma), supplemented with 10% fetal bovine serum (FBS, Biosera) and 1% antibiotic antimycotic solution (Biosera). The medium was changed every two days. When cells reached confluence, 0.25% trypsin-EDTA solution (Sigma) was used to harvest them. Cells at passage number 5 were

used. For the cell culture studies, PDMS substrates were rinsed with 70% ethanol and sterile phosphate buffered saline (PBS), followed by exposure to UV light for 1 h. Then, cells were cultured on PDMS substrates in non-treated 12-well cell culture plates (SPL Life Sciences) with a seeding density of 50,000 cells/well. Cells were incubated in a humidified incubator at 37°C with 5% CO_2 up to 21 days.

3.3.1 Cell Proliferation Assay

The proliferation of osteoblast cells on PDMS substrates was assessed by Alamar Blue assay for up to 7 days. At specific time points, culture media was replaced with the fresh one containing 10% Alamar blue and incubated at 37°C for 4 h. Then, optical absorbance values were measured at 570 and 595 nm by using a Micro-Plate Reader Spectrophotometer (BIO-RAD iMark) [144].

3.3.2 Morphological Staining

The actin cytoskeleton of the cells on PDMS substrates, was explored using Alexa Fluor 488 Phalloidin (Thermo Fisher) staining at the end of day 7. Briefly, cells were rinsed twice with PBS and fixed in 4% formaldehyde solution for 10 min, followed by rinsing with PBS three times for 5 min. To increase permeability, cells were immersed immediately in 0.1% Triton X-100 in PBS for 5 min. Nonspecific bindings were blocked with 1% bovine serum albumin (BSA) solution for 20 min. After the blocking step, Alexa Fluor 488 Phalloidin solution (in 1% BSA) was added to the cells. A counter-staining with DAPI was also performed to stain cell nuclei by incubating cells in DAPI staining solution (Thermo Fisher) for 3 min. Images were recorded under the fluorescence of excitation at 488 nm for f-actin cytoskeleton (green) and 358 nm for cell nuclei (blue) by using a fluorescence microscope (DM IL, Leica) [145].

3.3.3 Alkaline Phosphatase Activity Investigation

Intracellular ALP activity of osteoblasts was investigated by using Alkaline Phosphatase Activity Colorimetric Assay Kit (Biovision Research Products) according to the manufacturer's instructions. After days 3, 7, and 14 of incubation, cells were rinsed with PBS and immediately frost at -80°C. Following two freeze-thaw cycles, the cell suspension was centrifuged at 13,000 rpm for 10 min to remove supernatant. Then, cells were resuspended with assay buffer of the kit, and 5 mM p-nitrophenyl phosphate was added to each sample. After incubation for 60 min. at dark, stop solution was added to terminate ALP activity, and the absorbance values were recorded at 405 nm and calculated according to the standard curve by using the ALP enzyme of the assay kit.

3.3.4 Mineralization Staining

To observe the characteristic calcium deposition, a well-known alizarin red staining protocol was performed. In a typical staining, cells at days 7, 14, and 21 were washed with PBS and fixed in 4% formaldehyde solution for 10 min. Then cells were rinsed with PBS and distilled water, followed by incubation in 2% alizarin red solution (pH 4.2) for 20 min. Cells were rinsed with distilled water, and images were taken via optical microscopy [146].

3.4 Statistical Analysis

All of the results were reported as the mean ± standard deviation. Statistical differences between experimental groups were calculated by using one-way analysis of variance (ANOVA) followed by Tukey test. $p < 0.05$ was considered as being statistically significant.

3.5 Results

3.5.1 Characterization of Amino Acid Conjugated SAMs

^{1}H NMR data of the molecules are identical to our previous results [137]. In ^{1}H NMR data, recorded two doublet signals at around 8.25 ppm and two triplet signals around 7.60-7.80 ppm for Cbz-L-Leu-Bt and Cbz-L-His-Bt are characteristic signals for N-acylbenzotriazoles. These signals support the presence of benzotriazole in structure. After the reaction of APTES with benzotriazole-functionalized intermediates, benzotriazole signals were disappeared. Thus, one can conclude that benzotriazole was substituted with the amino groups. Amide signal for Cbz-L-Leu-SAM was recorded at 7.24 ppm and 6.80 ppm for Cbz-L-His-SAM, respectively. On the other hand, characteristic methylene (-CH_2-) singlet signal recorded at around 5.10 ppm supports the presence of Cbz-protecting group. Another characteristic signal is methylene (-CH_2-) signal, which is bonded to silicon atom in APTES. This signal is generally recorded at around 0.50-0.60 ppm because of Si-C bonding. Finally, after deprotection of Cbz-group characteristic multiplet signal at around 7.30-7.40 ppm and singlet signal around 5.00 ppm for Cbz-moiety were disappeared. Additionally, broad signal around 4.20 ppm supports presence of free -NH_2 group of amino acids.

^{1} NMR for L-His-SAM ($CDCl_3$ with 0.05% v/v TMS, 500 MHz,): δ 10.15 (broad, s, 1H, N**H** imidazole), 7.50 (s, 1H, Ar-**H** imidazole), 6.92 (s, 1H, Ar-**H** imidazole), 6.79 (s, 1H, amide N**H**), 4.55-4.43 (m, 1H, -C**H**-NH_2), 4.23 (broad, s, 2H, -N$\mathbf{H_2}$**)**, 3.83 (q, J= 6.90 Hz, 6H, OC$\mathbf{H_2}$**)**CH_3), 3.32-3.21 (m, 2H, -CONH-C$\mathbf{H_2}$**)**-), 3.12 (broad, s, 1H, CH-C$\mathbf{H_2}$**)**-imidazole), 2.98 (dd, J= 14,16, 5.00 Hz, 1H, CH-C$\mathbf{H_2}$**)**-imidazole), 1.62-1.44 (m, 2H, -CH2-C$\mathbf{H_2}$**)**-CH2-), 1.25 (t, J= 8.27 Hz, 9H, OCH2C$\mathbf{H_3}$**)**), 0.51-0.40 [m, 2H, -C$\mathbf{H_2}$**)**-Si(OEt_3)] ppm.

^{1} NMR for L-Leu-SAM ($CDCl_3$ with 0.05% v/v TMS, 500 MHz,): δ 7.24 (s, 1H, amide N**H**-), 4.25 (broad, s, 2H, -N$\mathbf{H_2}$**)**), 4.15 (dd, J= 8.29, 4.88 Hz, 1H, –C**H**-NH_2), 3.85 (q, J= 6.98 Hz, 6H, OC$\mathbf{H_2}CH_3$), 3.28 (dt, J= 11.92, 6.35 Hz, 2H, -CONH-C$\mathbf{H_2}CH_2$-), 1.72-1.60 (m, 2H, -CH_2-C$\mathbf{H_2}$-CH_2-), 1.55 (p, J= 8.40 Hz, 2H, -CH2-C$\mathbf{H_2}$-

CH_2-), 1.23 (t, J= 6.98 Hz, 9H, $OCH_2C\mathbf{H_3}$)), 0.98-0.91 (m, 6H, -CH($\mathbf{CH_3}$)**2**), 0.63 [t, J= 8.00 Hz, 2H, -$C\mathbf{H_2}$-Si(OEt_3)] ppm.

pH responsibility of SAMs from His-SAM was investigated via zeta potential measurements and cationic methylene blue (MB) - anionic eosin y disodium salt (EY) adsorption study at different pH values (pH = 5.0, 7.4 and 9.0). Zeta potential measurements of His-SAM functionalized silica nanoparticles (SNPs) are given in Figure 3.4. The zeta potential of SNPs at pH = 5.0 showed slightly positive charge, where His-SAM functionalization resulted strongly cationic SNP surfaces with an average zeta potential value of +37.9 ± 1.1 mV. Similarly, surface charge of anionic SNP with an average zeta potential of -27.6 ± 0.9 mV at pH = 7.4 was altered after His-SAM incorporation, which was found to be approximately neutral/slightly positive with an average zeta potential of +8.6 ± 0.6 mV. SNPs at pH = 9.0 have the most strongly anionic surface charge among all others and yet SNPs modified with His-SAM resulted approximately neutral/slightly negatively charged particles.

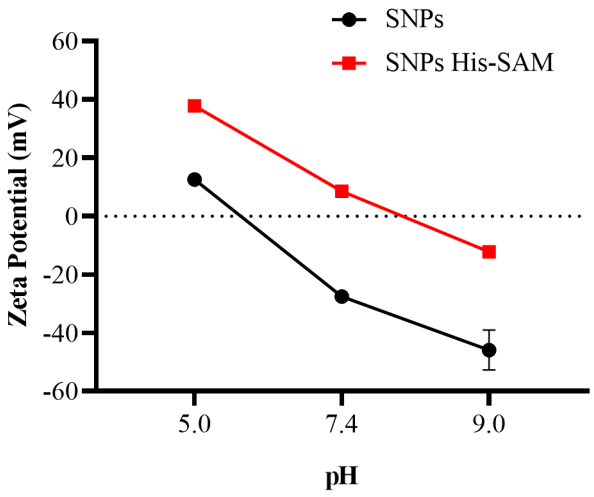

Figure 3.4 Surface zeta potentials (surface charges) of SNPs and His-SAM functionalized SNPs at pH = 5.0, 7.4 and 9.0.

3.5.2 Characterization of Modified PDMS Substrates

Characterization of surface chemistry was performed by XPS analysis and WCA measurements. Oxygen plasma treatment was used to activate PDMS surfaces. Fol-

lowing this treatment, substrates were modified with increasing concentrations (1-20 mM) of His-SAM for 2 h to investigate the optimum conditions for the SAM formation. PDMS is a synthetic polymer, which is made up of silicon, carbon, oxygen, and hydrogen atoms. Thus, modification of PDMS with His-SAM results in the presence of specific N1s signal in XPS spectra. Figure 3.5 (a) shows the high-resolution N1s core level overlay of PDMS substrates modified with increasing concentrations of His-SAM. From 1-5 mM His-SAM, the amount of nitrogen on substrate surface increases with increasing concentration, except for 10 mM, which provides the highest nitrogen content, and thereby the highest His-SAM coating of the surface. The decrease of N from 10-20 mM proves the maximum surface coverage was achieved with 10 mM and increasing the concentration caused the steric hindrance of imidazole rings. WCA measurements of His-SAM modified PDMS also prove the presence of hydrophilic histidine on surfaces and exhibit a decreasing trend with increasing concentration [Figure 3.5 (b)]. No statistical differences were found between WCAs of 10 mM and 20 mM His-SAM modified PDMS.

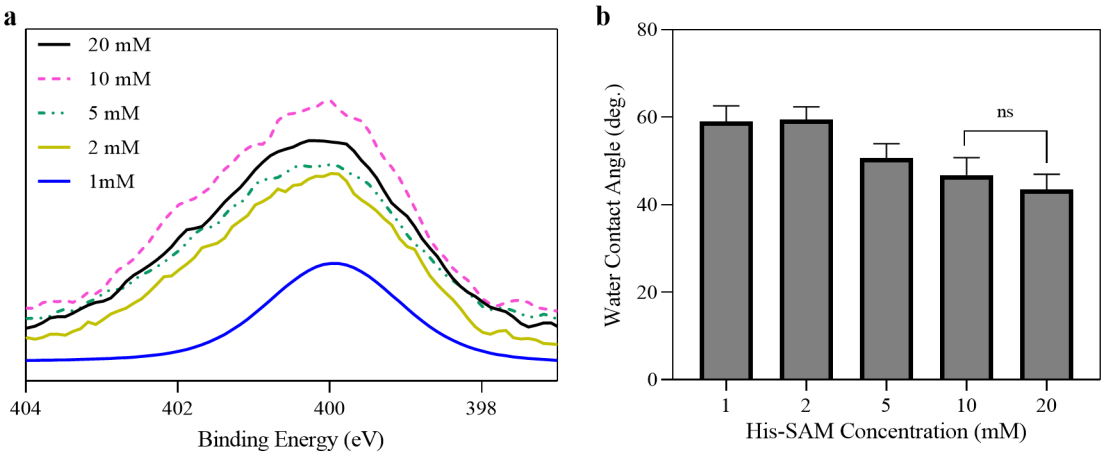

Figure 3.5 (a) High-resolution N1s spectra and (b) WCA measurements of PDMS modified with increasing concentrations (1-20 mM) of His-SAM.

For the optimum dipping time investigation, 10 mM His-SAM solution was used to modify substrates with varying incubation ranges and XPS detection of N1s shows that extended incubation period increased the amount of N atoms on the surface. Among them, 24 h modification results in the highest nitrogen peak [Figure 3.6 (a)].

WCAs of His-SAM modified PDMS were given in Figure 3.6 (b) according to the dipping time during functionalization. As shown in the figure, no statistical differences were found between WCAs, revealing that increasing the dipping time does not affect the wettability properties of His-SAM modified PDMS.

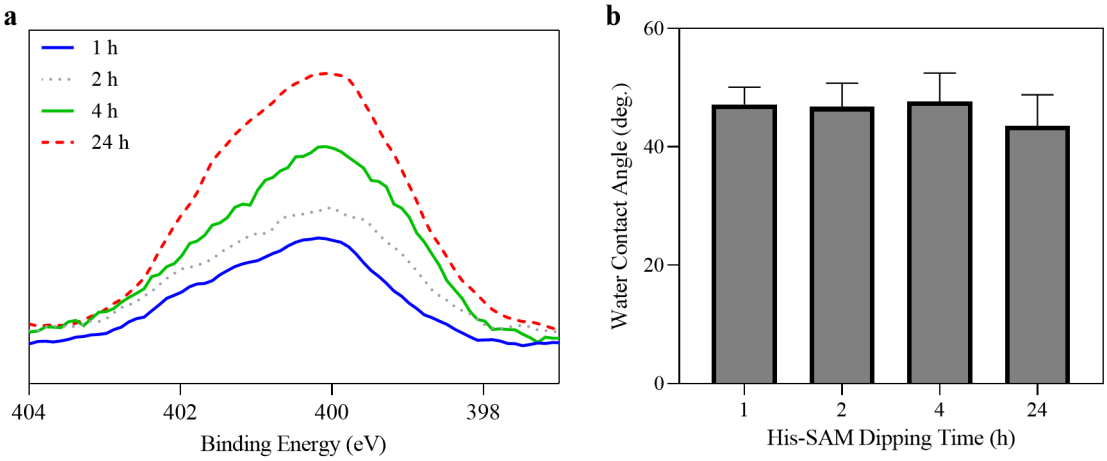

Figure 3.6 (a) High-resolution N1s spectra and (b) WCA measurements for His-SAM modification of PDMS with increasing dipping time (1-24 h).

From the high resolution XPS analysis and WCA measurements, 10 mM concentration and 24 h dipping time conditions are considered to be the optimum modification parameters for His-SAM. These parameters were also applied to Leu-SAM modification and all experiments were performed accordingly. Figure 3.7 (a) indicates the survey spectra of native and SAMs modified PDMS. Binding energies corresponding to O1s, C1s, Si2s, and Si2p PDMS-specific peaks at 532.8, 285.1, 154.0, and 102.7 eV were detected in all samples [147]. Besides, peaks at 401.1 eV appeared after Leu-SAM and His-SAM modifications, which were assigned to N1s core line. Observation of these peaks in both modified substrate surfaces was a certain indication for the presence of the molecules on PDMS substrates. When compared between modified surfaces, the increase of N1s peak in His-SAM modified PDMS showed relatively higher surface nitrogen content of the surface, due to the extra nitrogen atoms in the imidazole ring of the molecule.

Water contact angles (WCA) of hydrophilic and hydrophobic amino acid conju-

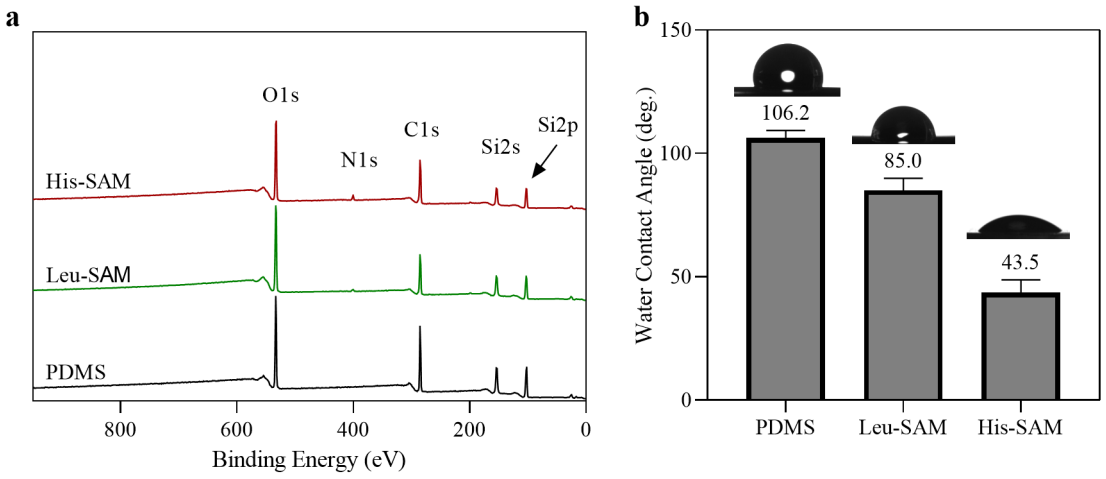

Figure 3.7 (a) XPS wide scan spectra and (b) WCA measurements of native, Leu-SAM modified, and His-SAM modified PDMS substrates.

gated SAMs modified PDMS substrate surfaces were utilized to confirm the alterations in surface wettability, as shown in Figure 3.7 (b). WCA of native PDMS was found in the hydrophobic region, which was measured to be 106.2±3.1°. After oxygen plasma treatment for 1 min, WCA was measured below 14°, showing the presence of Si-OH bonds. These bonds facilitated amino acid conjugated SAM modification of PDMS surfaces. After incorporation of Leu-SAM and His-SAM, very low WCA of plasma oxygenated PDMS was increased to 85.0±4.9° and 43.5±5.3°, creating hydrophobic and hydrophilic surfaces, respectively.

Table 3.1
Surface elemental composition of native and SAMs modified PDMS substrates.

	Theoretical %				Measured %			
Substrates	Si	C	N	O	Si	C	N	O
PDMS	25.00	50.00	-	25.00	29.99	43.18	-	26.83
Leu-SAM	21.05	47.37	10.53	21.05	27.90	37.59	1.35	33.16
His-SAM	19.00	43.00	19.00	19.00	24.00	42.20	2.96	30.72

The quantitative elemental composition of native and modified substrates was

summarized in Table 3.1. Compared to native PDMS, modification with Leu-SAM and His-SAM resulted in increased O% and N% with a concomitant decrease in Si%. Treatment with oxygen plasma prior to modification was responsible for the increase in oxygen content in both functionalized groups. The presence of N atom is an indication of SAMs modification, and the relation between theoretical and measured atomic percentages of N provides information about the surface coverage. In Leu-SAM group, the atomic percentage of N was expected to be 10.53% if the surface was fully covered, whereas XPS analysis shows that the surface N content was only 1.35%. Thus, approximately 13% of the surface is covered with Leu-SAM. Similarly, stoichiometric and measured values of N% in His-SAM modified PDMS are 19% and 2.96%, respectively, giving a surface density of 16%. Further investigation in pH responsibility of SAMs from His-SAM was also done on His-SAM modified PDMS via cationic methylene blue (MB) - anionic eosin y disodium salt (EY) adsorption study at different pH values (pH = 5.0, 7.4 and 9.0). Figure 3.8 shows the amount of MB and EY dyes adsorbed (Q, μg) on His-SAM modified PDMS. At pH = 5.0, His-SAM modified PDMS showed the weakest adsorption for cationic MB, due the repulsive forces between dye cations and positively charged His-SAM molecules on the PDMS surface; where a slight decrease in the positive charge was expressed at pH = 7.4, and at pH = 9.0 the highest adsorption capacity was obtained (due to the increased number of negative charges on His-SAM modified PDMS surface). Furthermore, the anionic EY dye adsorption study also confirmed the positively charged His-SAM molecules on the PDMS surface via electrostatic interactions.

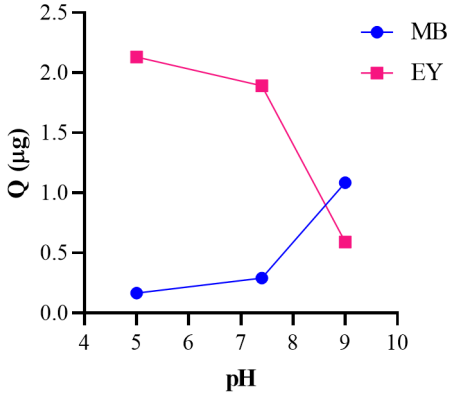

Figure 3.8 MB and EY dye adsorption capacity of His-SAM modified PDMS at various pHs.

The stability of SAMs modification was confirmed under constant flow regime for different time duration via XPS analyses and WCA measurements. Figure 3.9 (a) shows the XPS survey spectra of His-SAM modified PDMS surfaces under flow for 0.5 and 4 h with a control group. All His-SAM modified PDMS-related peaks corresponding to O1s, N1s, C1s, Si2s and Si2p were detected in all groups with no significant differences between the signal intensities. The standard deviation between measured N atomic percentages of His-SAM modified PDMS before or after constant flow was calculated as ±0.08%. Furthermore, similar atomic percentages of N atom in all experimental groups were a direct evidence for stable His-SAM modification, regardless of applied flow for different duration. Supporting the XPS analyses, WCA measurements of His-SAM modified PDMS surfaces [Figure 3.9 (b)] shows no statistically significant differences according to applied flow.

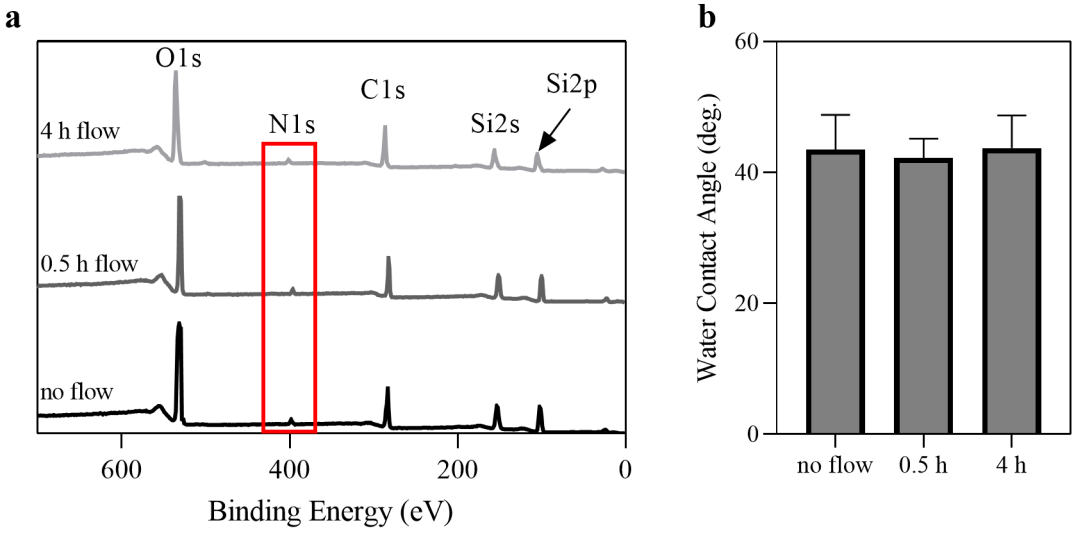

Figure 3.9 Stability of His-SAM modification under 2 mL/min flow for 0.5 and 4 h. (a) XPS wide scan spectra showing the specific O1s, N1s, C1s, Si2s and Si2p peaks of His-SAM modified PDMS before and after continuous flow. (b) WCAs of His-SAM modified PDMS before and after exposure to flow (No significant differences were observed between groups).

3.5.3 Osteoblastic Behavior on PDMS Substrates

Cytocompatibility and proliferation of amino acid conjugated SAMs modification on PDMS substrates were evaluated by *in vitro* hFOB cell culture. Cells were

cultured on native and modified substrates and incubated for 7 days. On days 1, 3, and 7 of cell culture, the metabolic activity of the cells was determined using Alamar Blue assay, which provides repeated investigation of the same samples. Figure 3.10 shows the reduced Alamar blue percentages relative to the cell proliferation on amino acid conjugated SAMs modified PDMS, native PDMS, and Tissue Culture Polystyrene (TCP), as a positive control. The increase in the reduced Alamar Blue percentage indicates the proliferation of cells on substrates. According to the results, cells in all experimental groups were remained viable and also in a tendency of growth in time, confirming the non-toxic nature of PDMS. Furthermore, cells on His-SAM modified PDMS affects proliferation in a similar way to TCP. For the whole culture period, both Leu-SAM and His-SAM modification improved the metabolic activity of cells significantly, when compared with the native PDMS.

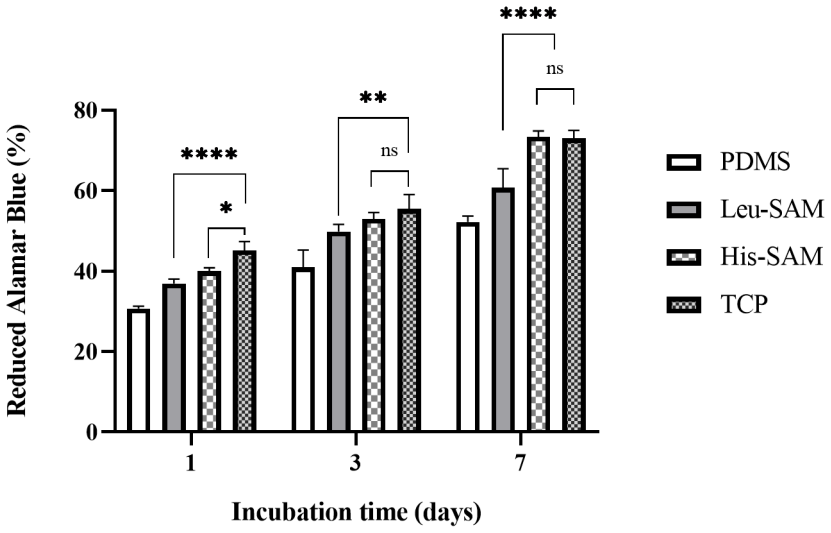

Figure 3.10 Reduced Alamar Blue percentages showing the relative hFOB cell proliferation on native, Leu-SAM, and His-SAM modified PDMS with positive control of TCP over 7 days. Data were given as means ± SD and n = 7. All groups were statistically significant respect to native PDMS, each day (****p < 0.0001; except for Leu-SAM on Day 1, ***p < 0.001), *p < 0.05, **p = 0.01.

Actin cytoskeleton organization of hFOB cells on PDMS substrates was investigated to show cellular morphology by dual fluorescent staining of Alexa Fluor 488-phalloidin and DAPI, 7 days post-seeding. As shown in Figure 3.11, modification of PDMS surface with both SAMs resulted in enhanced interactions. Only a few adhered cells were observed on native PDMS substrates as well as cells exhibiting poorly developed actin stress fibers, which might associate to the hydrophobic nature of the

material [148]. The aggregate formation was occurred as a reason for decreased cell attachment, supporting the low number of living cells found in Alamar blue assay.

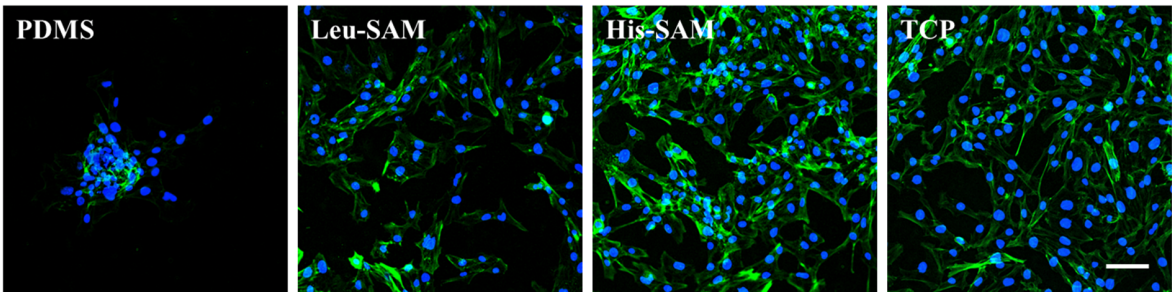

Figure 3.11 Fluorescence images of Alexa Fluor 488-phalloidin (green) and DAPI (blue) stained hFOBs on native, Leu-SAM, and His-SAM modified PDMS substrates and TCP. Scale bar = 100 μm.

Alkaline phosphatase is an early osteogenic marker which regulates bone-specific extracellular matrix mineralization [149]. hFOB cells are osteoblast precursors, and the increase in the ALP expression is an indication of a mature osteoblastic phenotype [150, 151]. Thus, osteoblastic behavior of hFOBs on PDMS substrates was investigated from the ALP activity for 14 days. As seen in Figure 3.12, ALP activity of cells on all substrates showed an ascending trend from day 3 to day 14. There was a significant increase in both SAMs modified surfaces relative to native PDMS until day 14. This trend is similar to the findings of Jones et al., where they documented the highest ALP activity of human osteoblasts on day 14 [152]. Throughout the culture period, His-SAM modified PDMS resulted in significantly higher ALP production when compared to native and Leu-SAM modified PDMS. An increase in the ALP activity was observed, especially when hydrophilic functional groups are higher on substrate surfaces [153]. Although Leu-SAM modified PDMS showed relatively hydrophobic surface properties, $-NH_2$ and $-CH_3$ functional groups of the molecule enabled enhanced osteogenic behavior when compared with native PDMS until day 14 [83]. His-SAM modified surfaces and control group, TCP, showed similar effects on cells with no significant differences until day 7, and on day 14 cells on His-SAM modified PDMS exhibited higher ALP activity than TCP ($p < 0.05$). The trend was agreed with the proliferation results and cytoskeleton organization of cells, as the increase in cell number was the highest in His-SAM and TCP groups until day 7. The increase in proliferation and accumulation of osteoblasts provokes cell maturation and accordingly ALP activity [148].

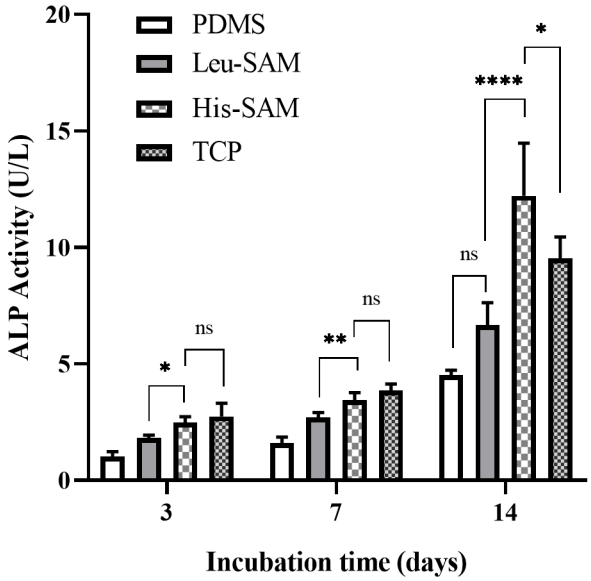

Figure 3.12 ALP activity (U/L) of hFOB cells on native, Leu-SAM and His-SAM modified PDMS with positive control of TCP at different incubation times. Data were given as means ± SD and n = 5. Statistical significance values were calculated for each day, $^{*}p < 0.05$, $^{**}p < 0.01$, and $^{****}p < 0.0001$ (All groups were statistically significant relative to native PDMS with $^{****}p < 0.0001$, each day, except for Leu-SAM on Day 3, $^{**}p < 0.01$).

Alizarin red staining is an indicator of calcium depositions in extracellular matrix [154]. Optical images of native and modified PDMS surfaces after alizarin red staining were depicted in Figure 3.13. As seen in the figure, subsequently from day 7 to 21, alizarin red staining was shown to be denser in all groups. Compatible with the ALP activity results, cell expansion and accumulation enabled them to progress into osteoblastic growth period after day 7 of culture on the substrates. After this day, ECM mineralization was accelerated [155]. The effect of surface modification on osteoblastic phenotype was supported here one more time, where on modified groups higher intensity of staining was recorded. Leu-SAM modified PDMS cells did not provide significantly increased ALP activity (relative to native PDMS) on day 14, however alizarin staining on the same day showed better osteogenic behavior than cells on native PDMS. Moreover, Leu-SAM modified PDMS leads to similar calcium deposition to TCP, thanks to its biomimetic functional groups [83]. Cells on His-SAM modified PDMS displayed a qualitatively higher amount of matrix mineralization among all groups for all time points. Especially on day 21, cells exhibited classical mineralization nodules and increased intensity of color with higher cell density. Biomineralization is

an indicator of osteogenic efficacy and bone formation [156].

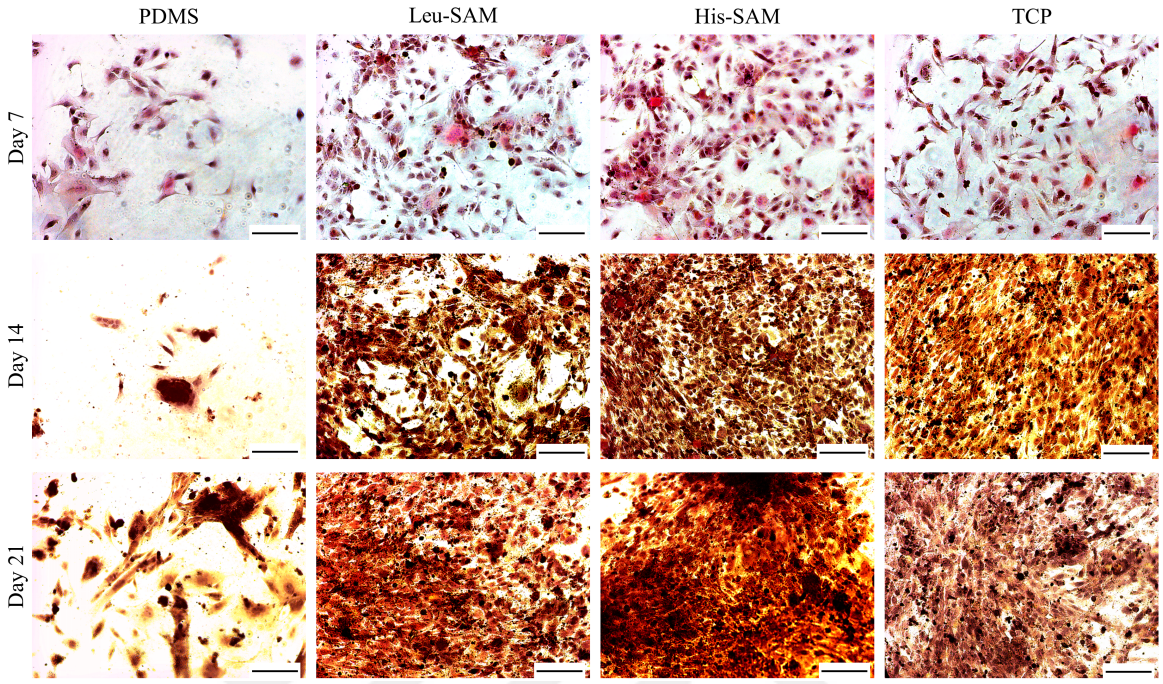

Figure 3.13 Alizarin red staining of hFOB cells on native, Leu-SAM, and His-SAM modified PDMS with positive control of TCP at different incubation times. Scale bar = 200 μm.

3.6 Discussion

In this chapter, hydrophilic and hydrophobic amino acid conjugated SAMs were prepared (Figure 3.1) and PDMS substrates modified to obtain stable, practical, and biomimetic substrate surfaces with varying wettability. By designing these amino acid incorporated SAMs, the main purpose was to enhance cell-biomaterial interactions and regulate biological signals, as extracellular matrix-like surfaces have the tendency of providing better cell culture environments. Since, essential amino acids are known to stimulate bone formation by enhancing alkaline phosphatase activity and collagen synthesis [44], human fetal osteoblastic cell line, hFOB 1.19, was chosen as a model. A recent work documented that hydrophilic hydroxyapatite/poly (amino acid) modified phosphodiester improved osteoblast adhesion, differentiation, and cranial bone formation [153].

PDMS is a biocompatible synthetic polymer and used in various applications due to its low toxicity and tunable surface properties. However, PDMS does not have any chemical cues for cell binding. Numerous techniques have been developed to improve surface characteristics of PDMS. A conventional and straightforward approach is increasing the substrate wettability by exposing to oxygen plasma [78], UV/ozone [157], or corona discharge [158]. Even though each of these treatments provides hydrophilic surfaces, long term stability cannot be achieved due to the hydrophobic recovery of PDMS [159]. This phenomenon results in an increased delamination tendency of cells from PDMS surfaces only a few days after seeding [160]. Extracellular matrix (ECM) protein coatings have also been widely used to produce cell microenvironment-like surfaces, leading to improved biocompatibility and enhanced cell behavior [30]. However, these interactions of proteins with surfaces are regulated by weak forces. As a result, cells on these surfaces tend to detach or being aggregated after they reached confluence due to protein dissociation [33, 32]. In the present part of the thesis, histidine and leucine conjugated SAMs were synthesized and characterized via 1H NMR spectroscopy. An optimized procedure was developed for the modification of PDMS substrates with these SAMs, by using His-SAM as a model (Figure 3.2). Increasing concentrations of His-SAM (1-20 mM) was prepared and PDMS surfaces were modified using these solutions for different dipping times (1-24 h). XPS results indicated that 10 mM His-SAM concentration provided the highest N content on substrates and more molecules could not bind the surface with His-SAM concentration higher than 10 mM due to the shielding effect of the accessible functional groups on the surface [Figure 3.5(a)]. WCA analysis supported the XPS results, by confirming the increased surface hydrophilicity with increased His-SAM concentration, where no significant differences were found between 10 mM and 20 mM His-SAM concentrations [Figure 3.5(b)]. After dipping time investigation, 24 h was found to be the optimum, as it XPS detection of N1s results in the highest nitrogen peak in 24 h group [Figure 3.5(a)]. Finally, 10 mM concentration and 24 h dipping time was considered as a standard and applied to both His-SAM and Leu-SAM modification of PDMS. XPS analysis was quantified as elemental compositions of native and SAMs modified PDMS in Table 3.1. The presence of N atom in both SAMs modified groups was a certain indication of successful modification and relative decreases and increases were also found in Si, C and O atoms.

When the theoretical and measured percentages of modified substrates were compared, measured percentages showed lower N%. Full surface coverage with SAMs may not be possible due to many issues: i) low surface densities (the number of activated surface functional groups), ii) the orientation of SAMs in a way to hinder accessible hydroxyl groups and iii) the repulsive forces between SAMs.

APTES modification is a well-known procedure and has been used in many applications to provide stable linkages under load or pressure; in microfluidics, introducing biomolecules for cell substrates, altering wettability properties, etc. Atomic Force Microscopy (AFM) is one of the techniques to confirm the long term APTES linkage supported stability of surface modification inside a microfluidic system under various flow rates and continuous flow at different shear stresses [161]. Specific properties of immobilized molecules (like enzymatic activity) have also used to verify APTES linkage supported stability for long term [162]. In this study, as the modification of PDMS substrates were completed through APTES based chemistry, amino acid SAMs modified surfaces are stable under flow, similar to the examples given above. PDMS surface keeps its stability under a constant and continuous flow regime at least up to 4 h (Figure 3.9), which is a critical time point for initial cell adhesion [163],and make these modifications suitable for cell culture studies.

Histidine is known as a hydrophilic amino acid with pH responsive characteristics due to its imidazole ring side chain [164]. In this study His-SAM modified PDMS demonstrated hydrophilic surfaces, as expected. The isoelectric point (pI) of histidine is 7.59, where pKa value 3N-H of the imidazole ring is pH = 6.0. Below pI, the net charge of the histidine amino acid will be positive [165]. However, in this study, histidine is conjugated to the APTES molecule‘s amino group through its carboxylic acid group. Due to the amide bond formation and loss of the acidic functional group (COOH), it is not possible to accurately calculate the pI of His-SAM molecules. Imidazole ring will be responsible for the protonation and deprotonation of the His-SAM molecule during SAM-cell interactions. pH responsibility of SAMs from His-SAM was investigated via zeta potential measurements and cationic MB - anionic EY adsorption study at different pH values (pH = 5.0, 7.4 and 9.0). Zeta potential measurements

of His-SAM functionalized SNPs are given in Figure 3.4. In the literature, it is very well-known that, nanoparticles having zeta potentials between -10 and +10 mV are regarded as approximately neutral, while nanoparticles are regarded to be strongly cationic and strongly anionic with greater zeta potentials than +30 mV or less zeta potentials than -30 mV, respectively [166]. According to the zeta potential analysis, SNPs exhibited a pH dependent trend like other nanoparticles; the more negative zeta potentials are obtained with increasing pH [167]. The zeta potential of SNPs at pH = 5.0 showed slightly positive charge, where His-SAM functionalization resulted strongly cationic SNP surfaces with an average zeta potential value of +37.9±1.1 mV. Similarly, surface charge of anionic SNP with an average zeta potential of -27.6±0.9 mV at pH = 7.4 [168] was confirmed to be altered after His-SAM incorporation, which was found to be approximately neutral/slightly positive with an average zeta potential of +8.6±0.6 mV. SNPs at pH = 9.0 have the most strongly anionic surface charge among all others and yet SNPs modified with His-SAM resulted approximately neutral/slightly negatively charged particles. To sum up, at pH 7.4, His-SAM modified SNP have shown approximately neutral/slightly positive surface charge. This finding does not fully support the positively charged His-SAM molecules at pH = 7.4. The phenomena may be explained as zeta potential analysis were conducted by using SNPs instead of PDMS surfaces and aggregation of these nanoparticles may affect the given results. Also, these findings at pH 7.4 may not represent the actual cell culture environment. In general, cell culture studies were performed at pH = 7.4, however pH of the medium could decrease to more acidic pH values due to metabolic activity of cells and possible cell debris. Under these conditions, imidazole side chain carrying unpaired electrons can bind a proton reversibly to make the molecule partially positively charged. For the clarification of this point, cationic MB and anionic EY adsorption study was also conducted to clarify zeta potential measurements by using directly His-SAM modified PDMS surfaces. Figure 3.8 shows the amount of MB and EY dyes adsorbed (Q, μg) on His-SAM modified PDMS. Here, the pH sensitivity of His-SAM modified PDMS surface's charge is clearly shown and the change in the surface charge is found to be not as sensitive to pH as histidine amino acid [164, 165]. Zeta potential measurements, together with MB - EY adsorption study confirmed the stability of positively charged His-SAM and related hydrophilic nature of His-SAM modified PDMS at physiological

pH and cell culture conditions.

hFOB cell proliferation study (Figure 3.10) indicated that cells on both hydrophilic and hydrophobic SAMs modified substrates were healthy and viable without any significant differences after day 3 of incubation, suggesting all modifications provided sufficient bioactivity. Increased cell proliferation on His-SAM can be attributed to surface hydrophilicity [169], but using a relatively hydrophobic molecule, Leu-SAM, could also have increased cellular metabolic activity for short time, due to its biomimetic nature. Besides, amino and carboxylic acid groups of Leu-SAM provide partially hydrophilic regions to these molecules, which could also be the reason for the enhanced expansion of the cells. After day 3, the number of viable cells was increased distinctively on His-SAM modified surfaces. This significant increase starting from day 3 of incubation showed that the wettability of surfaces influences cellular metabolic activity in long periods and also it confirmed the impact of hydrophilicity on improved osteoblast behavior and growth, leading to increased cellular proliferation [170]. Apart from being a hydrophilic amino acid, histidine is also one of the amino acids in FHRRIKA peptide sequence, which is a heparin-binding domain of bone sialoprotein [171]. Stile et al. documented that modification of hydrogels with this histidine-containing peptide enhanced proliferation and spreading of rat calvarial osteoblasts [172]. In another study with rat calvarial osteoblasts performed by Schuler et al., the enhanced proliferation of cells on FHRRIKA peptide-modified titanium was shown [173].

Morphological analysis of hFOBs on native and SAMs modified PDMS substrates was given in Figure 3.11 via f-actin staining. According to the analysis, hydrophobic Leu-SAM modified PDMS higher number of cells and showed better attachment than native PDMS, even though actin bundles of cells were short and disrupted. On the other hand, cells on hydrophilic His-SAM modified PDMS substrates exhibit a multilayer morphology, similar to cells on TCP, with well-defined and high number of actin fibers linking adjacent cells [174]. Toffoli et al documented similar effect of surface hydrophilicity on osteoblasts. They reported that thermally-induced hydrophilicity of titanium substrates enhanced actin cytoskeleton organization of MC3T3-E1 pre-

osteoblast cells [95]. Furthermore, a distinctive spindle-like morphology of cells was exhibited on both of His-SAM and TCP. These features may be contributed to a sign of osteogenic maturation [153]. Hence, surface hydrophilicity, in addition to different amino acid biochemistry, can impact substrate surface-osteoblast cell interaction in means of attachment and cellular extension.

Osteogenic functionality of hFOBs on PDMS substrates was examined via ALP activity and alizarin red staining. Figure 3.12 shows that cells on PDMS substrates reached confluence after day 7 and thus accumulation of cells, especially on hydrophilic His-SAM modified PDMS, promoted osteogenesis of hFOBs, confirming the effect of wettability [175] and in accordance to higher cell numbers on osteogenic differentiation [176]. Similarly, biomineralization of cells were the highest on His-SAM modified PDMS (Figure 3.13). The presence of qualitatively more calcium deposition of cells on His-SAM than other experimental groups is consistent with the other osteogenic marker, ALP activity, and proves that hFOBs on His-SAM modified PDMS differentiated enough to deposit higher amount of mineralized ECM than that of control group, TCP [149]. These ALP activity and calcium deposition overall results demonstrated the combination of a biomimetic and hydrophilic modification's superior effect on PDMS surfaces for *in vitro* osteoblast cell culture and maturation.

The results of this chapter indicated that both SAMs biointerface provided improved cell responses, relative to native PDMS and this study proved the predominant effects of biomimetic chemistry over wettability. Furthermore, hydrophilic histidine conjugated SAM modified PDMS facilitated superior osteoblastic maturation than other groups, including TCP for three weeks of culture. Moreover, cell culture studies showed that modification stability could be preserved successfully for at least three weeks. These findings will contribute greatly to the fields of biomaterial synthesis, surface modification, characterization and their relative cellular responses; and amino acid conjugated SAMs modifications of PDMS may be used in *in vitro* cell culture studies, regenerative medicine applications and as well as microfluidic systems.

4. CELL SUBSTRATE DESIGN FOR THE DIFFERENTIATION OF INDUCED PLURIPOTENT STEM CELLS INTO CARDIOMYOCYTES

4.1 Preparation and Characterization of PDMS Substrates with Healthy Myocardium-like Stiffness

PDMS substrates with wide range of stiffness were prepared to achieve the healthy myocardium-like environment. To produce cell substrates with varying stiffness, increasing pre-polymer and curing agent mass ratios (10:1, 20:1, 30:1, 50:1 and 70:1) of PDMS (Sylgard 184, Dow Corning) were combined, stirred rigorously and degassed for at least 30 min. Flat surfaces with equal substrate thickness were achieved by spin coating of these homogenous mixtures on glass slides at 2000 rpm (CEE 200X, Brewer Science). Afterwards, conventional curing method, at 70°C for 4 h [142], was applied and cellular behavior was subsequently investigated. Due to cell detachment issues 48 h post-seeding, conventional curing method was improved by increasing the curing time to 7 days while lowering the curing temperature to 60°C. After extensive curing, substrates were sonicated in absolute ethanol and DI water, respectively, for 30 min each and consecutively dried under a N_2 stream. All PDMS substrates were prepared under these conditions unless no other modification was specified.

Micromechanical properties of PDMS substrates with different pre-polymer and curing agent ratios were investigated by nanoindentation (Piuma Nanoindenter, Optics 11) in hydrated conditions. For samples with 10:1 - 30:1 ratio, using a probe with a calibrated spring constant of 13,4 N/m and a tip radius of 64 μm; for relatively sticky samples with 50:1 and 70:1 prepolymer & curing agent ratios, a probe with a spring constant of 0.51 N/m and a tip radius of 30 μm was selected. Sample size was 3 for each group and 3 spots of each sample were analyzed. The Olivier & Pharr approximation, integrated in the Piuma software, was used for the determination of Young's modulus.

4.2 Surface Chemical Modification and Characterization

PDMS surfaces were activated for 1 min by oxygen plasma treatment under 50 sccm flow of oxygen at 200 mTorr pressure before the modification with conventional or amino acid conjugated SAMs (PM, March Plasma Systems). This short treatment does not cause any cracks on the surface and provides reactive hydroxyl groups for following modifications [143]. Solutions of APTES, octadecyltrimethoxysilane (OTS), His-SAM or Leu-SAM (1% by volume in absolute ethanol) were prepared and activated PDMS substrates were immersed into these solutions at 25°C, overnight. After the modification, SAM solutions were discarded and PDMS substrates were washed extensively with absolute ethanol and DI H2O, respectively. Brief modification procedure of PDMS substrates with SAMs is shown in Figure 4.1.

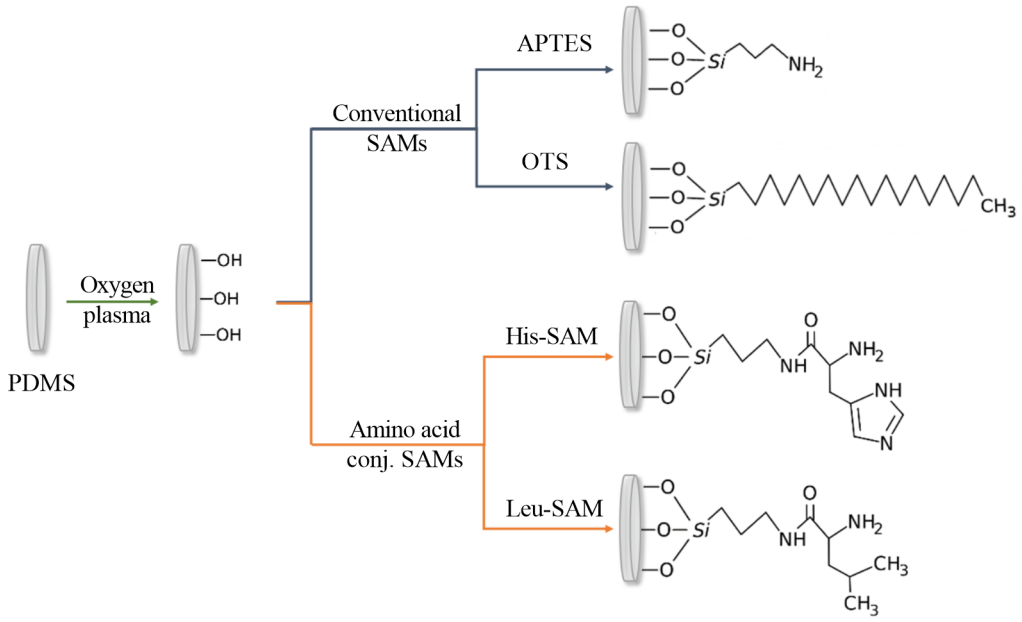

Figure 4.1 Modification procedure of PDMS substrates with conventional and amino acid conjugated SAMs.

PDMS surfaces modified with conventional and amino acid conjugated SAMs were characterized by water contact angle measurement (WCA) for wettability investigation and X-ray photoelectron spectroscopy (XPS) for the analysis of surface chemical composition.

Sessile water contact angle analysis was used to assess wettability properties of surfaces (CAM-100, KSV). Contact angle of DI water were measured at three random points of each PDMS surface.

XPS analysis was performed on K-Alpha XPS system with monochromatized Al K-Alpha source gun (Thermo Scientific). Survey spectra of PDMS surfaces were obtained at a pass energy of 150 eV, whereas high-resolution spectra were acquired at 50 eV pass energy.

4.3 Induced Pluripotent Stem Cell Culture

Murine iPSCs (clone TαP4 [177]) were cultured on gelatin coated (0.2%, aq) cell culture plates at 37°C and 5% CO_2 using a medium composed of Iscove's modified Dulbecco's medium (IMDM) with stable glutamine (Biosera) supplemented with 20% fetal bovine serum (FBS, Biosera), 1% non-essential amino acids (MEM, 100X, Biosera), 1% penicillin/streptomycin solution (100X, Biosera), 0.1 mM 2-mercaptoethanol (Thermofisher) and 1000 U/mL leukemia inhibitory factor (LIF, Orfgenetics) [178]. Cells were passaged every 2 days. PDMS coated glass slides were sterilized with ethanol (70% by volume) and sterile H_2O, followed by exposure to UV light for 1 h. iPSCs on cell culture plates were dissociated with 0.05% trypsin/ EDTA to single cells and seeded on sterilized PDMS surfaces in 12 well plates, with a density of $2x10^5$ cells/ well.

4.3.1 iPSCs Viability

Viability of iPSCs on PDMS surfaces was investigated 48 h after seeding via qualitative analysis with acridine orange (AO, Sigma) and propidium iodide (PI, Sigma) staining and quantitative analysis with (3-(4-5-dimethylthiasol-2-yl) diphenyl tetrazolium bromide) (MTT, Sigma) assay. AO stains viable cells and generates green fluorescent signal, whereas PI stains dead cells with red fluorescence. 2 μg/mL of

each solution was prepared and used to stain cells on PDMS surfaces. Images were recorded immediately after staining by using fluorescence microscopy (DMIL, Leica) [179]. Quantitative metabolic activities of iPSCs on PDMS were assessed by MTT analysis according to manufacturer's instructions. Briefly, cell culture media was refreshed and MTT assay (5 mg/mL) was added to each well [10% amount of the fresh media, v/v)]. Cells were re-incubated at 37°C for 4 h. Then, MTT solution was discarded and formed formazan crystals were dissolved in dimethyl sulfoxide (DMSO). Optical densities were recorded at 570 nm on the microplate reader (iMark, Bio-RAD). All values of experimental groups were normalized to TCP whereas five replicates were used in each group for statistical purpose.

4.3.2 Morphological Investigation

Morphology of iPSCs on PDMS was analyzed 48 h after cell culture, by using scanning electron microscopy (SEM). Cells were prepared for SEM as previously documented [180]. Briefly, surfaces were fixed with 2.% glutaraldehyde (Sigma) for 2 h, followed by dipping into increasing concentrations of ethanol (30-100% by volume) and hexamethyldisilazane (HMDS, Sigma) for dehydration. Finally, samples were sputter coated with a thin gold layer, prior to SEM imaging (XL30, Philips).

4.4 Cardiomyocyte Differentiation of iPSCs

iPSCs were grown on PDMS surfaces without LIF, and as soon as these cultures reached confluency; LIF was withdrawn and 50 μg/mL of ascorbic acid (AA, Sigma) was added to initiate cardiac differentiation [178, 181]. Cells were incubated with these induction conditions at 37°C and %5 CO_2 for the following 6 days while medium was refreshed in every 2 days. On day 7, AA addition was withdrawn whereas FBS concentration of cell culture medium was decreased to 5% and changing it every day. Differentiation on PDMS substrates was allowed up to day 12 at 37°C and %5 CO2 humidified incubator up to day 12. Herein, 0.2% gelatin coated TCPs were used as

controls.

4.4.1 Western Blot Analysis

Total protein extraction for western blotting was performed on the 12^{th} day of differentiation to evaluate the expression of cardiac markers. Cells on PDMS surfaces were scrapped and lysed in ice-cold 2X Laemmli buffer and protein concentrations were determined by using a spectrophotometer (Nanodrop 2000c, Thermo Scientific). Then, proteins were loaded to 4-10% polyacrylamide (Sigma-Aldrich) gels; resolved under 130 V (Mini Protean, Bio-RAD) and transferred (Transblot Turbo, Bio-RAD) to PVDF membranes (Millipore) [182]. After blocking for non-specific binding sites, membranes were probed with primary antibodies against anti-α-actinin (clone EA53, Sigma), anti-tropomyosin (TPM, sc-74480, Santa Cruz) and anti-cardiac troponin T (cTnT, sc-20025, Santa Cruz) at 4°C, overnight. Herein, anti-β-actin (ab8226, Abcam) was used as a loading control. Horseradish peroxidase (HRP)-labeled anti-mouse secondary antibody (ab6789, Abcam) was added on the membranes and incubated at room temperature for 1h, followed by visualization of specific bands by using 3,3',5,5'-tetramethylbenzidine chromogenic substrate (Thermo Fisher) while a quantification of bands was performed with ImageJ.

4.4.2 Immunocytochemistry

On differentiation day 12, cells were fixed in 4% paraformaldehyde (PFA, pH 7.4, Sigma) for 10 min and then permeabilized by Triton X-100 (0.1% by volume). After blocking in 1% bovine serum albumin (BSA, Biosera) supplemented with 22.52 mg/mL glycine (Sigma) for 2 h, cells were stained with monoclonal anti-cardiac troponin T antibody (cTnT, 1:100, sc-20025, Santa Cruz) at 4°C for overnight. Secondary detection was performed with anti- mouse IgG-AlexaFluor-555 (1:150, ab150106, Abcam) and nuclei were counterstained with DAPI (300 nM, Thermo Fisher). Images were recorded by using appropriate excitations filters with a fluorescence microscope

(DMIL, Leica) and fluorescence intensities were calculated with the ImageJ software.

4.4.3 Immunofluorescence Staining

For further examination with immunofluorescence staining, cells grown on PDMS surfaces were dissociated on differentiation day 12 and plated on fibronectin-coated plates. Cell culture was maintained for additional 24 h, followed by fixation and cTnT staining, as described in section 2.10. Then, actin cytoskeletons of cells were investigated with Alexa Fluor 488 Phalloidin (Thermo Fisher) solution in 1% BSA. DAPI counterstaining was performed for nuclei visualization and final staining were recorded under corresponding filters of fluorescence microscopy (DMIL, Leica). cTnT positive cell percentages and cTnT positive areas were analyzed on ImageJ software.

4.5 Statistical Analysis

All data were documented as the mean ± SD. Statistical analysis was completed on Graphpad (Prism) software by using one-way analysis of variance (ANOVA), followed by Tukey multiple comparison test. Given p values, which are lower than 0.05 were considered significant and presented as * for $p < 0.05$. Specific p values were indicated in the text.

4.6 Results

4.6.1 Nanoindentation Analysis

PDMS substrates with various stiffness values were prepared by mixing different mass ratios (10:1, 15:1, 20:1, 30:1, 50:1 and 70:1) of pre-polymer & cross-linker. Reducing PDMS's curing agent content results in an increase in the occurrence of uncured oligomers of the bulk substance. To make PDMS substrates thermodynamically more

stable, all samples were cured extensively for 7 days before experiments. Nanoindentation analysis of these extensively cured PDMS substrates are shown in Figure 4.2 and the decrease in curing agent amount resulted softer substrates with lower Young moduli (1.9 MPa-7.7 kPa for 10:1-70:1 PDMS, respectively). Each group significantly differed with any other ($p < 0.0001$). Among these various mixtures of PDMS with different micromechanical properties, the prepolymer & curing agent ratio of 50:1 has been considered to be in the range of healthy myocardium [49, 183] with a Young's modulus of 23.79±0.61 kPa and all following experiments were conducted using this ratio.

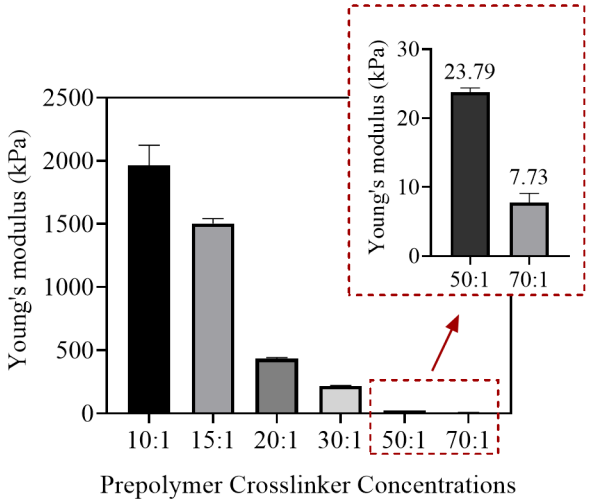

Figure 4.2 Young modulus values of PDMS with increasing pre-polymer & cross-linker ratios.

4.6.2 Characterization of Amino Acid-SAMs Modified PDMS

50:1 PDMS coated glass slides were activated and modified with conventional and amino acid conjugated SAMs. SAM modifications were confirmed by using XPS and WCA analyses.

4.6.2.1 XPS Analysis. Figure 4.3 (a) shows the survey spectra of native and modified PDMS, over the binding energy range of 0-800 eV and it clearly points out

the detected PDMS related peaks for Si2s, Si2p, C1s and O1s in all samples. In addition, presence of APTES, His-SAM and Leu-SAM specific N1s peaks on PDMS surfaces (given as PDMS-A, PDMS-H and PDMS-L, respectively) provides a primary confirmation of SAM modification.

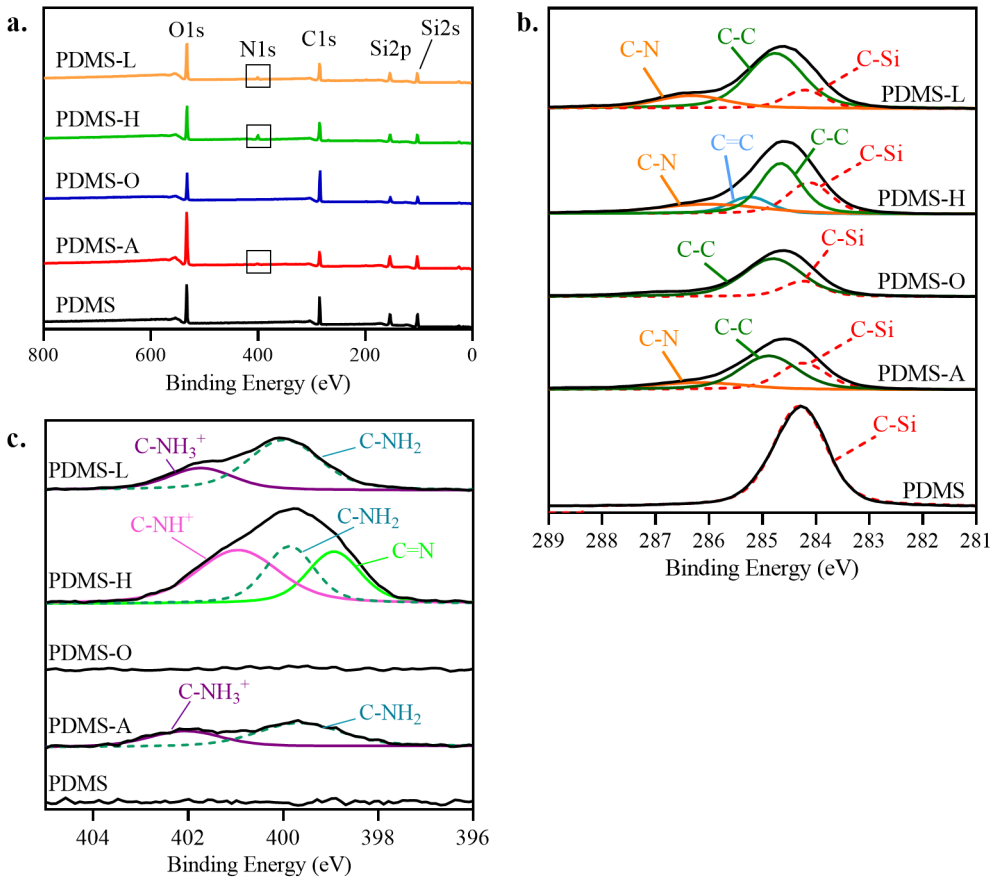

Figure 4.3 Characterization of native and SAMs modified PDMS with XPS (a) survey spectra, (b) high resolution C1s and (c) N1s spectra.

High-resolution C1s spectra of PDMS surfaces are shown in Figure 4.3 (b). Aside from the PDMS related main C-Si peak at 284.2 eV, additional photoemission peaks are present at higher binding energies for SAMs modified PDMS. The binding energy peak at 284.9 eV, for example, is found in all modified surfaces, corresponding to C-C [160] and this peak alone confirms the OTS modification (PDMS-O). For PDMS-A, PDMS-H and PDMS-L, peaks around 286.3 eV are detected and assigned to C-N [184]. The presence of these molecules on PDMS surfaces were further showed by the N1s spectrum [Figure 4.3 (c)] with peaks attributable to C-NH_2 at 399.9 eV [184, 185] and C-NH_3^+ at 401.8 eV [184, 186, 185] for both PDMS-A and PDMS-L and; to C=N at

398.9 [187], C-NH_2 at 399.9 eV [184] and C-NH^+ at 400.9 eV [187] for PDMS-H.

4.6.2.2 WCA Analysis. WCA measurements of native and SAMs modified PDMS were assessed to investigate the wettability properties. The values obtained from sessile drop method are given in Figure 4.4, and native PDMS surface was found to be in the hydrophobic region with a contact angle of 111.57°±2.32°. Oxygen plasma treatment resulted in very hydrophilic surfaces due to the insertion of hydroxyl groups. Modification of oxygen plasma treated PDMS with APTES or His-SAM provided hydrophilic surfaces with contact angles of 60.50°±1.92° (PDMS-A) and 64.26°±1.78° (PDMS-H), where PDMS-O and PDMS-L were found be hydrophobic surfaces with contact angles of 94.20°±3.24° and 88.7°±1.93°, respectively.

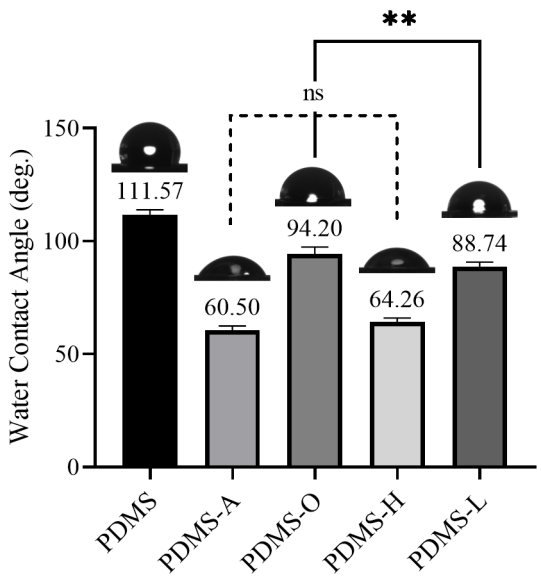

Figure 4.4 Characterization of native and SAMs modified PDMS with WCA measurements. The data are given as the mean ± SD. ****p $<$ 0.0001 for all comparisons between samples, except for **p $<$ 0.01 between PDMS-O and PDMS-L; no significant differences were found between PDMS-A and PDMS-H.

4.6.3 iPSC Response to PDMS Substrates

Both conventional SAMs and amino acid conjugated SAMs modified surfaces were used to assess iPSCs behavior to changes in surface functionality and wettability. Prior to these investigations, iPSC culture was tested on 50:1 PDMS surfaces, which

were cured using the conventional method (PDMS-conv). Cells were seeded as single cells on sterilized substrates and in the following 48 h, all cells were found to be detached from the surfaces and floating in the culture media by forming embryoid body-like structures gathering in the middle of wells [Figure 4.5(a)]. Then, curing time for 50:1 PDMS coated coverslips was extended to 7 days from 4 h and these substrates (PDMS-ext) provided better iPSC attachment, as shown in Figure 4.5(b). Cell viability on both substrates were analyzed by MTT assay, and obtained relative optical density measurements given in Figure 4.5(c) indicated the enhanced surface properties of 50:1 PDMS with increased curing time ($p < 0.0001$) for 48 h iPSC culture. Although these extended PDMS preparation conditions resulted in better cell behavior than the conventional one, iPSCs attached on the surfaces as clusters and did not spread well, revealing the need of surface modification.

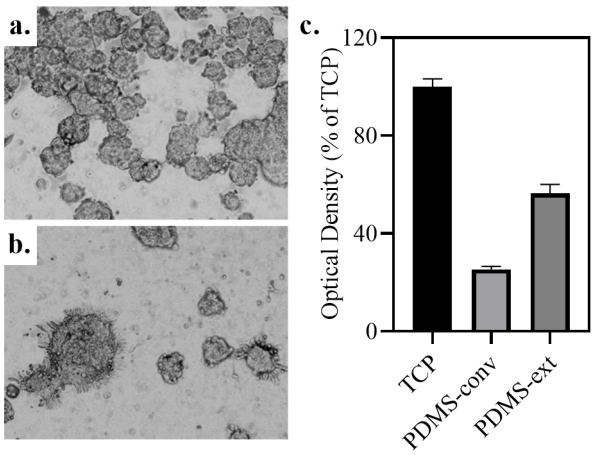

Figure 4.5 iPSC behavior 48 h after seeding on 50:1 PDMS-conv and PDMS-ext. (a) Optical microscopy images (10X) of cells on PDMS-conv and, (b) PDMS-ext. (c) Relative optical densities of iPSCs on TCP and PDMS substrates. The data are given as the mean ± SD. ****$p < 0.0001$ for all comparisons.

From this point, all PDMS substrates were prepared using 50:1 pre-polymer cross-linker ratio and cured for a week (PDMS-ext), for the whole study. iPSC behavior on native and SAMs modified surfaces were assessed for viability and attachment 48 h after cell culture. AO & PI vital staining of iPSC on PDMS surfaces shows viable (green) and dead (red) cells, and as given in Figure 4.6, only a few to none dead cells are present in each experimental group, which proves the nontoxic nature of both native and SAMs modified PDMS. In addition, iPSC number and spreading are enhanced after

each of SAM modification, in comparison to native PDMS. Among these functionalized surfaces, PDMS-L provided the highest cell covered area.

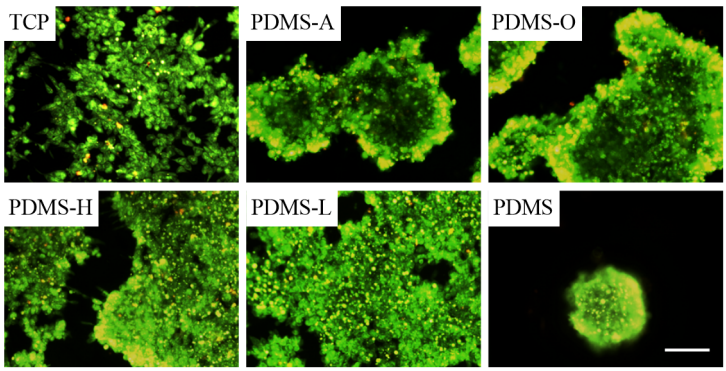

Figure 4.6 iPSC viability on native and SAM modified PDMS surfaces. Qualitative investigation of different PDMS surfaces' toxicity on cells by using acridine orange (green) and propidium iodide (red) staining (Scale bar = 100 μm).

Cell viability on PDMS surfaces was quantified through MTT analysis (Figure. 4.7). According to relative (% of TCP) optical density measurements, each type of surface modification was found to increase viable iPSC number ($p < 0.0001$), in respect to native PDMS. Also, in each conventional and amino acid conjugated SAMs groups; hydrophobic surfaces (PDMS-O and PDMS-L) allowed better viabilities than hydrophilic ones (PDMS-A and PDMS-H). Moreover, similar to AO & PI staining, hydrophobic PDMS-L surfaces supported the highest cell viability among all other experimental groups, including TCP, with a statistically significant difference of $p < 0.0001$ compared to each of all groups.

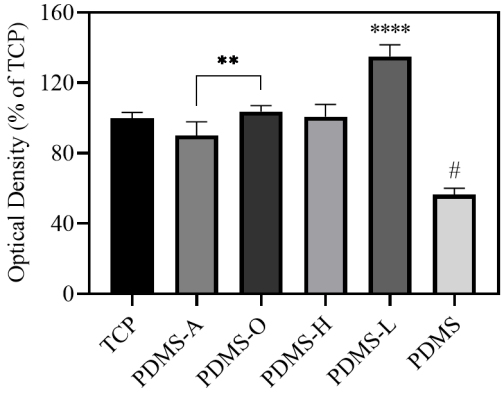

Figure 4.7 iPSC viability on native and SAMs modified PDMS surfaces. Quantification of iPSC viability on native and modified PDMS surfaces with MTT assay according to the relative optical densities (**$p < 0.01$, **** and # indicate $p < 0.0001$ when compared to all other groups).

SEM images (Figure 4.8) confirmed the promotive effect of PDMS-L surface on iPSCs, by showing the spread-out morphologies and quite extended cell spreading, whereas all other functionalized surfaces resulted in relatively lower cell coverage. Furthermore, native PDMS resulted in almost no visible cell adhesion sites.

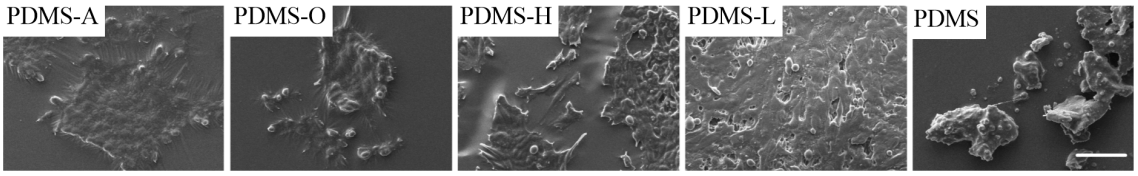

Figure 4.8 SEM images of iPSCs on native and SAM modified PDMS surfaces over 48 h (Scale bar = 50 μm).

4.6.4 Differentiation of iPSC into Cardiomyocytes on PDMS Substrates

Cardiac differentiation of iPSCs on PDMS surfaces was evaluated on the day 12 of onset differentiation, through western blot analysis, cell beating areas and immunofluorescence staining. Fold changes of cardiomyocyte specific markers; actinin, TPM and cTnT are given in Figure 4.9 (a-c) and according to overall results, PDMS-L significantly elevated total levels of all cardiac markers.

Actinin expression of cells is shown to be the highest on PDMS-L, followed by the other amino acid SAM modified surface: PDMS-H, and gelatin coated TCP. All these three surfaces result in a significant increase in this cardiac marker, when compared with native PDMS. Conventional SAMs modified surfaces' effects on actinin expression were significantly lower than PDMS-L and also higher than native PDMS with no statistical differences.

For TPM marker, there are significant differences showing PDMS-L's superiority over all PDMS surfaces, as well as for cTnT, showing that PDMS-L provided enhanced cardiac differentiation among other groups, however, statistical analysis showed differences for TCP and native PDMS groups only, with $^{*}p < 0.05$. Interestingly, native

PDMS acted in the same way as gelatin coated TCPs on cardiomyocyte differentiation for TPM and cTnT. While, for the same cardiac markers, native PDMS also resulted in a similar expression with PDMS-A, PDMS-O and PDMS-H, indicating the predominant effect of substrate stiffness over surface chemistry.

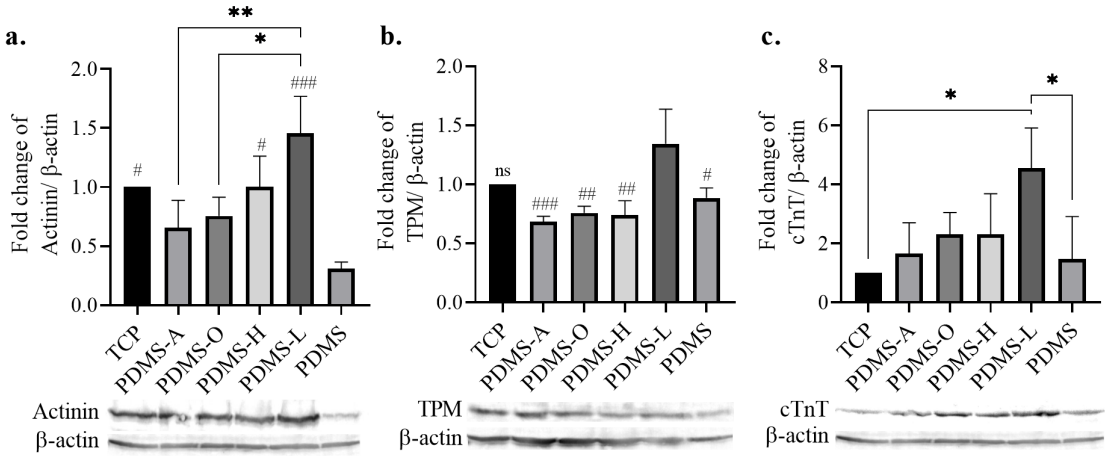

Figure 4.9 Western blot analysis for the cardiac markers of (a) α-actinin; (b) TPM, and (c) cTnT with the control of β-actin. The data are presented as the mean ± SD; $^{*}p < 0.05$, $^{**}p < 0.01$, $^{***}p < 0.001$, and # indicate significant differences when compared to native PDMS in (a); and PDMS-L in (b).

In Figure 4.10 (a), beating areas on all experimental groups are shown in white marks on day 12 of differentiation. Among given images, all cells were beating only on PDMS-L, supporting the western blot analysis. In addition, first beating areas were also found 6 days after cardiac initiation on PDMS-L, compared to a minimum of 7 days for cells cultured on other surfaces. Other SAMs-modified PDMS surfaces also provided sufficiently broad areas relative to native PDMS and gelatin coated TCP. Effect of substrate stiffness on cardiac differentiation is shown here with native PDMS of myocardium-like mechanical properties and TCP, where they resulted in similar beating areas. Furthermore, according to these recordings, frequencies [Figure 4.10 (b)] and areas [Figure 4.10 (c)] of spontaneously contracting cardiomyocyes were investigated.

Figure 4.11 (a) shows immunostaining for one of the most important cardiomyocyte specific proteins; cTnT in red with nuclei in blue. As given in the figure, all experimental groups give positive signals with different patterns. Similar to its effect

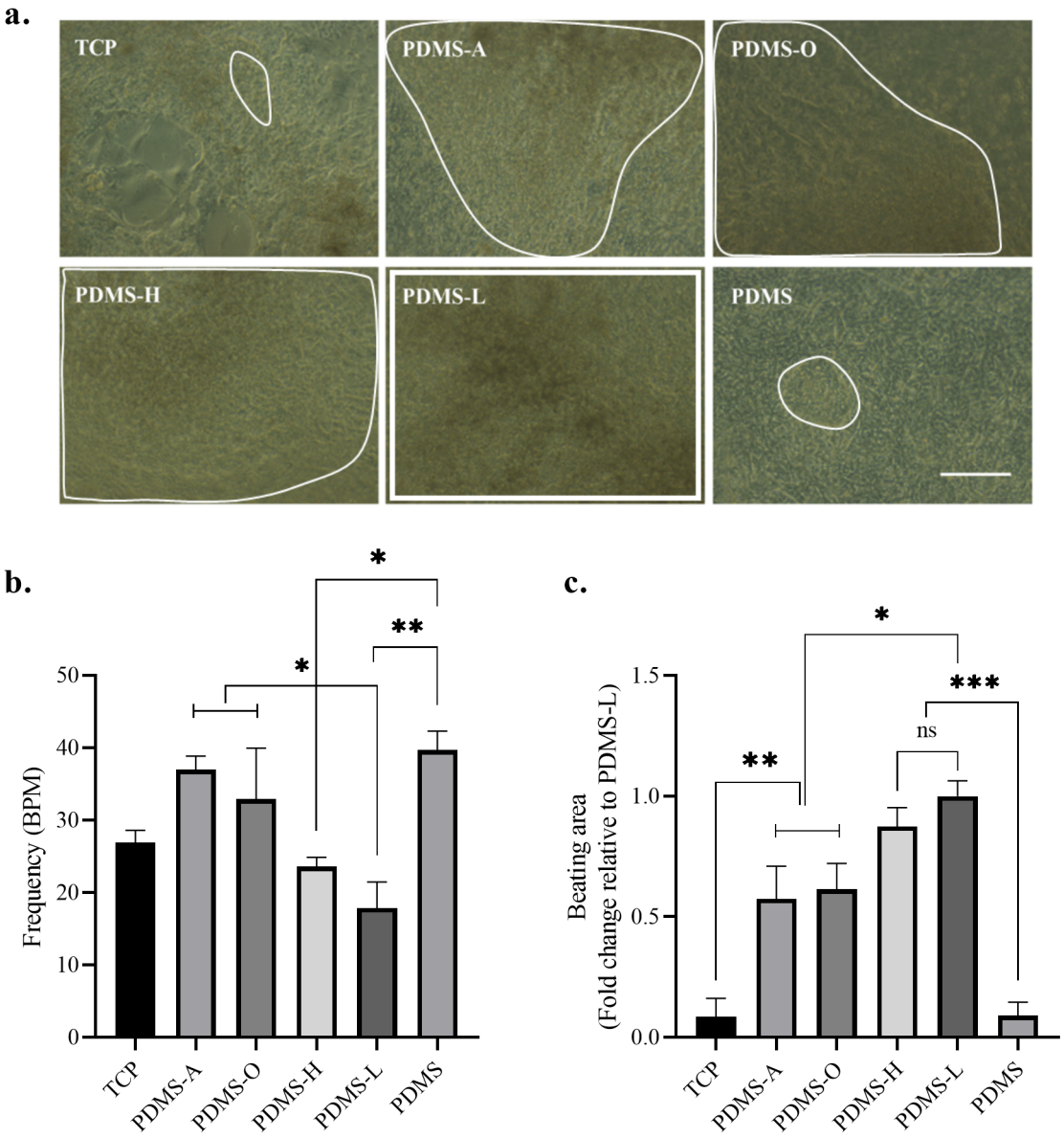

Figure 4.10 (a) Optical microscopy images of beating areas (in white) on TCP and various PDMS substrates (Scale bar = 200 μm). (b) Frequency and (c) areas of beating cardiomyocyes on the 12^th day of differentiation. The data are presented as the mean ± SD (n = 3); *p <0.05, **p < 0.01 and ***p < 0.001.

on iPSCs behavior and on differentiation, which is characterized by western blot analysis, native PDMS group results the least number of differentiated cells in all substrates. On the other hand, cells especially on amino acid conjugated SAM modified PDMS substrates were observed to be densely populated with intense cTnT staining. Furthermore, cTnT positive cells on PDMS-H showed more elongated morphology, similar

to mature cardiomyocytes. Quantitative comparison of fluorescence densities [Figure 4.11 (b)] clearly indicates the significant cTnT abundance on hydrophobic PDMS-L. The other amino acid conjugated SAM modified PDMS, PDMS-H, follows PDMS-L. Although PDMS-O is also a hydrophobic surface like PDMS-L, hydrophilic PDMS-H results in higher cTnT signal ($p < 0.001$), where all SAM modification, regardless of conventional or amino acid conjugated, provides more differentiated cells than native PDMS ($p < 0.0001$). This result may depend on the multifunctionality of His-SAM, which includes amine, amide, carbonyl and imidazole groups in addition to carbon-based skeleton. The signal pattern on quantitative intensities of cTnT is similar to western blot analysis with the same marker and demonstrates the relation between groups on cardiac differentiation.

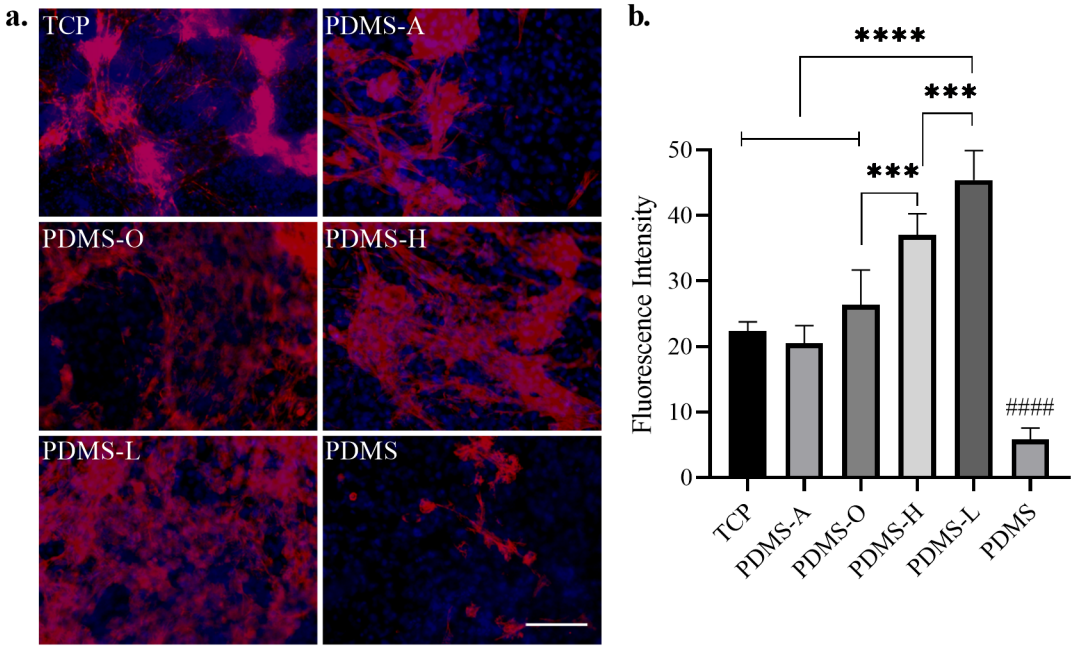

Figure 4.11 Immunostaining for the cardiac marker, cTnT (red) with DAPI (blue) counterstain for nuclei. (a) Cells on day 12 of differentiation on TCP and different PDMS surfaces (Scale bar = 100 μm). (b) Quantification of cTnT fluorescent intensity of staining on day 12 of differentiation. The data are presented as the mean ± SD (n = 3); ***p < 0.001, ****p < 0.0001 and ####p < 0.0001. #p indicates significant difference when compared to all other groups.

cTnT positive cell percentages and cTnT positive areas were analyzed after 12 days of cardiac differentiation. Cells were trypsinized and plated on fibronectin coated well plates. On the next day, cTnT immunostaining (with DAPI counterstain) was performed and images were analyzed on ImageJ software. cTnT positive and negative cell

nuclei were counted and the percentage of cTnT positive cells were quantified as shown in Figure 4.12(a). Then, cTnT positive fluorescence areas were quantified on ImageJ and given in Figure 4.12(b). Supporting the western blot analysis, PDMS-L provided the highest number of cardiomyocytes and all conventional and amino acid conjugated SAMs-modification increased the number of cardiomyocytes, when compared to native PDMS and gelatin coated TCP. Furthermore, no significant differences were found between native PDMS and gelatin coated TCP, showing the predominant effect of healthy myocardium-like stiffness on the differentiation of iPSCs into cardiomyocytes.

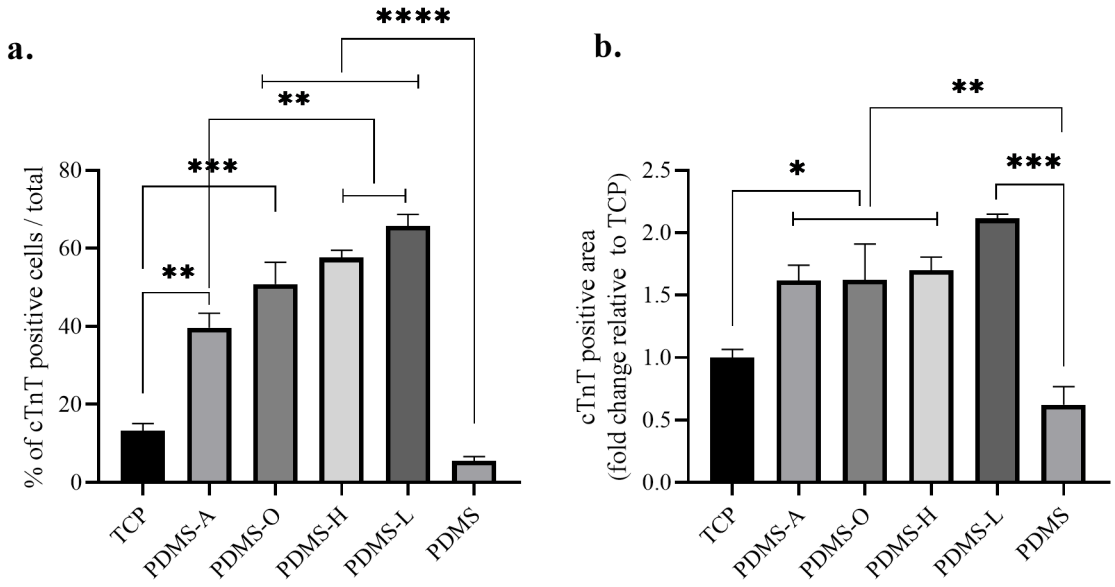

Figure 4.12 (a) Quantification of cTnT positive cells (%) and (b) area. The data are presented as the mean ± SD (n = 3); *p < 0.05, **p < 0.01, ***p < 0.001 and ****p < 0.0001.

In both cTnT immunostaining and western blot analysis, PDMS-L showed enhancing effects on cardiac differentiation of iPSCs. To examine superiority of this modification on differentiation with the effect of substrate stiffness, cells on PDMS-L, positive control-gelatin coated TCP and negative control-native PDMS were trypsinized on the day 12 of inducement and plated on fibronectin coated well plates. On the next day cell cytoskeleton and cardiac properties (cTnT) were investigated with fluorescence imaging (Figure 4.13). Cell adhesion and cell number on fibronectin-coated wells was similar for all groups, regardless of their growing conditions. However, the number of

cardiomyocyte-like cells was the highest on when PDMS-L was used as a substrate for the differentiation. Thus, the promotive effect of both substrate stiffness and Leu-SAM modification on cardiac differentiation of iPSC was once more shown, confirming the western blot analysis and immunostaining performed in the study.

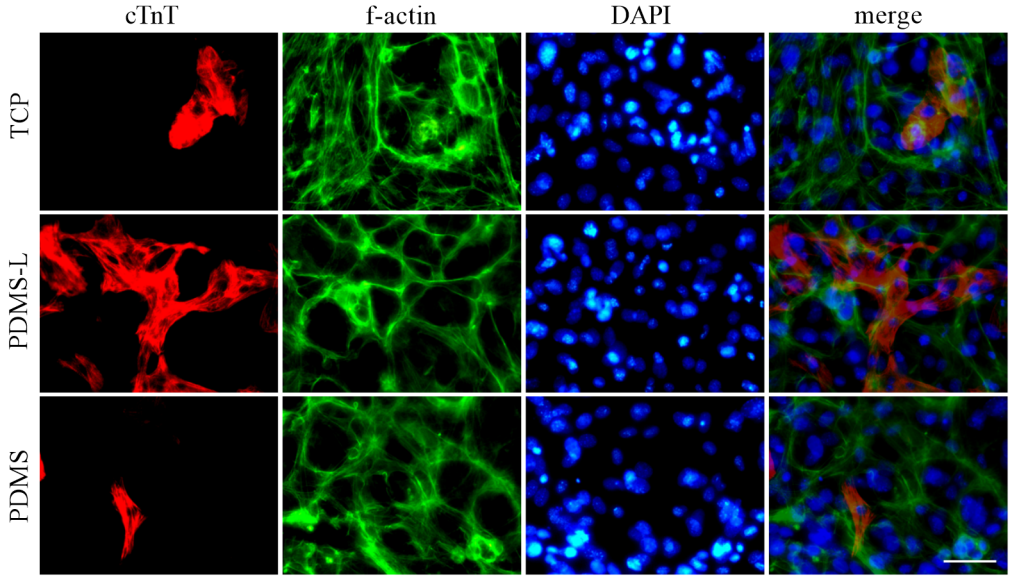

Figure 4.13 cTnT (red) and F-actin (green) staining of cells differentiated for 12 days on gelatin coated TCP, PDMS-L and PDMS, respectively and re-plated on fibronectin-coated TCP (Scale bar = 50 μm).

4.7 Discussion

In this chapter, PDMS was used to produce cell substrates for *in vitro* cardiac differentiation of iPSCs. Surface chemical properties of PDMS were enhanced for cell culture via conventional and synthesized amino acid conjugated SAMs, by using a straightforward modification technique. Additionally, our goal was to achieve an optimal substrate stiffness considering that the stiffness of healthy myocardial tissue ranges from 12 to 30 kPa [49, 188, 177, 183]. Among all prepared PDMS substrates of varying curing agent concentrations (10:1-70:1), 50:1 PDMS was found in this range with a Young's modulus of 23.79±0.61 kPa (Figure 4.2). Numerous studies on cardiomyocytes concluded and confirmed that, cardiac cells perform their functions better on substrates with healthy myocardium stiffness during *in vitro* culture [178, 114, 189, 190]. Simi-

larly, cardiac differentiation of stem cells was enhanced on these mimicked substrates [116, 19]. All experiments in this study were conducted by using 50:1 PDMS, however in the preliminary cell culture studies we encountered an important drawback while using PDMS: cell detachment was high due to the leaching of uncured oligomers [191, 192]. Uncrosslinked low molecular weight (LMW) species are the reason of this problem. They diffuse from the bulk to the surface and cause a lubricating effect [193, 28]. As the amount of curing agent is already very low in 50:1 PDMS, iPSC cultured on PDMS substrates started to detach from the surfaces, 48 h after seeding [Figure 4.5(a)] and almost no attached cells were left in the following days. To solve this issue, curing conditions of substrates were optimized from 70°C and 4 h to 60°C and 7 days with additional ethanol and water washing steps being incorporated to the protocol [194, 192]. Enhanced iPSC adhesion and viability was achieved and elimination of LMW chains also made PDMS surfaces thermodynamically more stable after oxygen plasma treatment and following surface modification [191].

Once the optimum substrate stiffness had been established, suitable surface chemical modification of PDMS was investigated for both iPSC behavior and their cardiac differentiation, as untreated PDMS surface does not support cell attachment and growth [195]. We used SAMs for the modification (Figure 4.1), as those molecules provide well-defined stable linkages [34, 161], in addition to their straightforward production without any request of expensive and complicated devices [35, 196]. Functional groups and related tunable wettability properties of these molecules enable their use for enhanced and biomimetic cell interaction purposes, as these functional groups are found in natural biological environments of cells [42]. Here, we aimed to increase the bio-mimicry of PDMS surfaces, by preparation of amino acid conjugated SAMs. With conventional (APTES and OTS) and amino acid conjugated (His-SAM and Leu-SAM) SAMs, we showed the effects of different functional groups and wettability separately and comparatively. For the characterization of the surface modification with SAMs, specific N1s signals were confirmation for PDMS-A, PDMS-H and PDMS-L on XPS survey spectra [Figure 4.3(a)] showing the presence of SAMs. Detailed investigations of bonds are given with high resolution C1s and N1s spectra [Figure 4.3(b-c)], which show PDMS-related C-Si bonds, in addition to SAMs specific ones. Both PDMS-A and

PDMS-L have the same C1s and N1s peaks, as expected from their molecular structures [197, 198, 186]. The difference between these modifications is clearly seen by the length of these specific signals, as in PDMS-L, nitrogen content is 2 times higher than in PDMS-A. Also, additional C-C chain and methyl groups of the amino acid resulted an increased C-C peak on PDMS-L [186]. In PDMS-H, total three peaks of nitrogen atoms are shown in the N1s spectra with a distinctive bond of C=N [Figure 4.3(c)], which is resulted from the imidazole side-chain of histidine amino acid (Figure 4.1) [199, 200]. All these components are expected to be present in the spectrum of a surface that has been successfully modified with SAMs and additionally, stability of SAMs modified PDMS was tested and confirmed in our previous study for both 21 days of cell culture and also under flow conditions [138]. To support XPS results of surface modification in the wettability manner, WCA measurements were conducted and PDMS-A and PDMS-H surfaces were found to be hydrophilic, as expected, due to the amine [32] and imidazole groups [199]. On the other hand, methyl groups, which are the main functional groups on PDMS-O, and are also predominant on PDMS-L make these surfaces hydrophobic, but their contact angles were not as high as native PDMS.

Altogether, cell viability, morphology, cardiac marker expression and beating areas demonstrated the combined effects of soft cell substrates with various functional groups and relative wettability on murine iPSCs. The main goal of the study was to enhance PDMS surface chemical properties for the differentiation of iPSCs into cardiomyocytes. To achieve that, short-term iPSC attachment and viability was proposed, until the required confluency was obtained for differentiation. Both AO & PI staining (Figure 4.6) and MTT analysis (Figure 4.7) clearly showed that all SAMs modified surfaces increased the number of viable iPSCs, when compared to native PDMS, moreover, these enhanced cell responses confirmed their potential use for short term surfaces for iPSCs, *in vitro*. Among all experimental groups, hydrophobic PDMS-L supported a significantly higher number of viable cells after 48 h of culture ($p < 0.0001$) and similarly, extended cell spreading and enhanced cell coverage was also observed on PDMS-L (Figure 4.8). Like hydrophobic PDMS-L, hydrophobic PDMS-O also resulted in a relatively higher cell number than the other conventional SAM; PDMS-A, which is

hydrophilic. These improved responses of iPSC to hydrophobic surfaces are compatible to the behavior of ESC [201] and confirm the significant benefits of using hydrophobic Leu-SAM modified PDMS on iPSCs over other groups, including gelatin coated TCP. For the evaluation of cardiac maturation, the expression of sarcomeric α-actinin is an important indicator, as sarcomere formation is a fundamental marker of cardiomyocte contraction. Additionally, regulatory proteins like cTnT [202] and TPM modulate the activation of contractions [202, 203]. Effects of surface chemical composition were similar for all three cardiac marker expressions with a dominant abundance on PDMS-L. Interestingly, abundance of TPM and cTnT markers were similar in native PDMS and the positive control group, gelatin coated TCP [Figure 4.9(b-c)]. Here, we showed that cardiac myocardium-like substrate stiffness is predominant for cardiac differentiation over surface chemistry, although this effect cannot be proved with actinin. Immunostaining of cells against cTnT (Figure 4.11 and Figure 4.12) or beating areas (Figure 4.10) demonstrate and confirm the promotive effect of amino acid conjugated SAMs on iPSC cardiac differentiation. As shown in Figure 4.11(a), cTnT positive cells on PDMS-H appeared to be more elongated, similar to mature cardiomyocytes in their native environment [204]. Moreover, PDMS-H provided a large beating area [Figure 4.10(b)]. On the other hand, hydrophobic PDMS-L resulted with significantly higher cTnT fluorescence intensity ($^{***}p < 0.001$) than hydrophilic PDMS-H [Figure 4.11(b)]. Another important contribution of PDMS-L on differentiation was found in the contraction of cells, which indicates the cardiac lineage commitment. Cells on PDMS-L started beating on the 6th day of initiation, whereas it took at least 7 days for cells on other surfaces. This enhanced effect of Leu-SAM modified PDMS on cardiac specification can be explained by leucine-rich proteoglycans, which are one of the critical components of myocardial ECM [205, 206, 207]. In addition to surface chemical composition, wettability is also an important surface characteristic for cellular behavior and its effects depend on the cell type. For example, hydrophobic culture environments were found to enable uniform embryoid body formation of ESCs, in addition to better viability and differentiation [201]. In cardiac ECM, specific proteins like elastin [208] and fibronectin [209], are known to show hydrophobic properties, therefore cell culture environments with higher water contact angles are expected to be better for *in vitro* culture of cardiomyocytes. Zong et al. and Mehrotra et al. confirmed that,

primary cardiomyocytes expressed better structural and functional maturation on relatively hydrophobic surfaces (WCA=107° and 81.79°, respectively) [210, 211], other studies reported the preference of neonatal rat cardiomyocytes [212, 213] and ESC derived-cardiomyocytes for hydrophilic substrates [212]. In this study, hydrophobic conventional SAM, OTS; and amino acid conjugated SAM, Leu-SAM with dominant -CH_3 functional groups resulted in better cardiac environments than their hydrophilic partners; PDMS-A and PDMS-H, respectively.

These results not only demonstrate the previous literature on the choice of substrate elastic moduli and promotive effects of healthy myocardium-like stiffness on cardiac differentiation of iPSCs, but also offer a facile, comparative and biomimetic approach to alter surface biochemistry of PDMS substrates. PDMS is an inexpensive, transparent and easy to prepare polymer and unlike other cell substrate materials in this area, like polyacrylamide, its mechanical properties can be easily altered while expensive linker molecules for surface chemical modification is not required [178]. In addition to the advantageous properties of PDMS, soft substrates used here were thermodynamically more stable due to extensive curing conditions and this comparative study offers enhanced cell substrate surface properties of PDMS via only a single-step modification procedure using our synthesized amino acid conjugated SAMs and conventional SAMs, which make these substrates a superior and promising alternative over other polymers for cell culture applications.

5. CELL SUBSTRATE DESIGN FOR ENHANCED CORNEAL ENDOTHELIAL CELL RESPONSE

5.1 Preparation and Characterization of PDMS Substrates

White (Rosa Pascali) and red roses (Rosa Damascena) were purchased from a local flower shop. Soft lithography was used to produce rose petal relief negative pattern on PDMS cell substrates. To use the same pattern, the first rose petal relief negative replicate was copied for several times by using the first positive replicate (gold coated) as a mold. Rose petal topography mimicked negative (-) replica was prepared by mixing 10:1 ratio of PDMS pre-polymer and curing agent (PDMS, Sylgard 184; Dow). Rigorously stirred mixture was degassed completely and poured onto rose petals. Red and white rose petals were used both in fresh and dried (petals were fixed onto a cork board and allowed to dry under room conditions) form. After 4 h of curing at 70°C, replicas were cleaned by sonicating in DI water, absolute ethanol and DI water, respectively. Both negative and positive replicas were sputter coated with a thin layer of gold (Quorum SC7640 high resolution sputter coater, 1.5 kV, 10 mA), before using as a mold. 15:1 PDMS pre-polymer to curing agent ratio was used for the positive (+) replica, as it would be easier to peel off while using PDMS with different pre-polymer to curing agent ratios. Finally, (white) rose petal topography mimicked cell substrates were prepared with 30:1 PDMS. This procedure is schematically given in Figure 5.1.

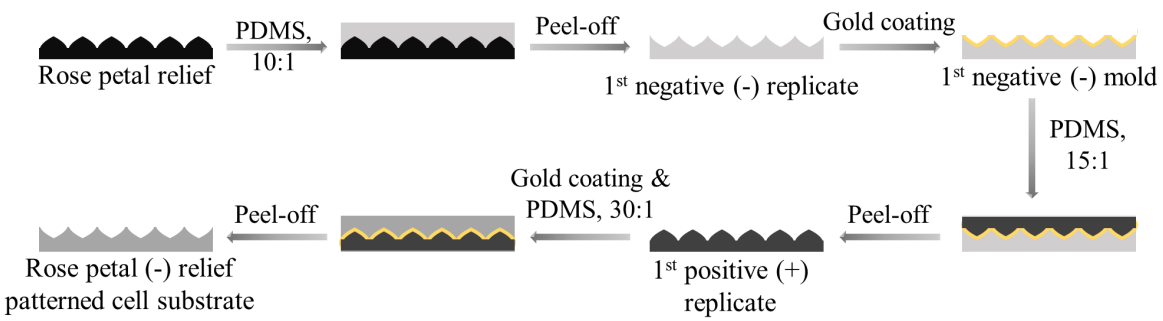

Figure 5.1 Schematic procedure of rose petal topography mimicked PDMS substrate preparation.

Mimicked substrates were characterized by a SEM (XL30, Philips) and optical profilometer (Zygo, CT) for determining the morphology and pattern dimensions, respectively. SEM was also used to examine successful replication cycle of a single PDMS mold.

Young's modulus of PDMS substrates with various pre-polymer and curing agent concentrations (10:1, 15:1, 20:1 and 30:1) were measured using a nanoindenter (CellHesion®200, JPK) in hydrated conditions. Measurements were performed with a CONT cantilever (0.2 N/m force constant and 13 kHz resonance frequency, Nanoworld) in contact mode and 7 samples were analyzed for each type. Young's moduli of different PDMS substrates were calculated according to the Hertz model.

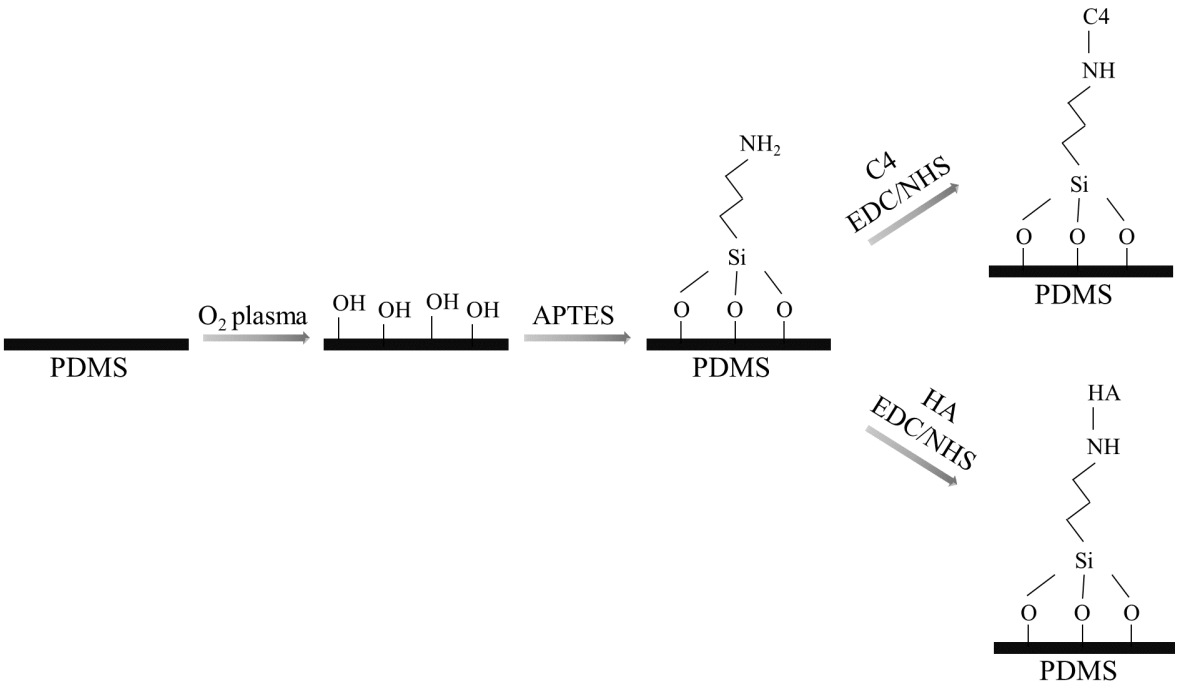

Figure 5.2 Functionalization of PDMS substrates with COL 4 and HA.

PDMS substrate surfaces were modified with COL 4 and HA using EDC/NHS coupling chemistry. First, surfaces were activated via oxygen plasma for 60 s (50 sccm O_2 flow at 200 mTorr pressure, March Plasma Systems) [143] and then they were immersed into 10% APTES in absolute ethanol to form amine groups (PDMS-NH_2) [143, 32]. 1 mg/mL HA (Acros, 251770010) and 0.5 mg/mL COL 4 (Sigma C5533)

solutions were prepared in 1:1 EDC and NHS containing MES buffer (50 mM, pH 5.0) and stirred for 30 min [214, 215]. Finally, PDMS-NH_2 substrates were incubated in these solutions at room temperature (RT) overnight with subsequent rinsing with MES buffer and DI water (Figure 5.2).

5.2 Corneal Endothelial Cell Culture

Bovine CECs (BCE C/D-1b, ATCC® CRL-2048™) were cultured on PDMS substrates in 24 well tissue culture plates (TCP) with a density of $1x10^5$ cells/well, using 10% Fetal Bovine Serum (FBS, Merck) supplemented DMEM High glucose with L-Glutamine and Sodium Pyruvate (Biosera). Cells were incubated at 37°C with 5% CO2 in a humidified environment. PDMS substrates were sterilized before cell culture with 70% ethanol, sterile DI water and UV exposure. CEC cell behavior was investigated on both flat native PDMS (PDMS), COL 4 functionalized PDMS (PDMS-C4), HA functionalized PDMS (PDMS-HA) and white rose petal negative relief topography mimicked versions of these substrates (PDMS-R, PDMS-C4-R and PDMS-HA-R, respectively) with a control group of TCP.

5.2.1 Cell Proliferation Assay

Alamar blue assay (AlamarBlue™, Bio-Rad) was used to investigate CEC proliferation on various PDMS substrates on days 1, 3 and 7. Briefly, cell culture media was removed and 10% alamar blue containing fresh media was added on cells on these specific days. Cells were incubated for 4 h and optical absorbance of each experimental group was recorded on a micro plate reader spectrophotometer (Bio-Rad, iMark) at 570 and 595 nm [138].

5.2.2 Morphological Staining

Cellular morphology on functionalized and white rose petal patterned PDMS substrates was investigated via actin cytoskeleton staining (Alexa Fluor 488 Phalloidin, Thermo Fisher) on the 7^{th} day of CEC culture. Cells were fixed in 4% formaldehyde and permeabilized by immersing into 0.1% Triton X-100 containing PBS. After blocking was completed in 1% BSA for 20 min, actin cytoskeleton staining solution (in 1% BSA) was applied. DAPI counterstaining (Thermo Fisher) was used to visualize cell nuclei. Images were recorded with appropriate filters of a fluorescence microscope (DM IL, Leica) [138].

5.2.3 Immunocytochemistry

On the 7^{th} day of CEC culture on substrates, cells were fixed and permeabilized as instructed in Section 5.2.2. Blocking and immunocytochemical staining were performed using the same procedure as in Section 5.1. Anti-sodium potassium ATPase primary antibody (ab76020, EP1845Y, 1:100) and anti-rabbit IgG H&L secondary antibody (ab150062, Alexa Fluor™555, 1:200) were used to label Na^+/K^+ ATPase, and DAPI was used to visualize cell nuclei.

5.2.4 Western Blot Analysis

Western blot analyses were performed on the 7^{th} day of CEC culture and expressions of CEC-relative markers Na^+/K^+ ATPase, collagen type IV, N-cadherin and zonula occludens-1 (ZO-1) were investigated on PDMS substrates. Briefly, total proteins were extracted and lysed in 2X Laemmli buffer and equalized amounts of proteins were loaded into 4-10% polyacrylamide gels (Sigma-Aldrich). Then, they were resolved under 130 V (Mini protean, Bio-Rad) and transferred to PVDF membranes (Transblot Turbo, Bio-Rad). After blocking was completed using 5% non-fat milk containing PBST, membranes were incubated with anti-sodium potassium ATPase (ab76020,

EP1845Y), anti-collagen IV (ab6586), anti-N-cadherin (ab18203) primary antibodies overnight at 4°C. Anti-β-actin (ab8226) was chosen to be the loading control. On the following day, membranes were rinsed extensively with PBST and incubated with corresponding horseradish peroxidase (HRP)-labeled secondary antibodies (ab6721, and ab6789) for 1 h. 3,3',5,5'-tetramethylbenzidine chromogenic substrate (Thermo Fisher) was used for the visualization of bands on the membranes and their intensities were calculated using ImageJ.

5.3 Statistical Analysis

Graphpad (Prism) software was used to conduct all statistical analyses with one-way analysis of variance (ANOVA) and Tukey multiple comparison test. p values lower than 0.05 were regarded as statistically significant. Data were given as mean $\pm$ SD.

5.4 Results

5.4.1 Topographical Investigation of Patterned PDMS Substrates

Soft lithography was used to transfer rose petal's positive and negative reliefs topographical cues on PDMS substrates. Figure 5.3(a) summarizes SEM images of (i) fresh red rose, (ii) dry red rose, (iii) fresh white rose and (iv) dry white rose petal patterned features on 15:1 PDMS surfaces (positive replicas). Herein, both micro and nano-sized cues were successfully replicated. Due to the shrinkage of cells in dry petals, cell forms were disrupted leading to reduced cell number and increased cell-to-cell distances. Therefore, they were not preferred as cell substrates for CECs. In both fresh rose petals patterned ones; cell number is in the range of physiologically relevant CEC density ($\approx$ 2000 cells/mm^2). Microgroove mean depths (n=30 measurements using optical profilometer over 3 PDMS replicas) of the patterned PDMS were calculated to

be 12.9 μm and 6.6 μm for red and white rose, respectively [Figure 5.3(b)]. Among them, white rose patterned one ensured CEC-like depth [216]. Furthermore, fresh white rose petal provided better CEC shape-imitative hexagonal cells than red ones. Thus, we used white rose petals (Rosa Pascali) for the fabrication of patterned cell substrates in the study. In Figure 5.3(c), SEM images of (i) white rose petal replicating mold and (ii) white rose petal topography mimicked PDMS cell surfaces were given. Highly ordered hexagonal shapes and nano-scale cues in Figure 5.3(c-ii) proved both successful replication and CEC shape-imitative cell substrate production.

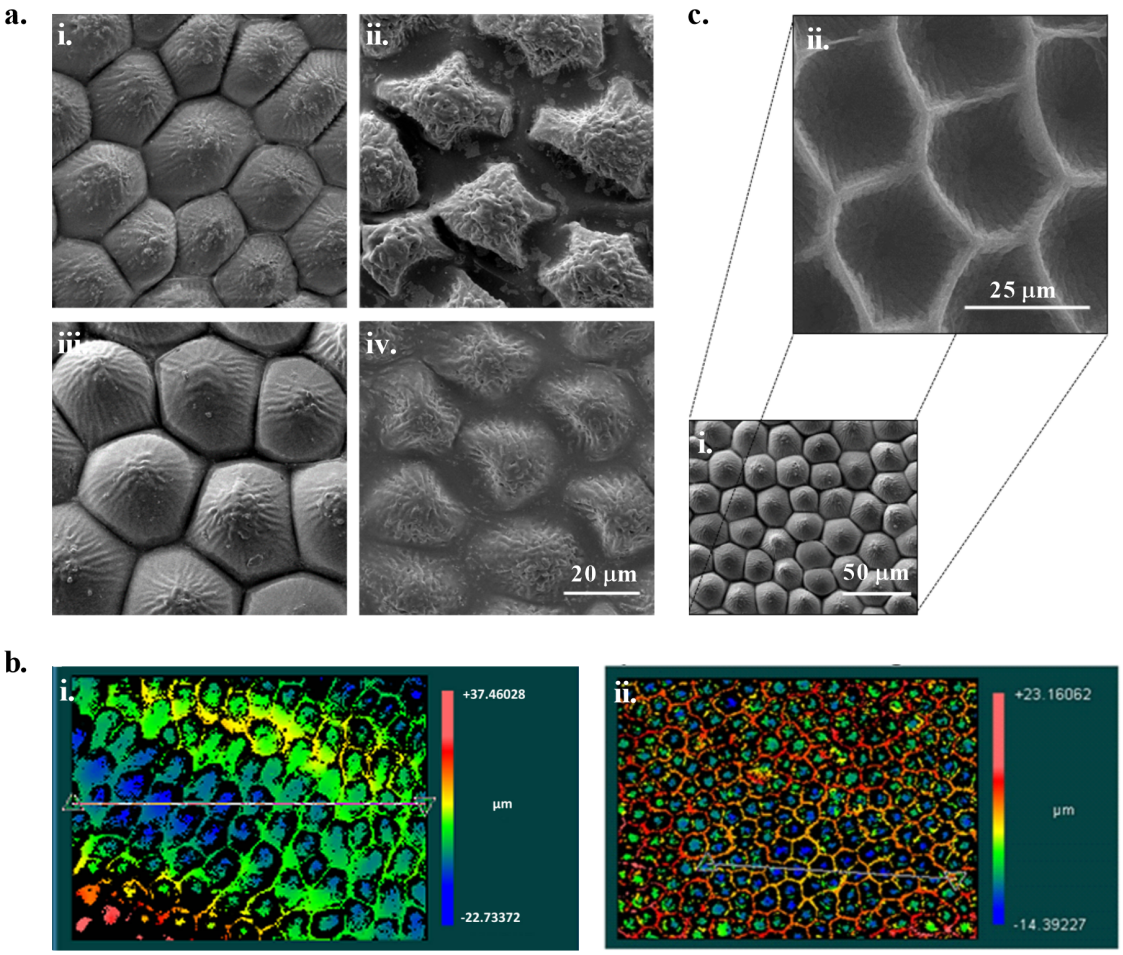

Figure 5.3 SEM images of rose petal patterns on PDMS surfaces; (a) positive replicas of (i) fresh and (ii) dry red rose, (iii) fresh and (iv) dry white rose petal patterns; (b) surface topography measurements of fresh (i) white and (ii) red rose petal patterned PDMS; (c) fresh white rose patterned (i) mold and (ii) cell substrate.

Replicating capacity of PDMS molds were tested by using a marked PDMS

mold for 10 replications. 1^{st} positive replicate was coated with gold and used as mold to produce cell substrates (Figure 5.1). In Figure 5.4, a marked PDMS mold (a) and its negative replicates (b-f) were shown. From these images it was implied that a mold could be used for at least 10 times for the preparation of cell substrates by maintaining the pattern structures with good precision.

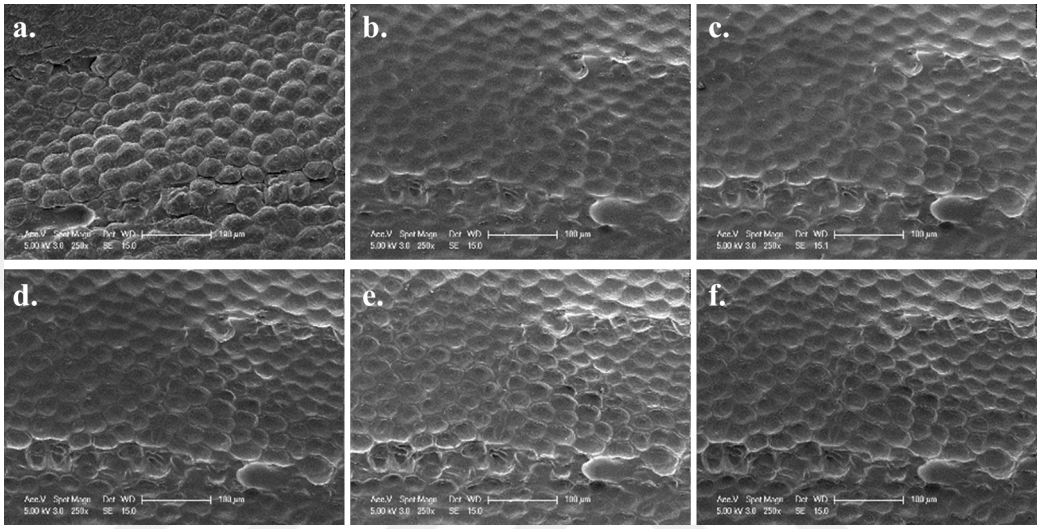

Figure 5.4 SEM images of rose petal mimicked PDMS (a) mold (positive replicate) with marked area, (b) 1^{st} replicate, (c) 3^{rd} replicate, (d) 5^{th} replicate, (e) 7^{th} replicate and (f) 10^{th} replicate (Scale bar = 100 μm).

5.4.2 Nanoindentation Analysis

PDMS substrates were prepared in decreasing curing agent concentrations (10:1, 15:1, 20:1 and 30:1) to obtain substrates with a wide stiffness range. Nanoindentation was used for the characterization of these various PDMS substrates and Young's modulus values were given in Figure 5.5, as 2105.3±155.6, 1387.57±152.9, 683.43±188.7 and 211.85±74.9 kPa for 10:1, 15:1, 20:1 and 30:1 PDMS pre-polymer and curing agent ratios, respectively. All these formulations provided successful pattern replications, whereas lower amounts of PDMS curing agent than 30:1 resulted sticky substrates. Among 10:1-30:1 PDMS substrates, the Young's modulus of 30:1 PDMS (211.85±74.9 kPa) was found in the cornea-friendly range, which is between 200-290 kPa [217, 218, 219, 220] and PDMS with 30:1 pre-polymer to curing agent ratio was used for the fabrication of all cell substrates.

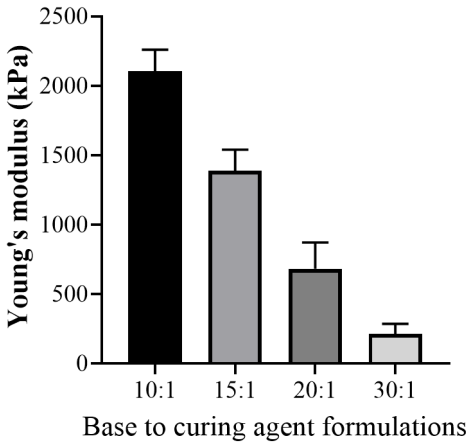

Figure 5.5 Nanoindentation measurements of varying PDMS pre-polymer and curing agent formulations (****$p < 0.0001$).

5.4.3 Characterization of Surface Chemical Modification

COL 4 and HA functionalization of PDMS substrates were confirmed via WCA measurements for the alteration in surface hydrophobicity, XPS analysis and immunofluorescent staining for surface chemical and biochemical investigation.

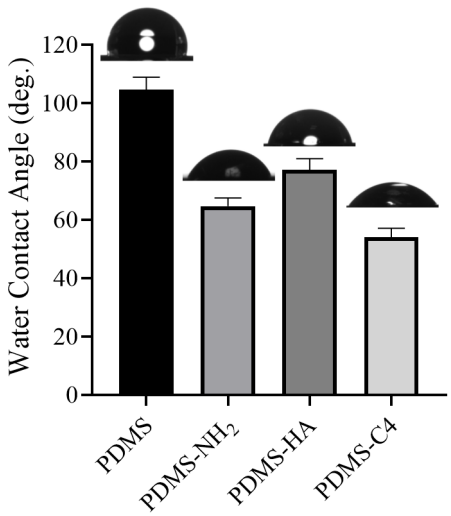

Figure 5.6 WCA analysis of native PDMS and APTES, HA and COL 4 functionalized PDMS. The data are presented as the mean ± SD (n = 3); ****$p < 0.0001$ for all comparisons, except ***p =0.0002 for PDMS-NH2 vs PDMS-HA and **p =0.0012 for PDMS-NH_2 vs PDMS C4.

5.4.3.1 WCA Measurements. Wettability properties of various PDMS substrates were investigated to show the effect of surface functionalization and results are given in Figure 5.6. Untreated PDMS surfaces displayed a hydrophobic nature with a water contact angle of 104.6°±4.3°, which was strongly reduced after oxygen plasma treatment and APTES modification (64.7°±2.8°) due to the formation of hydrophilic amine groups. After HA functionalization, PDMS surfaces became more hydrophobic than PDMS-NH_2 with a WCA of 77.2°±3.8°, whereas PDMS-C4 showed the lowest contact angle of 54.1°±3.1°.

5.4.3.2 XPS Analysis. XPS survey [Figure 5.7(a)] and high-resolution spectra were shown [Figure 5.7(b-e)] for PDMS, PDMS-NH_2, PDMS-HA and PDMS-C4.

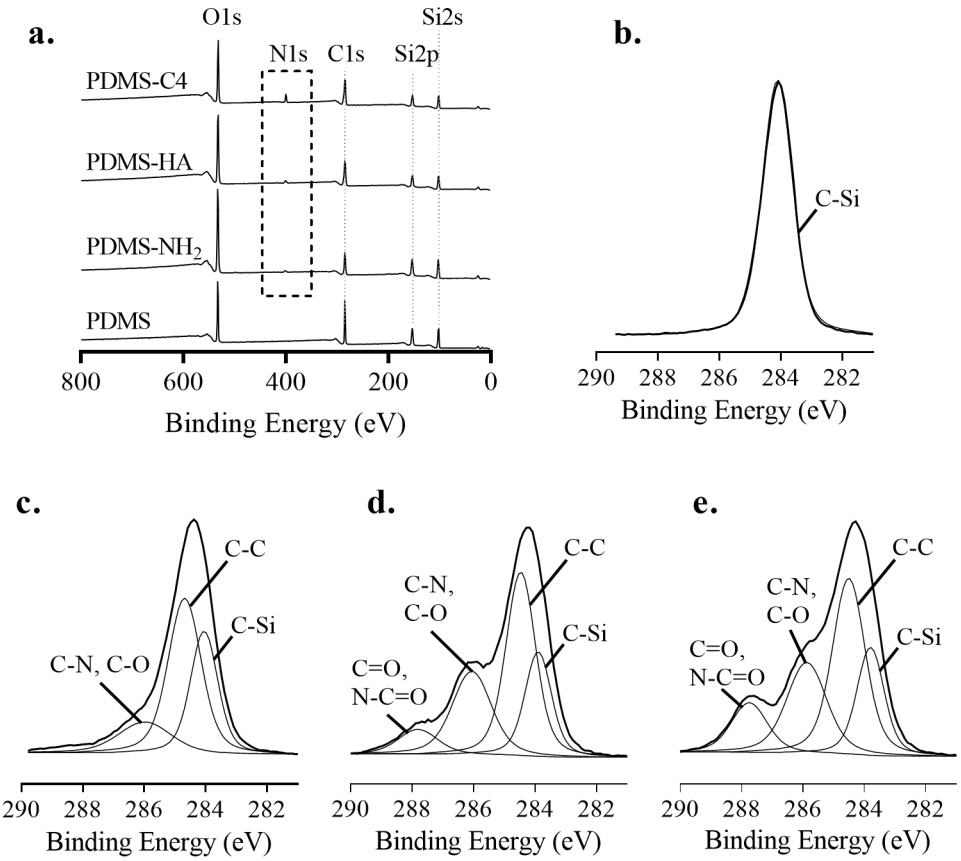

Figure 5.7 (a) XPS survey spectra of native PDMS and APTES, HA and COL 4 functionalized PDMS. (b) High resolution C1s spectra of native PDMS, (c) PDMS-NH_2, (d) PDMS-HA and (e) PDMS-C4.

In survey spectra, all PDMS related peaks of Si2s, Si2p, C1s and O1s were

detected [138]. After modification with APTES, N1s peak was shown at 400.4 eV to confirm the incorporation of -NH_2 functional group. When HA or COL 4 were immobilized on PDMS surfaces, there were significant rises in C1s and N1s. This is a clear indication of introducing biomolecules to PDMS surfaces featuring various carbon-nitrogen functionalities. Further investigation was supplied by the high-resolution C1s core-level spectra. Four different C species were specified based on their binding energies, C-Si at $\approx$ 283.7 eV, C-H, C-C at $\approx$ 284.5 eV, C-N, C-O at $\approx$ 285.8 eV and N-C=O, C=O at $\approx$ 287.8 eV [214, 221, 222]. The appearance of C-C, C-O, and C-N was attributed to the successful chemical modification with APTES, HA and COL 4. Furthermore, the presence of surface amide-type functionalities (N-C=O) confirms the conjugation of PDMS-NH_2 with HA or COL 4.

5.4.3.3 Immunofluorescence Staining. Immunofluorescent staining was further used to show the uniformity of HA or COL 4 functionalization on PDMS-NH2 (Figure 5.8). No fluorescent signals were observed in native PDMS for both anti-hyaluronic acid and anti-collagen IV staining [Figure 5.8(a and c)], whereas uniform staining of HA (in green) and COL 4 (in red) were visualized, attributable to the HA or C4 functionalization [Figure 5.8(b and d)] [214, 223].

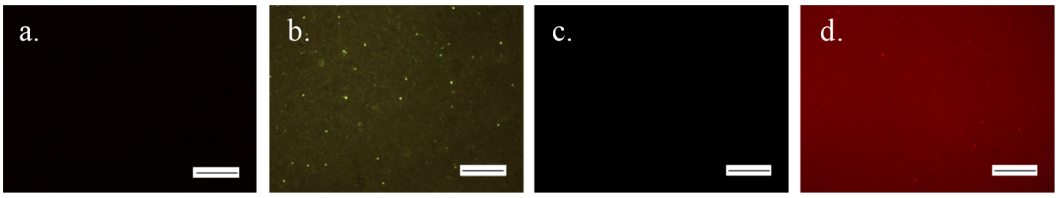

Figure 5.8 Immunofluorescent staining against anti-hyaluronic acid on (a) PDMS and (b) PDMS-HA; against anti-collagen IV on (c) PDMS and (d) PDMS-C4. Scale bar = 200 μm.

5.4.4 CEC Behavior on PDMS Substrates

CEC proliferation was evaluated on flat and white rose negative relief patterned native, HA functionalized and COL 4 functionalized PDMS surfaces over 7 days. The metabolic activity of CECs on various PDMS substrates was determined via Alamar

blue assay on days 1, 3 and 7. The effect of only surface chemical modification on CEC proliferation was given in Figure 5.9(a), relative to reduced alamar blue percentages. According to the figure, CECs on all substrates were in a tendency of increasing in number with time and remained viable for 7 days. This is a certain indication of non-toxic effect of both native and modified PDMS. Among all PDMS substrates, PDMS-C4 clearly enhanced CEC proliferation significantly ($p < 0.0001$) for the whole cell culture period. White rose negative relief patterning of PDMS increased the cell number on all PDMS surfaces [Figure 5.9(b)] and with PDMS-C4-R, a TCP-like proliferative environment was achieved for CECs on days 3 and 7. HA functionalization of PDMS did not show any improvements on CEC proliferation relative to native PDMS. Thus, white rose patterning-related cell proliferation was investigated on native and COL 4 modified PDMS [Figure 5.9(c)]. This effect was clearly visible on day 7 with a statistically increased cell metabolic activity on patterned versions of each group ($p < 0.0001$). In addition to promotive effect of white rose mimicked patterning, COL 4 functionalization resulted an improved CEC bioactivity ($p < 0.0001$).

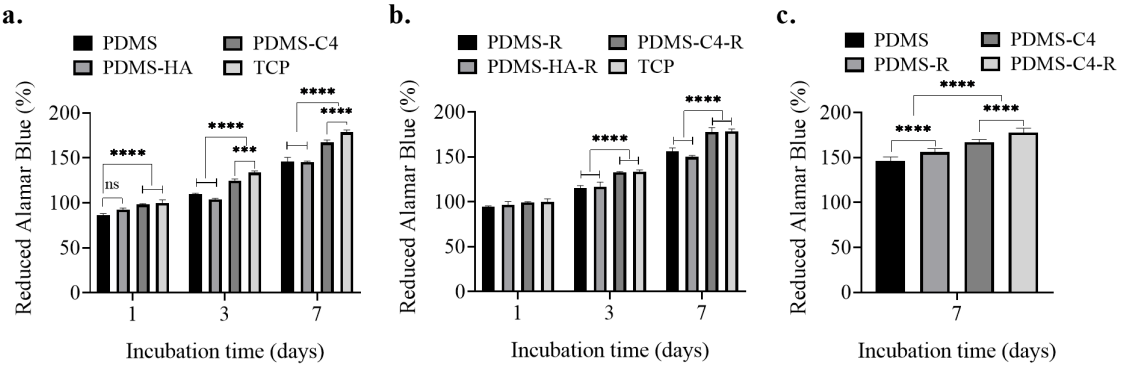

Figure 5.9 Reduced alamar blue (%) with relative CEC proliferation on (a) flat and (b) white rose patterned native PDMS, PDMS-HA, PDMS-C4 and TCP over 7 days and (c) CEC proliferation on flat and white rose patterned PDMS and COL 4 on day 7 (***$p < 0.001$ and ****$p < 0.0001$).

Cellular morphology on PDMS substrates were investigated on day 7 via actin cytoskeleton staining and fluorescence images of CECs on various surfaces were given in Figure 5.10. Very few attached cells were found on flat native PDMS, supporting the proliferation analysis. Both patterning and surface chemical modification increased the number of attached cells on PDMS surfaces. Furthermore, patterned PDMS-C4

provided the most densely CECs population with well-defined actin fibers organization.

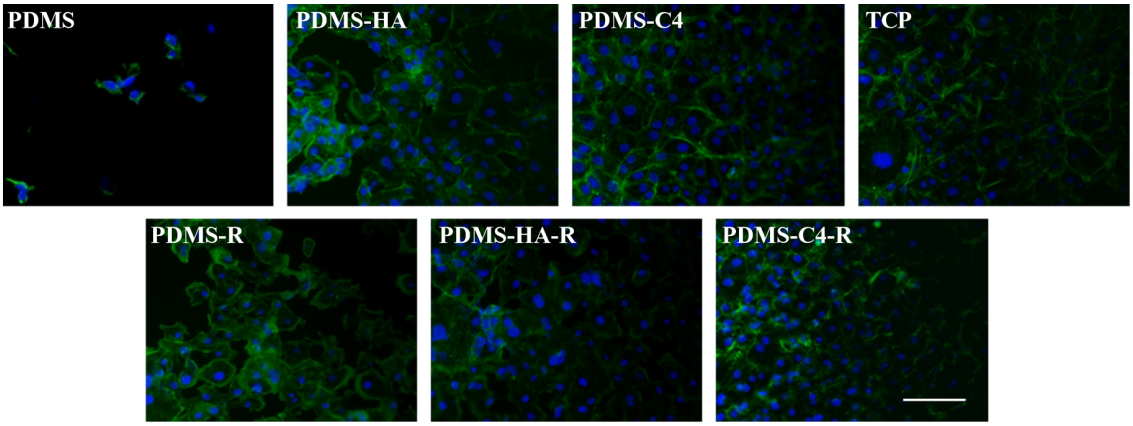

Figure 5.10 Actin cytoskeleton (green) and nuclei (blue) staining of CECs on PDMS substrates (Scale bar = 100 μm).

Expression of CEC-relative marker Na^+/K^+ ATPase was investigated (Figure 5.11) to verify the CEC phenotype via immunofluorescent staining. All experimental groups gave positive signals with varying dispersion. In flat native and HA functionalized PDMS, Na^+/K^+ ATPase signals were not intense, whereas PDMS-C4 provided the highest Na^+/K^+ ATPase activity, including the positive control group-TCP. White rose patterning resulted in an increase of stained areas in all groups. Among patterned substrates, uniform distribution and the highest staining intensity were achieved on PDMS-C4-R with densely populated CECs.

Further investigation of CEC phenotype specific markers was conducted with the cell substrates that showed enhanced cell responses in Na^+/K^+ ATPase immunostaining: PDMS-C4, PDMS-C4-R and TCP. Western blot analysis on Figure 5.12 demonstrated that depositions of CEC-related functional proteins, Na^+/K^+ ATPase, N-Cadherin and Collagen IV were detected on all these substrates with relatively highest expressions on PDMS-C4-R. Confirming immunostaining results, Na^+/K^+ ATPase expression of cells was significantly higher on patterned PDMS-C4, than flat one ($^*p < 0.05$), similar to another CEC-specific marker, N-Cadherin. Although PDMS-C4-R group showed the highest expression, the difference between PDMS-C4-R and TCP was not significant for both Na^+/K^+ ATPase and N-Cadherin [Figure 5.12(a-b)]. However,

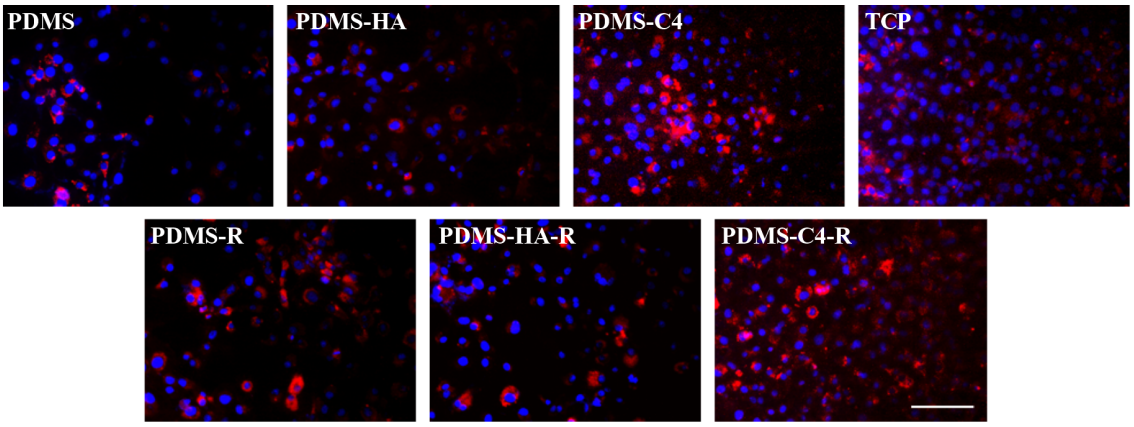

Figure 5.11 Immunofluorescent staining of CECs for Na^+/K^+ ATPase (red) and DAPI (blue). Scale bar = 100 μm).

deposition of Collagen IV [Figure 5.12(c)] was significantly up-regulated on patterned PDMS-C4-R than its flat version ($^{**}p < 0.01$) and TCP ($^{*}p < 0.05$). Collagen IV is one the most important ECM components for the maintenance of healthy CEC hexagonal morphology. Increased expression of Collagen IV, in addition to Na^+/K^+ ATPase and N-Cadherin implied that white rose negative relief patterned PDMS substrates enhanced CEC-specific functions, *in vitro*.

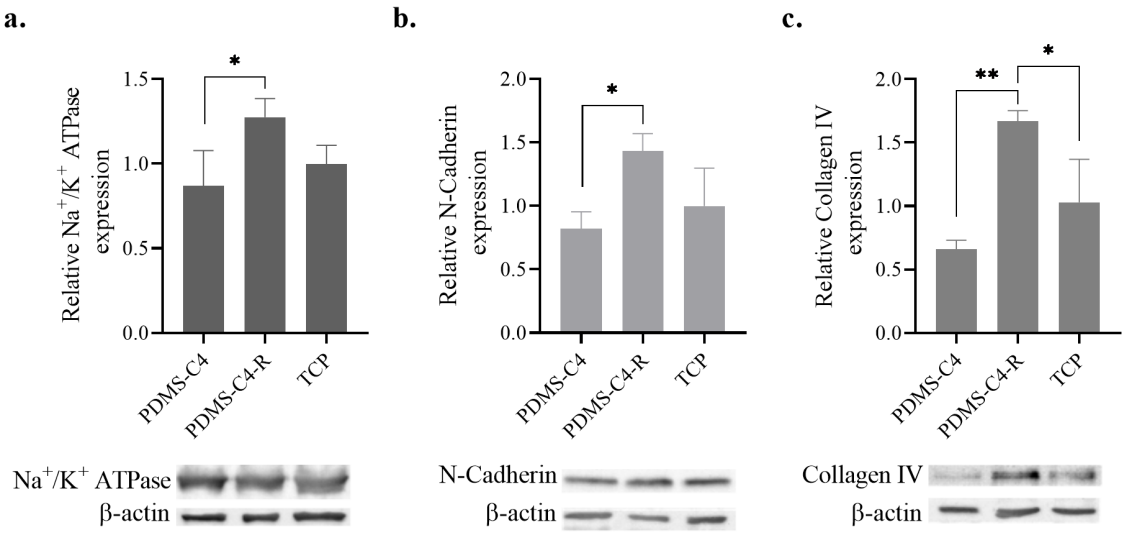

Figure 5.12 Western blot analysis of CECs on PDMS-C4, PDMS-C4-R and TCP. Quantification of (a) Na^+/K^+ ATPase, (b) N-Cadherin and (c) Collagen IV markers relative to β-actin ($^{*}p < 0.05$ and $^{**}p < 0.01$).

5.5 Discussion

In this study, biomimetic PDMS cell substrates having a cornea-friendly stiffness, white rose petal negative relief patterned surface topography and corneal ECM-like surface biochemistry were developed. A successful cell substrate should support *in vitro* cell attachment, proliferation and cell type specific functions, as if those cells are at their own *in vivo* environment. Therefore, there is growing interest on preparation of natural cell microenvironment-like substrates having well-regulated mechanical, physical and biochemical properties. Here, we focused on CECs, as they are one of the cell types, which cannot regenerate *in vivo* and the decrease in cell number would eventually cause certain diseases and vision loss [127, 117]. Keratoplasty has been the main treatment of such corneal endothelial diseases, however due to the limited availability of donor tissues, new approaches are required [224]. The major challenge in the development of alternative methods is the expansion of functional CECs *in vitro*. Production of successful cell substrates for functional CECs proliferation *in vitro* would not only enable treatment opportunities to more patients using lower number of donor corneas, but also would provide an alternative environment to drug design or cell therapy applications. To address this need, we have developed a cell substrate for *in vitro* CEC culture (PDMS-C4-R) with optimized surface properties.

Micro- to nano-scale topographical features on materials are sensed by cells and modulate their behavior [225, 226]. Various cell types, like fibroblasts [227], osteoblasts [228] or MSCs [229], have been investigated to show the effect of substrate surface topography on cell response. Similarly, in corneal regeneration and reconstruction, numerous studies demonstrated the influence of micro- and nanoscale geometrical cues on cell adhesion, maturation, proliferation, morphology or differentiation [86]. Simple pattern cues (grooves, wells, pillars, pits, etc.) have been fabricated for corneal epithelial cells [230], corneal keratinocytes [231], corneal keratocytes [232], corneal stromal cells [233] or CECs [234]. However high precision design considerations on natural microenvironment architecture are required to produce substrate surfaces with enhanced biomimetic topography. In their native microenvironment, CECs are in direct contact with the nanotopography of underlying Descemet's membrane [235]. Inspired by

these isotropic cues, micro- and nanoscale pillars and wells were formed on various substrates, like PDMS or TCP, and these patterned substrates provided enhanced CEC proliferation and functional marker expression [135, 234, 126]. Instead of producing geometrical structures on cell substrates, we took the advantage of naturally occurring nano- and micropatterns with healthy corneal endothelium-like topography: rose petals. Red and white (both in dry and fresh form) rose petal topographies were investigated with SEM after PDMS replication [Figure 5.3(a)]. Fresh white rose petal mimicked surfaces showed healthy CEC shape-like hexagonal patterns [Figure 5.3(c-i)] [224]. Furthermore, the density of these patterns ($\approx$ 2000 cells/mm^2) was in the physiologically relevant range of corneal endothelium (well above the critical level, which is between 400-500 cells/mm^2 [236]), depth of hexagonal shapes ($\approx$ 6.6 μm), were similar to CECs ($\approx$ 5 μm) [216] and nanotopographical cues were naturally formed inside each hexagon [Figure 5.3(b-i) and Figure 5.3(c-ii)]. SEM images of copies confirmed that a PDMS mold could be used for at least 10 times with excellent pattern fidelity (Figure 5.4).

For the production of cell substrates, we investigated Young's modulus of PDMS with various pre-polymer and curing agent ratios, as cells are also responsive to the stiffness of their environment [127, 237]. Palchesko et al. confirmed that substrates with Descemet's membrane-like chemo-mechanical properties resulted improved CEC behavior. Among other ECM proteins and substrates with various stiffness, Collagen IV coated PDMS with an elastic modulus of 50 kPa was found to enhance CEC proliferation ($>$ 3000 fold) and the expression of phenotypic markers [51]. We used 10:1 to 30:1 PDMS pre-polymer to curing agent ratios in this study and 30:1 PDMS with 211.85$\pm$74.9 kPa Young's modulus (Figure 5.5) was found in the bulk modulus range of cornea, which is between 200-290 kPa [217, 218, 219, 220]. All patterned cell substrates were prepared using 30:1, as using PDMS with lower curing agent amounts did not allow successful replication. By adjusting PDMS stiffness to this cornea-friendly range, biomimetic properties of cell substrates were enhanced.

In addition to the optimized topographical and mechanical properties of PDMS substrates, we have also functionalized their surfaces with two corneal ECM compo-

nents: HA and COL 4. Although patterning resulted a significant increase in CEC proliferation ($p < 0.0001$, Figure 5.9) and the number of attached cells (Figure 5.10), actin fibers were disrupted on native PDMS and did not provide linking between adjacent cells, revealing the importance of surface chemical modification. Functionalization of PDMS surfaces with HA or COL 4 was completed using NHS/EDC chemistry (Figure 5.2) and demonstrated by WCA measurements, XPS analysis and immunofluorescent staining (Figures 5.6, 5.7 and 5.8). The presence of N-C=O, C=O and the significant increase in C-N and C-C peaks in high resolution C1s spectra of PDMS-HA [Figure 5.7(d)] and PDMS-C4 [Figure 5.7(e)] indicated that modification was achieved successfully [238, 214, 221]. Additionally, wettability properties of HA and COL 4 modified PDMS (Figure 5.6) were consistent with the literature with hydrophilic PDMS-C4 [239] and relatively hydrophobic nature of PDMS-HA [240]. After successful functionalization of PDMS substrates with these corneal ECM components, proliferation of CECs was enhanced, as seen in Figure 5.9. This effect was more distinctive in PDMS-C4, as collagen type IV is one of the main constituents of Descemet's membrane [241]. Accordingly, PDMS-C4 successfully mimics the natural microenvironment of CECs. Among all flat PDMS substrates, PDMS-C4 provided the most suitable environment for CEC expansion [Figure 5.9(a)], whereas white rose patterning of PDMS-C4 enhanced proliferative capacity of CECs significantly ($p < 0.0001$) and showed similar effects with the control group, TCP [Figure 5.9(b-c)]. Although HA modification of PDMS did not change CEC metabolic activities, it ensured cellular attachment and better cytoskeleton formation, when compared to native PDMS (Figure 5.10). HA is a naturally occurring glycosaminoglycan and known to facilitate cell adhesion [131]. Especially on PDMS-HA-R, cell adhesion was considerably higher, due to the enhanced biomimetic properties of substrates. However, even flat PDMS-C4 provided better cell adhesion than patterned PDMS-HA, with improved interconnections between cells and increased attached cell number. Moreover, cells on patterned PDMS-C4 showed typical CEC polygonal shapes and formed a confluent cell monolayer, whereas elongated CEC shapes with relatively low number of cells were found on TCP. Actin cytoskeleton staining of CECs on patterned PDMS showed the guidance effect of white rose petal negative relief topography, with enhanced interconnections between adjacent cells and maintenance of uniform hexagonal CEC shape.

PDMS-C4-R cell substrates were not only effective for *in vitro* CEC proliferation, but also for their physiological functionality. Na^+/K^+ ATPase expression of cells on substrates was investigated to evaluate the activity and vitality of CECs. Localization of Na^+/K^+ ATPase is very crucial for the regulation of corneal pumping function. This pump function prevents stroma from overhydration and maintains optical transparency [242]. Positive immunostaining of Na^+/K^+ ATPase was observed on all substrates (Figure 5.11); however, the staining intensity was higher in flat and patterned, COL 4 modified PDMS. Teo et al. reported that laminin coated micro- and nanopatterned PDMS with 10:1 pre-polymer to curing agent ratio enhanced Na^+/K^+ ATPase expression of CECs [135]. Similarly, CECs on micro- and nanoscale patterned TCP showed enhanced functional marker expression [126]. In our study, among all substrates including TCP, PDMS-C4-R facilitated the highest immunofluorescent intensity against Na^+/K^+ ATPase, whereas both PDMS-C4-R and TCP showed similar CEC proliferation. Western blot analysis confirmed immunostaining results with enhanced CEC phenotype specific marker expressions arising from white rose petal mimicked surface topography (Figure 5.12). Significantly higher up-regulations of healthy corneal endothelium related morphological and functional proteins of Collagen IV [124], Na^+/K^+ ATPase [243] and N-Cadherin [120] indicated that combination of cornea-friendly substrate stiffness with biomimetic surface chemistry and topography predominates over the positive effects of TCP on CECs and PDMS-C4-R provided functional expansion of CECs.

6. CONCLUSION

This thesis described single or simultaneous influences of biomimetic chemical modification, tissue type-specific mechanical adjustments and topographical alteration of PDMS substrates on osteoblasts, iPSCs and their differentiation into cardiomyocytes and CECs. In Chapter 3, His-SAM and Leu-SAM were synthesized; optimum parameters to modify PDMS were investigated and successful modifications were confirmed via XPS and WCA analyses. Both AA-SAMs modified PDMS substrates provided improved osteoblast cell proliferation and maturation; however, at the longer culture duration, hydrophilic His-SAM facilitated a superior osteoblastic behavior than Leu-SAM and the positive control, TCP. Moreover, His-SAM and Leu-SAM provided a supportive environment to hFOB cells for three weeks of culture, proving that modification stability could be preserved with SAMs for at least three weeks. In Chapter 4, PDMS substrate stiffness was adjusted to the stiffness of healthy cardiac environment by using 50:1 mass ratio. Surface modifications with conventional (APTES, OTS) and AA-SAMs (His-SAM, Leu-SAM) were completed and confirmed. All SAMs modifications were found to improve iPSC behavior and cardiac differentiation, when compared with native PDMS. Moreover, specifically PDMS-L was found to be highly supportive for cardiac differentiation of iPSC with statistically increased cardiac marker expression. In Chapter 5, similarities between white rose petal topography and natural healthy CEC microenvironment have been demonstrated for the first time in the literature. Moreover, PDMS substrates were prepared in a cornea-friendly stiffness range and modified with two of the important CEC microenvironment components: COL 4 and HA. White rose petal patterned and COL 4 modified PDMS with optimized stiffness provided enhanced bovine CEC response with higher density monolayers and increased phenotypic marker expression. Taken all these together, we have not only shown the single and synergetic effects of substrate chemical, mechanical and topographical properties, but also provided cell type specific, simple and effective production strategies for highly supportive cell substrates, which can be applied to *in vitro* cell culture studies, regenerative medicine applications and as well as microfluidics.

REFERENCES

1. Huang, G., F. Li, X. Zhao, Y. Ma, Y. Li, M. Lin, G. Jin, T. J. Lu, G. M. Genin, and F. Xu, "Functional and Biomimetic Materials for Engineering of the Three-Dimensional Cell Microenvironment," *Chemical Reviews*, Vol. 17, no. 20, pp. 12764–12850, 2017.

2. Schoen, F. J., and R. N. Mitchell, "Tissues, the Extracellular Matrix, and Cell-Biomaterial Interactions," in *Biomaterials Science: An Introduction to Materials*, Academic Press, 3rd ed., 2013.

3. Urbanczyk, M., S. L. Layland, and K. Schenke-Layland, "The role of extracellular matrix in biomechanics and its impact on bioengineering of cells and 3D tissues," *Matrix Biology*, Vol. 85–86, pp. 1–14, 2020.

4. Rizwan, M., J. W. Tse, A. Nori, K. W. Leong, and E. K. F. Yim, "Cell-Substrate Interactions," in *Principles of Regenerative Medicine* (Atala, A., R. Lanza, A. G. Mikos, and R. B. T. P. o. R. M. T. E. Nerem, eds.), ch. 27, pp. 437–468, Boston: Academic Press, 2019.

5. Amani, H., H. Arzaghi, M. Bayandori, A. S. Dezfuli, H. Pazoki-Toroudi, A. Shafiee, and L. Moradi, "Controlling Cell Behavior through the Design of Biomaterial Surfaces: A Focus on Surface Modification Techniques," *Advanced Materials Interfaces*, Vol. 6, no. 13, p. 1900572, 2019.

6. Teixeira, A. I., G. A. Abrams, P. J. Bertics, C. J. Murphy, and P. F. Nealey, "Epithelial contact guidance on well-defined micro- and nanostructured substrates," *Journal of Cell Science*, Vol. 116, pp. 1881–1892, 2003.

7. Fraser, S. A., Y. H. Ting, K. S. Mallon, A. E. Wendt, C. J. Murphy, and P. F. Nealey, "Sub-micron and nanoscale feature depth modulates alignment of stromal fibroblasts and corneal epithelial cells in serum-rich and serum-free media," *Journal of Biomedical Materials Research - Part A*, Vol. 86, no. 3, pp. 725–735, 2008.

8. Teixeira, A. I., G. A. McKie, J. D. Foley, P. J. Bertics, P. F. Nealey, and C. J. Murphy, "The effect of environmental factors on the response of human corneal epithelial cells to nanoscale substrate topography," *Biomaterials*, Vol. 27, pp. 3945–3954, 2006.

9. Han, Y. L., S. Wang, X. Zhang, Y. Li, G. Huang, H. Qi, B. Pingguan-Murphy, Y. Li, T. J. Lu, and F. Xu, "Engineering physical microenvironment for stem cell based regenerative medicine," *Drug Discovery Today*, Vol. 19, no. 6, pp. 763–773, 2014.

10. Takahashi, K., K. Tanabe, M. Ohnuki, M. Narita, T. Ichisaka, K. Tomoda, and S. Yamanaka, "Induction of Pluripotent Stem Cells from Adult Human Fibroblasts by Defined Factors," *Cell*, Vol. 131, pp. 861–872, 2007.

11. Kanzaki, Y., F. Terasaki, M. Okabe, S. Fujita, T. Katashima, K. Otsuka, and N. Ishizaka, "Three-dimensional architecture of cardiomyocytes and connective tissue in human heart revealed by scanning electron microscopy," *Circulation*, Vol. 122, no. 19, pp. 1973–1974, 2010.

12. Gerbin, K. A., K. A. Mitzelfelt, X. Guan, A. M. Martinson, and C. E. Murry, "Delta-1 Functionalized Hydrogel Promotes hESC-Cardiomyocyte Graft Proliferation and Maintains Heart Function Post-Injury," *Molecular Therapy - Methods and Clinical Development*, Vol. 17, pp. 986–998, 2020.

13. Park, S. J., R. Y. Kim, B. W. Park, S. Lee, S. W. Choi, J. H. Park, J. J. Choi, S. W. Kim, J. Jang, D. W. Cho, H. M. Chung, S. H. Moon, K. Ban, and H. J. Park, "Dual stem cell therapy synergistically improves cardiac function and vascular regeneration following myocardial infarction," *Nature Communications*, Vol. 10, p. 3123, 2019.

14. Park, J., C. W. Anderson, L. R. Sewanan, M. H. Kural, Y. Huang, J. Luo, L. Gui, M. Riaz, C. A. Lopez, R. Ng, S. K. Das, J. Wang, L. Niklason, S. G. Campbell, and Y. Qyang, "Modular design of a tissue engineered pulsatile conduit using human induced pluripotent stem cell-derived cardiomyocytes," *Acta Biomaterialia*, Vol. 102, pp. 220–230, 2020.

15. Agarwal, A., J. A. Goss, A. Cho, M. L. McCain, and K. K. Parker, "Microfluidic heart on a chip for higher throughput pharmacological studies," *Lab on a Chip*, Vol. 13, no. 18, pp. 3599–3608, 2013.

16. Jeong, Y. J., D. S. Kim, J. Y. Kim, N. E. Oyunbaatar, B. K. Lee, E. S. Kim, and D. W. Lee, "Drug-induced changes in mechanical behavior of electrically synchronized cardiomyocytes on surface-patterned polydimethylsiloxane diaphragm," *Sensors and Actuators, A: Physical*, Vol. 301, p. 111760, 2020.

17. Kolanowski, T. J., M. Busek, M. Schubert, A. Dmitrieva, B. Binnewerg, J. Pöche, K. Fisher, F. Schmieder, S. Grünzner, S. Hansen, A. Richter, A. El-Armouche, F. Sonntag, and K. Guan, "Enhanced structural maturation of human induced pluripotent stem cell-derived cardiomyocytes under a controlled microenvironment in a microfluidic system," *Acta Biomaterialia*, Vol. 102, pp. 273–286, 2020.

18. Mastikhina, O., B. U. Moon, K. Williams, R. Hatkar, D. Gustafson, O. Mourad, X. Sun, M. Koo, A. Y. Lam, Y. Sun, J. E. Fish, E. W. Young, and S. S. Nunes, "Human cardiac fibrosis-on-a-chip model recapitulates disease hallmarks and can serve as a platform for drug testing," *Biomaterials*, Vol. 233, p. 119741, 2020.

19. Fu, J., Y. J. Chuah, J. Liu, S. Y. Tan, and D. A. Wang, "Respective Effects of Gelatin-Coated Polydimethylsiloxane (PDMS) Substrates on Self-renewal and Cardiac Differentiation of Induced Pluripotent Stem Cells (iPSCs)," *ACS Biomaterials Science and Engineering*, Vol. 4, no. 12, pp. 4321–4330, 2018.

20. Chuah, Y. J., Z. T. Heng, J. S. Tan, L. M. Tay, C. S. Lim, Y. Kang, and D. A. Wang, "Surface modifications to polydimethylsiloxane substrate for stabilizing prolonged bone marrow stromal cell culture," *Colloids and Surfaces B: Biointerfaces*, Vol. 191, p. 110995, 2020.

21. Hassler, C., T. Boretius, and T. Stieglitz, "Polymers for neural implants," *Journal of Polymer Science, Part B: Polymer Physics*, Vol. 49, pp. 18–33, 2011.

22. Poojari, Y., "Silicones for Encapsulation of Medical Device Implants," *Silicon*, Vol. 9, pp. 645–649, 2017.

23. El-Ali, J., P. K. Sorger, and K. F. Jensen, "Cells on chips," *Nature*, Vol. 442, pp. 403–411, 2006.

24. Quirós-Solano, W. F., N. Gaio, O. M. Stassen, Y. B. Arik, C. Silvestri, N. C. Van Engeland, A. Van der Meer, R. Passier, C. M. Sahlgren, C. V. Bouten, A. van den Berg, R. Dekker, and P. M. Sarro, "Microfabricated tuneable and transferable porous PDMS membranes for Organs-on-Chips," *Scientific Reports*, Vol. 8, p. 13524, 2018.

25. Dittrich, P. S., and A. Manz, "Lab-on-a-chip: Microfluidics in drug discovery," *Nature Reviews Drug Discovery*, Vol. 5, pp. 210–218, 2006.

26. Wei, C., B. Fan, D. Chen, C. Liu, Y. Wei, B. Huo, L. You, J. Wang, and J. Chen, "Osteocyte culture in microfluidic devices," *Biomicrofluidics*, Vol. 9, no. 1, p. 014109, 2015.

27. Tu, Q., J. C. Wang, Y. Zhang, R. Liu, W. Liu, L. Ren, S. Shen, J. Xu, L. Zhao, and J. Wang, "Surface modification of poly(dimethylsiloxane) and its applications in microfluidics-based biological analysis," *Reviews in Analytical Chemistry*, Vol. 31, pp. 177–192, 2012.

28. Bodas, D., and C. Khan-Malek, "Hydrophilization and hydrophobic recovery of PDMS by oxygen plasma and chemical treatment-An SEM investigation," *Sensors and Actuators, B: Chemical*, Vol. 123, pp. 368–373, 2007.

29. Palchesko, R. N., L. Zhang, Y. Sun, and A. W. Feinberg, "Development of Polydimethylsiloxane Substrates with Tunable Elastic Modulus to Study Cell Mechanobiology in Muscle and Nerve," *Plos One*, Vol. 7, p. e51499, 2012.

30. Pan, C. J., H. Qin, Y. D. Nie, and H. Y. Ding, "Control of osteoblast cells adhesion and spreading by microcontact printing of extracellular matrix protein patterns," *Colloids and Surfaces B: Biointerfaces*, Vol. 104, pp. 18–26, 2013.

31. Ribeiro, A. J., K. Zaleta-Rivera, E. A. Ashley, and B. L. Pruitt, "Stable, covalent attachment of laminin to microposts improves the contractility of mouse neonatal cardiomyocytes," *ACS Applied Materials and Interfaces*, Vol. 6, pp. 15516–15526, 2014.

32. Chuah, Y. J., Y. T. Koh, K. Lim, N. V. Menon, Y. Wu, and Y. Kang, "Simple surface engineering of polydimethylsiloxane with polydopamine for stabilized mesenchymal stem cell adhesion and multipotency," *Scientific Reports*, 2015.

33. Kuddannaya, S., Y. J. Chuah, M. H. A. Lee, N. V. Menon, Y. Kang, and Y. Zhang, "Surface chemical modification of poly(dimethylsiloxane) for the enhanced adhesion and proliferation of mesenchymal stem cells," *ACS Applied Materials and Interfaces*, Vol. 5, pp. 9777–9784, 2013.

34. Bhairamadgi, N. S., S. P. Pujari, F. G. Trovela, A. Debrassi, A. A. Khamis, J. M. Alonso, A. A. Al Zahrani, T. Wennekes, H. A. Al-Turaif, C. Van Rijn, Y. A. Alhamed, and H. Zuilhof, "Hydrolytic and thermal stability of organic monolayers on various inorganic substrates," *Langmuir*, Vol. 30, pp. 5829–5839, 2014.

35. Hasan, A., S. K. Pattanayek, and L. M. Pandey, "Effect of Functional Groups of Self-Assembled Monolayers on Protein Adsorption and Initial Cell Adhesion," *ACS Biomaterials Science & Engineering*, Vol. 4, pp. 3224–3233, 9 2018.

36. Hasan, A., and L. M. Pandey, "Surface modification of Ti6Al4V by forming hybrid self-assembled monolayers and its effect on collagen-I adsorption, osteoblast adhesion and integrin expression," *Applied Surface Science*, Vol. 505, p. 144611, 2019.

37. Mani, G., D. M. Johnson, D. Marton, M. D. Feldman, D. Patel, A. A. Ayon, and C. M. Agrawal, "Drug delivery from gold and titanium surfaces using self-assembled monolayers," *Biomaterials*, Vol. 29, pp. 4561–4573, 2008.

38. Alonso, J. M., A. A. Bielen, W. Olthuis, S. W. Kengen, H. Zuilhof, and M. C. Franssen, "Self-assembled monolayers of 1-alkenes on oxidized platinum surfaces as platforms for immobilized enzymes for biosensing," *Applied Surface Science*, Vol. 383, pp. 283–293, 2016.

39. Nanci, A., J. D. Wuest, L. Peru, P. Brunet, V. Sharma, S. Zalzal, and M. D. McKee, "Chemical modification of titanium surfaces for covalent attachment of biological molecules," *Journal of Biomedical Materials Research*, Vol. 40, pp. 324–335, 1998.

40. Pandey, L. M., and S. K. Pattanayek, "Hybrid surface from self-assembled layer and its effect on protein adsorption," *Applied Surface Science*, Vol. 257, pp. 4731–4737, 2011.

41. Marín-Pareja, N., M. Cantini, C. González-García, E. Salvagni, M. Salmerón-Sánchez, and M. P. Ginebra, "Different Organization of Type I Collagen Immobilized on Silanized and Nonsilanized Titanium Surfaces Affects Fibroblast Adhesion and Fibronectin Secretion," *ACS Applied Materials and Interfaces*, Vol. 7, pp. 20667–20677, 2015.

42. Cao, B., Y. Peng, X. Liu, and J. Ding, "Effects of Functional Groups of Materials on Nonspecific Adhesion and Chondrogenic Induction of Mesenchymal Stem Cells on Free and Micropatterned Surfaces," *ACS Applied Materials & Interfaces*, Vol. 9, pp. 23574–23585, 7 2017.

43. Padial-Molina, M., P. Galindo-Moreno, J. E. Fernández-Barbero, F. O'Valle, A. B. Jódar-Reyes, J. L. Ortega-Vinuesa, and P. J. Ramón-Torregrosa, "Role of wettability and nanoroughness on interactions between osteoblast and modified silicon surfaces," *Acta Biomaterialia*, Vol. 7, pp. 771–778, 2011.

44. Conconi, M. T., M. Tommasini, E. Muratori, and P. P. Parnigotto, "Essential amino acids increase the growth and alkaline phosphatase activity in osteoblasts cultured in vitro," *Farmaco*, Vol. 56, pp. 755–61, 2001.

45. Sun, S., H. Shi, S. Moore, C. Wang, A. Ash-Shakoor, P. T. Mather, J. H. Henderson, and Z. Ma, "Progressive Myofibril Reorganization of Human Cardiomyocytes on a Dynamic Nanotopographic Substrate," *ACS Applied Materials and Interfaces*, Vol. 12, pp. 21450–21462, 2020.

46. Sung, T.-C., H. C. Su, Q.-D. Ling, S. S. Kumar, Y. Chang, S.-T. Hsu, and A. Higuchi, "Efficient differentiation of human pluripotent stem cells into cardiomyocytes on cell sorting thermoresponsive surface," *Biomaterials*, Vol. 253, p. 120060, 2020.

47. Berry, M. F., A. J. Engler, Y. J. Woo, T. J. Pirolli, L. T. Bish, V. Jayasankar, K. J. Morine, T. J. Gardner, D. E. Discher, and H. L. Sweeney, "Mesenchymal stem cell injection after myocardial infarction improves myocardial compliance," *American Journal of Physiology-Heart and Circulatory Physiology*, Vol. 290, pp. H2196–H2203, 6 2006.

48. Breitbach, M., T. Bostani, W. Roell, Y. Xia, O. Dewald, J. M. Nygren, J. W. Fries, K. Tiemann, H. Bohlen, J. Hescheler, A. Welz, W. Bloch, S. E. W. Jacobsen, and B. K. Fleischmann, "Potential risks of bone marrow cell transplantation into infarcted hearts," *Blood*, Vol. 110, pp. 1362–1369, 2007.

49. Engler, A. J., C. Carag-Krieger, C. P. Johnson, M. Raab, H.-Y. Tang, D. W. Speicher, J. W. Sanger, J. M. Sanger, and D. E. Discher, "Embryonic cardiomyocytes beat best on a matrix with heart-like elasticity: scar-like rigidity inhibits beating," *Journal of Cell Science*, Vol. 121, pp. 3794–3802, 2008.

50. Engler, A. J., S. Sen, H. L. Sweeney, and D. E. Discher, "Matrix Elasticity Directs Stem Cell Lineage Specification," *Cell*, Vol. 126, pp. 677–689, 2006.

51. Palchesko, R. N., K. L. Lathrop, J. L. Funderburgh, and A. W. Feinberg, "In vitro expansion of corneal endothelial cells on biomimetic substrates.," *Scientific reports*, Vol. 5, p. 7955, 2015.

52. Velve-Casquillas, G., M. Le Berre, M. Piel, and P. T. Tran, "Microfluidic tools for cell biological research," *Nano Today*, Vol. 5, no. 1, pp. 28–47, 2010.

53. Wu, M. H., S. B. Huang, and G. B. Lee, "Microfluidic cell culture systems for drug research," *Lab on a Chip*, Vol. 10, no. 8, pp. 939–956, 2010.

54. Mount, N. M., S. J. Ward, P. Kefalas, and J. Hyllner, "Cell-based therapy technology classifications and translational challenges," *Philosophical Transactions of the Royal Society B: Biological Sciences*, Vol. 370, 2015.

55. Khot, M. I., M. A. Levenstein, G. N. de Boer, G. Armstrong, T. Maisey, H. S. Svavarsdottir, H. Andrew, S. L. Perry, N. Kapur, and D. G. Jayne, "Characterising a PDMS based 3D cell culturing microfluidic platform for screening chemotherapeutic drug cytotoxic activity," *Scientific Reports*, Vol. 10, 2020.

56. Warrick, J. W., W. L. Murphy, and D. J. Beebe, "Screening the Cellular Microenvironment: A Role for Microfluidics," *IEEE Reviews in Biomedical Engineering*, Vol. 1, pp. 75–93, 2008.

57. Barthes, J., H. Ozcelik, M. Hindie, A. Ndreu-Halili, A. Hasan, and N. E. Vrana, "Cell microenvironment engineering and monitoring for tissue engineering and regenerative medicine: the recent advances.," *BioMed research international*, Vol. 2014, p. 921905, 2014.

58. Öztürk Öncel, M. Ö., and B. Garipcan, "Stem Cell Behavior on Microenvironment Mimicked Surfaces," in *Advanced Surfaces for Stem Cell Research*, pp. 425–452, Wiley, 2016.

59. Yeste, J., X. Illa, M. Alvarez, and R. Villa, "Engineering and monitoring cellular barrier models," *Journal of Biological Engineering*, Vol. 12, no. 18, 2018.

60. Carmagnola, I., E. Ranzato, and V. Chiono, "Scaffold functionalization to support a tissue biocompatibility," in *Functional 3D Tissue Engineering Scaffolds: Materials, Technologies, and Applications*, ch. 11, pp. 255–277, Woodhead Publishing, 2018.

61. Mattson, J. M., R. Turcotte, and Y. Zhang, "Glycosaminoglycans contribute to extracellular matrix fiber recruitment and arterial wall mechanics," *Biomechanics and Modeling in Mechanobiology*, Vol. 16, pp. 213–225, 2017.

62. Hynes, R. O., "The extracellular matrix: not just pretty fibrils.," *Science (New York, N.Y.)*, Vol. 326, pp. 1216–1219, 2009.

63. Patterson, J., M. M. Martino, and J. A. Hubbell, "Biomimetic materials in tissue engineering," *Materials Today*, Vol. 13, pp. 14–22, 2010.

64. Kim, Y., H. Ko, I. K. Kwon, and K. Shin, "Extracellular Matrix Revisited: Roles in Tissue Engineering," *International neurourology journal*, Vol. 20, pp. S23–S29, 5 2016.

65. Sainio, A., and H. Järveläinen, "Extracellular matrix-cell interactions: Focus on therapeutic applications," *Cellular Signalling*, Vol. 66, 2020.

66. McMillen, P., and S. A. Holley, "Integration of cell-cell and cell-ECM adhesion in vertebrate morphogenesis," *Current Opinion in Cell Biology*, Vol. 36, pp. 48–53, 2015.

67. Li, Y., Y. Xiao, and C. Liu, "The Horizon of Materiobiology: A Perspective on Material-Guided Cell Behaviors and Tissue Engineering," *Chemical Reviews*, Vol. 117, pp. 4376–4421, 2017.

68. Ezashi, T., P. Das, and R. M. Roberts, "Low O2 tensions and the prevention of differentiation of hES cells," *Proceedings of the National Academy of Sciences of the United States of America*, Vol. 102, pp. 4783–4788, 2005.

69. Forristal, C. E., K. L. Wright, N. A. Hanley, R. O. Oreffo, and F. D. Houghton, "Hypoxia inducible factors regulate pluripotency and proliferation in human embryonic stem cells cultured at reduced oxygen tensions," *Reproduction*, Vol. 139, pp. 85–97, 2010.

70. Nakada, Y., D. C. Canseco, S. Thet, S. Abdisalaam, A. Asaithamby, C. X. Santos, A. M. Shah, H. Zhang, J. E. Faber, M. T. Kinter, L. I. Szweda, C. Xing, Z. Hu, R. J. Deberardinis, G. Schiattarella, J. A. Hill, O. Oz, Z. Lu, C. C. Zhang, W. Kimura, and H. A. Sadek, "Hypoxia induces heart regeneration in adult mice," *Nature*, Vol. 541, pp. 222–227, 2017.

71. Martinive, P., F. Defresne, C. Bouzin, J. Saliez, F. Lair, V. Grégoire, C. Michiels, C. Dessy, and O. Feron, "Preconditioning of the tumor vasculature and tumor cells by intermittent hypoxia: Implications for anticancer therapies," *Cancer Research*, Vol. 66, pp. 11736–44, 2006.

72. Brizzi, M. F., G. Tarone, and P. Defilippi, "Extracellular matrix, integrins, and growth factors as tailors of the stem cell niche," *Current Opinion in Cell Biology*, Vol. 24, pp. 645–51, 2012.

73. Geiger, B., J. P. Spatz, and A. D. Bershadsky, "Environmental sensing through focal adhesions," *Nature Reviews Molecular Cell Biology*, Vol. 10, pp. 21–33, 2009.

74. Sun, Y., C. S. Chen, and J. Fu, "Forcing stem cells to behave: A biophysical perspective of the cellular microenvironment," *Annual Review of Biophysics*, Vol. 41, pp. 519–42, 2012.

75. Yamamoto, K., T. Sokabe, T. Watabe, K. Miyazono, J. K. Yamashita, S. Obi, N. Ohura, A. Matsushita, A. Kamiya, and J. Ando, "Fluid shear stress induces differentiation of Flk-1-positive embryonic stem cells into vascular endothelial cells in vitro," *American Journal of Physiology - Heart and Circulatory Physiology*, Vol. 288, pp. H1915–24, 2005.

76. Folkman, J., and A. Moscona, "Role of cell shape in growth control," *Nature*, Vol. 273, pp. 345–349, 1978.

77. Stevens, M. M., and J. H. George, "Exploring and engineering the cell surface interface," *Science*, Vol. 310, pp. 1135–1138, 2005.

78. Wong, I., and C. M. Ho, "Surface molecular property modifications for poly(dimethylsiloxane) (PDMS) based microfluidic devices," *Microfluidics and Nanofluidics*, Vol. 7, 2009.

79. Manchineella, S., G. Thrivikraman, B. Basu, and T. Govindaraju, "Surface-functionalized silk fibroin films as a platform to guide neuron-like differentiation of human mesenchymal stem cells," *ACS Applied Materials and Interfaces*, Vol. 8, pp. 22849–59, 2016.

80. Kuddannaya, S., J. Bao, and Y. Zhang, "Enhanced in Vitro Biocompatibility of Chemically Modified Poly(dimethylsiloxane) Surfaces for Stable Adhesion and Long-term Investigation of Brain Cerebral Cortex Cells," *ACS Applied Materials and Interfaces*, Vol. 7, pp. 25529–38, 2015.

81. Yang, X., X. Wang, F. Yu, L. Ma, X. Pan, G. Luo, S. Lin, X. Mo, C. He, and H. Wang, "Hyaluronic acid/EDC/NHS-crosslinked green electrospun silk fibroin nanofibrous scaffolds for tissue engineering," *RSC Advances*, Vol. 6, pp. 99720–99728, 2016.

82. Sangsanoh, P., N. Israsena, O. Suwantong, and P. Supaphol, "Effect of the surface topography and chemistry of poly(3-hydroxybutyrate) substrates on cellular behavior of the murine neuroblastoma Neuro2a cell line," *Polymer Bulletin*, Vol. 74, pp. 4101–4118, 2017.

83. Curran, J. M., R. Chen, and J. A. Hunt, "The guidance of human mesenchymal stem cell differentiation in vitro by controlled modifications to the cell substrate," *Biomaterials*, Vol. 27, pp. 4783–93, 2006.

84. Curran, J. M., S. Fawcett, L. Hamilton, N. P. Rhodes, C. V. Rahman, M. Alexander, K. Shakesheff, and J. A. Hunt, "The osteogenic response of mesenchymal stem cells to an injectable PLGA bone regeneration system," *Biomaterials*, Vol. 34, pp. 9352–9364, 2013.

85. Chen, M., Y. Zhang, Y. Zhou, Y. Zhang, M. Lang, Z. Ye, and W. S. Tan, "Pendant small functional groups on poly(ϵ-caprolactone) substrate modulate adhesion, proliferation and differentiation of human mesenchymal stem cells," *Colloids and Surfaces B: Biointerfaces*, Vol. 134, pp. 322–331, 2015.

86. Xiong, S., H. C. Gao, L. Qin, Y. G. Jia, and L. Ren, "Engineering topography: Effects on corneal cell behavior and integration into corneal tissue engineering," *Bioactive Materials*, Vol. 4, pp. 293–302, 2019.

87. Ventre, M., F. Causa, and P. A. Netti, "Determinants of cell-material crosstalk at the interface: Towards engineering of cell instructive materials," *Journal of the Royal Society Interface*, Vol. 9, pp. 2017–32, 2012.

88. Cun, X., and L. Hosta-Rigau, "Topography: A biophysical approach to direct the fate of mesenchymal stem cells in tissue engineering applications," *Nanomaterials*, Vol. 10, 2020.

89. Lv, L., Y. Liu, P. Zhang, X. Zhang, J. Liu, T. Chen, P. Su, H. Li, and Y. Zhou, "The nanoscale geometry of TiO2 nanotubes influences the osteogenic differentiation of human adipose-derived stem cells by modulating H3K4 trimethylation," *Biomaterials*, Vol. 39, pp. 193–205, 2015.

90. Oh, S., K. S. Brammer, Y. S. Li, D. Teng, A. J. Engler, S. Chien, and S. Jin, "Stem cell fate dictated solely by altered nanotube dimension," *Proceedings of the National Academy of Sciences of the United States of America*, Vol. 106, pp. 2130–5, 2009.

91. Qiu, J., J. Li, S. Wang, B. Ma, S. Zhang, W. Guo, X. Zhang, W. Tang, Y. Sang, and H. Liu, "TiO2 Nanorod Array Constructed Nanotopography for Regulation of Mesenchymal Stem Cells Fate and the Realization of Location-Committed Stem Cell Differentiation," *Small*, Vol. 12, pp. 1770–1778, 2016.

92. Patra, S., S. Sarkar, S. K. Bera, G. K. Paul, and R. Ghosh, "Influence of surface topography and chemical structure on wettability of electrodeposited ZnO thin films," *Journal of Applied Physics*, Vol. 108, 2010.

93. Tengvall, P., "4.6 Protein Interactions With Biomaterials," in *Comprehensive Biomaterials II* (Ducheyne, P. B. T., ed.), pp. 70–84, Oxford: Elsevier, 2017.

94. Ferrari, M., F. Cirisano, and M. C. Morán, "Mammalian Cell Behavior on Hydrophobic Substrates: Influence of Surface Properties," *Colloids and Interfaces*, Vol. 3, 2019.

95. Toffoli, A., L. Parisi, M. G. Bianchi, S. Lumetti, O. Bussolati, and G. M. Macaluso, "Thermal treatment to increase titanium wettability induces selective proteins adsorption from blood serum thus affecting osteoblasts adhesion," *Materials Science and Engineering C*, Vol. 107, 2020.

96. Cai, S., C. Wu, W. Yang, W. Liang, H. Yu, and L. Liu, "Recent advance in surface modification for regulating cell adhesion and behaviors," *Nanotechnology Reviews*, Vol. 9, 2020.

97. Ayala, R., C. Zhang, D. Yang, Y. Hwang, A. Aung, S. S. Shroff, F. T. Arce, R. Lal, G. Arya, and S. Varghese, "Engineering the cell-material interface for controlling stem cell adhesion, migration, and differentiation," *Biomaterials*, Vol. 32, no. 15, pp. 3700–3711, 2011.

98. Yang, C. Y., L. Y. Huang, T. L. Shen, and J. Andrew Yeh, "Cell adhesion, morphology and biochemistry on nanotopographic oxidized silicon surfaces," *European Cells and Materials*, Vol. 20, pp. 415–30, 2010.

99. Padhi, A., and A. S. Nain, "ECM in Differentiation: A Review of Matrix Structure, Composition and Mechanical Properties," *Annals of Biomedical Engineering*, Vol. 48, no. 3, pp. 1071–1089, 2020.

100. Chaudhuri, O., J. Cooper-White, P. A. Janmey, D. J. Mooney, and V. B. Shenoy, "Effects of extracellular matrix viscoelasticity on cellular behaviour," *Nature*, Vol. 584, pp. 535–546, 2020.

101. Jiang, L., Z. Sun, X. Chen, J. Li, Y. Xu, Y. Zu, J. Hu, D. Han, and C. Yang, "Cells sensing mechanical cues: Stiffness influences the lifetime of cell-extracellular matrix interactions by affecting the loading rate," *ACS Nano*, Vol. 10, pp. 207–217, 2016.

102. Gerardo, H., A. Lima, J. Carvalho, J. R. D. Ramos, S. Couceiro, R. D. M. Travasso, R. Pires das Neves, and M. Grãos, "Soft culture substrates favor stem-like cellular phenotype and facilitate reprogramming of human mesenchymal stem/stromal cells (hMSCs) through mechanotransduction," *Scientific Reports*, Vol. 9, no. 1, p. 9086, 2019.

103. Xu, Y., S. Patnaik, X. Guo, Z. Li, W. Lo, R. Butler, A. Claude, Z. Liu, G. Zhang, J. Liao, P. M. Anderson, and J. Guan, "Cardiac differentiation of cardiosphere-derived cells in scaffolds mimicking morphology of the cardiac extracellular matrix," *Acta Biomaterialia*, Vol. 10, pp. 3449–3462, 2014.

104. Anselme, K., "Osteoblast adhesion on biomaterials," *Biomaterials*, Vol. 21, pp. 667–681, 2000.

105. Kazimierczak, P., and A. Przekora, "Osteoconductive and osteoinductive surface modifications of biomaterials for bone regeneration: A concise review," *Coatings*, Vol. 10, no. 10, 2020.

106. Xie, Y., C. Hu, Y. Feng, D. Li, T. Ai, Y. Huang, X. Chen, L. Huang, and J. Tan, "Osteoimmunomodulatory effects of biomaterial modification strategies on macrophage polarization and bone regeneration," *Regenerative Biomaterials*, Vol. 7, pp. 233–245, 2020.

107. Li, J., X. Liu, J. M. Crook, and G. G. Wallace, "3D Printing of Cytocompatible Graphene/Alginate Scaffolds for Mimetic Tissue Constructs," *Frontiers in bioengineering and biotechnology*, Vol. 8, p. 824, 7 2020.

108. Ullah, S., and X. Chen, "Fabrication, applications and challenges of natural biomaterials in tissue engineering," *Applied Materials Today*, Vol. 20, 2020.

109. Xing, H., R. Li, Y. Wei, B. Ying, D. Li, and Y. Qin, "Improved Osteogenesis of Selective-Laser-Melted Titanium Alloy by Coating Strontium-Doped Phosphate With High-Efficiency Air-Plasma Treatment," *Frontiers in Bioengineering and Biotechnology*, Vol. 8, p. 367, 2020.

110. Keselowsky, B. G., D. M. Collard, and A. J. García, "Integrin binding specificity regulates biomaterial surface chemistry effects on cell differentiation," *Proceedings of the National Academy of Sciences of the United States of America*, Vol. 102, pp. 5953–5957, 2005.

111. Kikuchi, K., and K. D. Poss, "Cardiac regenerative capacity and mechanisms," *Annual Review of Cell and Developmental Biology*, Vol. 28, pp. 719–741, 2012.

112. Sun, R., X. Li, M. Liu, Y. Zeng, S. Chen, and P. Zhang, "Advances in stem cell therapy for cardiovascular disease (Review)," *International Journal of Molecular Medicine*, Vol. 38, no. 1, pp. 23–29, 2016.

113. Sinnecker, D., K. L. Laugwitz, and A. Moretti, "Induced pluripotent stem cell-derived cardiomyocytes for drug development and toxicity testing," *Pharmacology and Therapeutics*, Vol. 143, pp. 246–252, 2014.

114. Xie, J., Q. Zhang, T. Zhu, Y. Zhang, B. Liu, J. Xu, and H. Zhao, "Substrate stiffness-regulated matrix metalloproteinase output in myocardial cells and cardiac fibroblasts: Implications for myocardial fibrosis," *Acta Biomaterialia*, Vol. 10, pp. 2463–72, 2014.

115. Fu, J., Y. J. Chuah, W. T. Ang, N. Zheng, and D.-A. Wang, "Optimization of a polydopamine (PD)-based coating method and polydimethylsiloxane (PDMS) substrates for improved mouse embryonic stem cell (ESC) pluripotency maintenance and cardiac differentiation.," *Biomaterials science*, Vol. 5, pp. 1156–1173, 5 2017.

116. Qiu, Y., A. F. Bayomy, M. V. Gomez, M. Bauer, P. Du, Y. Yang, X. Zhang, and R. Liao, "A role for matrix stiffness in the regulation of cardiac side population cell function," *American Journal of Physiology - Heart and Circulatory Physiology*, Vol. 308, no. 9, pp. H990–H997, 2015.

117. Tsao, Y. T., C. M. Cheng, W. C. Wu, and H. C. Chen, "Bioengineering of Human Corneal Endothelial Cells from Single- to Four-Dimensional Cultures," *Current Ophthalmology Reports*, Vol. 8, pp. 172–184, 2020.

118. Sanchis-Gimeno, J. A., A. Lleó-Pérez, L. Alonso, M. S. Rahhal, and F. Martínez-Soriano, "Corneal endothelial cell density decreases with age in emmetropic eyes," *Histology and Histopathology*, Vol. 20, pp. 423–427, 2005.

119. Hutcheon, A. E., J. D. Zieske, and X. Guo, "3D in vitro model for human corneal endothelial cell maturation," *Experimental Eye Research*, Vol. 184, pp. 183–191, 2019.

120. Sun, P., L. Shen, C. Zhang, L. Du, and X. Wu, "Promoting the expansion and function of human corneal endothelial cells with an orbital adipose-derived stem cell-conditioned medium," *Stem Cell Research and Therapy*, Vol. 8, p. 287, 2017.

121. Van den Bogerd, B., S. N. Dhubhghaill, C. Koppen, M. J. Tassignon, and N. Zakaria, "A review of the evidence for in vivo corneal endothelial regeneration," *Survey of Ophthalmology*, Vol. 63, no. 2, pp. 149–165, 2018.

122. Peh, G. S., R. W. Beuerman, A. Colman, D. T. Tan, and J. S. Mehta, "Human corneal endothelial cell expansion for corneal endothelium transplantation: An overview," *Transplantation*, Vol. 91, pp. 811–819, 2011.

123. Okumura, N., D. Matsumoto, Y. Fukui, M. Teramoto, H. Imai, T. Kurosawa, T. Shimada, F. Kruse, U. Schlötzer-Schrehardt, S. Kinoshita, and N. Koizumi, "Feasibility of cell-based therapy combined with descemetorhexis for treating Fuchs endothelial corneal dystrophy in rabbit model," *Plos One*, Vol. 13, p. e0191306, 2018.

124. Wang, Y.-H., T.-H. Young, and T.-J. Wang, "Investigating the effect of chitosan/ polycaprolactone blends in differentiation of corneal endothelial cells and extracellular matrix compositions," *Experimental Eye Research*, Vol. 185, p. 107679, 2019.

125. Chen, Z., X. Liu, J. You, Y. Song, E. Tomaskovic-Crook, G. Sutton, J. M. Crook, and G. G. Wallace, "Biomimetic corneal stroma using electro-compacted collagen," *Acta Biomaterialia*, Vol. 113, pp. 360–371, 2020.

126. Muhammad, R., G. S. Peh, K. Adnan, J. B. Law, J. S. Mehta, and E. K. Yim, "Micro- and nano-topography to enhance proliferation and sustain functional markers of donor-derived primary human corneal endothelial cells," *Acta Biomaterialia*, Vol. 19, pp. 138–148, 2015.

127. Mahdavi, S. S., M. J. Abdekhodaie, S. Mashayekhan, A. Baradaran-Rafii, and A. R. Djalilian, "Bioengineering Approaches for Corneal Regenerative Medicine," *Tissue Engineering and Regenerative Medicine*, Vol. 17, pp. 567–593, 2020.

128. Rafat, M., F. Li, P. Fagerholm, N. S. Lagali, M. A. Watsky, R. Munger, T. Matsuura, and M. Griffith, "PEG-stabilized carbodiimide crosslinked collagen-chitosan hydrogels for corneal tissue engineering," *Biomaterials*, Vol. 29, pp. 3960–3972, 2008.

129. Wang, T. J., I. J. Wang, S. Chen, Y. H. Chen, and T. H. Young, "The phenotypic response of bovine corneal endothelial cells on chitosan/polycaprolactone blends," *Colloids and Surfaces B: Biointerfaces*, Vol. 90, pp. 236–243, 2012.

130. Koivusalo, L., J. Karvinen, E. Sorsa, I. Jönkkäri, J. Väliaho, P. Kallio, T. Ilmarinen, S. Miettinen, H. Skottman, and M. Kellomäki, "Hydrazone crosslinked hyaluronan-based hydrogels for therapeutic delivery of adipose stem cells to treat corneal defects," *Materials Science and Engineering C*, Vol. 85, pp. 68–78, 2018.

131. Liu, Y., L. Ren, and Y. Wang, "Crosslinked collagen-gelatin-hyaluronic acid biomimetic film for cornea tissue engineering applications," *Materials Science and Engineering C*, Vol. 33, pp. 196–201, 2013.

132. An, J. H., S. Y. Park, G. H. Kim, I. P. Mo, S. Kim, H. M. Woo, and K. M. Park, "Tissue engineered ultra-thin descemet stripping corneal endothelial layers using porcine cornea and stem cells," *Experimental Eye Research*, Vol. 199, 2020.

133. El-Sherbiny, I. M., and M. H. Yacoub, "Hydrogel scaffolds for tissue engineering: Progress and challenges," *Global Cardiology Science and Practice*, Vol. 2013, pp. 316–342, 2013.

134. Teichmann, J., M. Valtink, M. Nitschke, S. Gramm, R. Funk, K. Engelmann, and C. Werner, "Tissue Engineering of the Corneal Endothelium: A Review of Carrier Materials," *Journal of Functional Biomaterials*, Vol. 4, pp. 178–208, 2013.

135. Teo, B. K. K., K. J. Goh, Z. J. Ng, S. Koo, and E. K. F. Yim, "Functional reconstruction of corneal endothelium using nanotopography for tissue-engineering applications," *Acta Biomaterialia*, Vol. 8, no. 8, pp. 2941–2952, 2012.

136. Gutermuth, A., J. Maassen, E. Harnisch, D. Kuhlen, A. Sauer-Budge, C. Skazik-Voogt, and K. Engelmann, "Descemet's Membrane Biomimetic Microtopography Differentiates Human Mesenchymal Stem Cells into Corneal Endothelial-Like Cells," *Cornea*, Vol. 38, pp. 110–119, 2019.

137. Katritzky, A. R., P. Angrish, D. Hür, and K. Suzuki, "N-(Cbz- and Fmoc-α-aminoacyl)benzotriazoles: Stable derivatives enabling peptide coupling of Tyr, Trp, Cys, Met, and Gln with free amino acids in aqueous media with complete retention of chirality," *Synthesis*, Vol. 3, pp. 397–402, 2005.

138. Öztürk-Öncel, M. Ö., S. Odabaş, L. Uzun, D. Hür, and B. Garipcan, "A facile surface modification of poly(dimethylsiloxane) with amino acid conjugated self-assembled monolayers for enhanced osteoblast cell behavior," *Colloids and Surfaces B: Biointerfaces*, Vol. 196, 2020.

139. Kangwansupamonkon, W., N. Klaikaew, and S. Kiatkamjornwong, "Green synthesis of titanium dioxide/acrylamide-based hydrogel composite, self degradation and environmental applications," *European Polymer Journal*, Vol. 107, pp. 118–131, 2018.

140. Fita, P., M. Fedoseeva, and E. Vauthey, "Ultrafast excited-state dynamics of eosin b: A potential probe of the hydrogen-bonding properties of the environment," *Journal of Physical Chemistry A*, Vol. 115, pp. 2465–2470, 2011.

141. Natarajan, T. S., H. C. Bajaj, and R. J. Tayade, "Preferential adsorption behavior of methylene blue dye onto surface hydroxyl group enriched TiO2 nanotube and its photocatalytic regeneration," *Journal of Colloid and Interface Science*, Vol. 433, pp. 104–114, 2014.

142. Cattoni, A., J. Chen, D. Decanini, J. Shi, and A.-M. Haghiri-Gosnet, "Soft UV Nanoimprint Lithography: A Versatile Tool for Nanostructuration at the 20nm Scale," in *Recent Advances in Nanofabrication Techniques and Applications*, IntechOpen, 2011.

143. Wipff, P. J., H. Majd, C. Acharya, L. Buscemi, J. J. Meister, and B. Hinz, "The covalent attachment of adhesion molecules to silicone membranes for cell stretching applications," *Biomaterials*, Vol. 30, pp. 1781–1789, 2009.

144. Ateş, G. B., A. Ak, B. Garipcan, and M. Gülsoy, "Indocyanine green-mediated photobiomodulation on human osteoblast cells," *Lasers in Medical Science*, Vol. 33, pp. 1591–1599, 2018.

145. D'Sa, R. A., J. Raj, P. J. Dickinson, F. McCabe, and B. J. Meenan, "Human Fetal Osteoblast Response on Poly(Methyl Methacrylate)/Polystyrene Demixed Thin Film Blends: Surface Chemistry Vs Topography Effects," *ACS Applied Materials & Interfaces*, Vol. 8, pp. 14920–14931, 6 2016.

146. Zhu, Y., Z. Cao, Y. Peng, L. Hu, T. Guney, and B. Tang, "Facile Surface Modification Method for Synergistically Enhancing the Biocompatibility and Bioactivity of Poly(ether ether ketone) That Induced Osteodifferentiation," *ACS Applied Materials and Interfaces*, Vol. 11, pp. 27503–27511, 2019.

147. Qin, X. H., B. Senturk, J. Valentin, V. Malheiro, G. Fortunato, Q. Ren, M. Rottmar, and K. Maniura-Weber, "Cell-Membrane-Inspired Silicone Interfaces that Mitigate Proinflammatory Macrophage Activation and Bacterial Adhesion," *Langmuir*, Vol. 35, pp. 1882–1894, 2019.

148. Liu, B., L. Chen, C. Shao, F. Zhang, K. Zhou, J. Cao, and D. Zhang, "Improved osteoblasts growth on osteomimetic hydroxyapatite/BaTiO3 composites with aligned lamellar porous structure," *Materials Science and Engineering: C*, Vol. 61, pp. 8–14, 2016.

149. Gupta, D., J. Venugopal, S. Mitra, V. R. Giri Dev, and S. Ramakrishna, "Nanostructured biocomposite substrates by electrospinning and electrospraying for the mineralization of osteoblasts," *Biomaterials*, Vol. 30, pp. 2085–2094, 2009.

150. Harris, S. A., R. J. Enger, L. B. Riggs, and T. C. Spelsberg, "Development and characterization of a conditionally immortalized human fetal osteoblastic cell line," *Journal of Bone and Mineral Research*, Vol. 10, pp. 178–186, 1995.

151. Hicok, K. C., T. Thomas, F. Gori, D. J. Rickard, T. C. Spelsberg, and B. L. Riggs, "Development and characterization of conditionally immortalized osteoblast precursor cell lines from human bone marrow stroma," *Journal of Bone and Mineral Research*, Vol. 13, pp. 205–217, 1998.

152. Jones, J. R., O. Tsigkou, E. E. Coates, M. M. Stevens, J. M. Polak, and L. L. Hench, "Extracellular matrix formation and mineralization on a phosphate-free porous bioactive glass scaffold using primary human osteoblast (HOB) cells," *Biomaterials*, Vol. 28, pp. 1653–1663, 2007.

153. Xiong, Y., J. Huang, L. Fu, H. Ren, S. Li, W. Xia, and Y. Yan, "Enhancement of osteoblast cells osteogenic differentiation and bone regeneration by hydroxyapatite/phosphoester modified poly(amino acid)," *Materials Science and Engineering: C*, Vol. 111, p. 110769, 2020.

154. Razafiarison, T., U. Silván, D. Meier, and J. G. Snedeker, "Surface-Driven Collagen Self-Assembly Affects Early Osteogenic Stem Cell Signaling," *Advanced Healthcare Materials*, Vol. 5, pp. 1481–1492, 2016.

155. Huang, R., L. Zhang, L. Huang, and J. Zhu, "Enhanced in-vitro osteoblastic functions on β-type titanium alloy using surface mechanical attrition treatment," *Materials Science and Engineering C*, Vol. 97, pp. 688–697, 2019.

156. Yang, H., S. Chen, L. Liu, C. Lai, and X. Shi, "Synthesis, characterization and osteogenesis of phosphorylated methacrylamide chitosan hydrogels," *RSC Advances*, Vol. 8, pp. 36331–36337, 2018.

157. Hillborg, H., N. Tomczak, A. Olàh, H. Schönherr, and G. J. Vancso, "Nanoscale hydrophobic recovery: A chemical force microscopy study of UV/ozone-treated cross-linked poly(dimethylsiloxane)," *Langmuir*, Vol. 20, pp. 785–794, 2004.

158. Hillborg, H., and U. W. Gedde, "Hydrophobicity recovery of polydimethylsiloxane after exposure to corona discharges," *Polymer*, Vol. 39, pp. 1991–1998, 1998.

159. Senzai, T., and S. Fujikawa, "Fast Hydrophobicity Recovery of the Surface-Hydrophilic Poly(dimethylsiloxane) Films Caused by Rechemisorption of Dimethylsiloxane Derivatives," *Langmuir*, Vol. 35, pp. 9747–9752, 7 2019.

160. Genchi, G. G., G. Ciofani, I. Liakos, L. Ricotti, L. Ceseracciu, A. Athanassiou, B. Mazzolai, A. Menciassi, and V. Mattoli, "Bio/non-bio interfaces: A straightforward method for obtaining long term PDMS/muscle cell biohybrid constructs," *Colloids and Surfaces B: Biointerfaces*, Vol. 105, pp. 144–151, 2013.

161. Siddique, A., T. Meckel, R. W. Stark, and S. Narayan, "Improved cell adhesion under shear stress in PDMS microfluidic devices," *Colloids and Surfaces B: Biointerfaces*, Vol. 150, pp. 456–464, 2017.

162. Hernández-Maya, F. M., and M. P. Cañizares-Macías, "Evaluation of the activity of β-glucosidase immobilized on polydimethylsiloxane (PDMS) with a microfluidic flow injection analyzer with embedded optical fibers," *Talanta*, Vol. 185, pp. 53–60, 2018.

163. Liu, X., J. Y. Lim, H. J. Donahue, R. Dhurjati, A. M. Mastro, and E. A. Vogler, "Influence of substratum surface chemistry/energy and topography on the human fetal osteoblastic cell line hFOB 1.19: Phenotypic and genotypic responses observed in vitro," *Biomaterials*, Vol. 28, pp. 4535–50, 2007.

164. Tu, Z., A. Young, C. Murphy, and J. F. Liang, "The pH sensitivity of histidine-containing lytic peptides," *Journal of Peptide Science*, Vol. 15, pp. 790–795, 2009.

165. Campbell, M. K., and S. O. Farrel, "Amino Acids and Peptides," in *Biochemistry*, ch. 3, pp. 69–70, Cengage Learning, 7th ed., 2012.

166. Clogston, J. D., and A. K. Patri, "Zeta potential measurement," *Methods in molecular biology (Clifton, N.J.)*, Vol. 697, pp. 63–70, 2011.

167. Kim, K. M., H. M. Kim, W. J. Lee, C. W. Lee, T. I. Kim, J. K. Lee, J. Jeong, S. M. Paek, and J. M. Oh, "Surface treatment of silica nanoparticles for stable and charge-controlled colloidal silica," *International Journal of Nanomedicine*, Vol. 9, pp. 29–40, 2014.

168. Alkhammash, H. I., N. Li, R. Berthier, and M. R. De Planque, "Native silica nanoparticles are powerful membrane disruptors," *Physical Chemistry Chemical Physics*, Vol. 17, pp. 15547–15560, 2015.

169. Yang, S. Y., E. S. Kim, G. Jeon, K. Y. Choi, and J. K. Kim, "Enhanced adhesion of osteoblastic cells on polystyrene films by independent control of surface topography and wettability," *Materials Science and Engineering C*, Vol. 33, pp. 1689–1695, 2013.

170. Fu, C., X. Yang, S. Tan, and L. Song, "Enhancing Cell Proliferation and Osteogenic Differentiation of MC3T3-E1 Pre-osteoblasts by BMP-2 Delivery in Graphene Oxide-Incorporated PLGA/HA Biodegradable Microcarriers," *Scientific Reports*, Vol. 7, 2017.

171. Pountos, I., M. Panteli, A. Lampropoulos, E. Jones, G. M. Calori, and P. V. Giannoudis, "The role of peptides in bone healing and regeneration: A systematic review," *BMC Medicine*, Vol. 14, 2016.

172. Stile, R. A., and K. E. Healy, "Thermo-responsive peptide-modified hydrogels for tissue regeneration," *Biomacromolecules*, Vol. 2, pp. 185–194, 2001.

173. Schuler, M., D. W. Hamilton, T. P. Kunzler, C. M. Sprecher, M. De Wild, D. M. Brunette, M. Textor, and S. G. Tosatti, "Comparison of the response of cultured osteoblasts and osteoblasts outgrown from rat calvarial bone chips to nonfouling KRSR and FHRRIKA-peptide modified rough titanium surfaces," *Journal of Biomedical Materials Research - Part B Applied Biomaterials*, Vol. 91, pp. 517–527, 2009.

174. Kitsara, M., A. Blanquer, G. Murillo, V. Humblot, S. De Bragança Vieira, C. Nogués, E. Ibáñez, J. Esteve, and L. Barrios, "Permanently hydrophilic, piezoelectric PVDF nanofibrous scaffolds promoting unaided electromechanical stimulation on osteoblasts," *Nanoscale*, Vol. 11, pp. 8906–8917, 2019.

175. Rafieerad, A. R., A. R. Bushroa, B. Nasiri-Tabrizi, S. Baradaran, A. Amiri, S. Saber-Samandari, S. Khanahmadi, E. Zeimaran, W. J. Basirun, K. Kalaiselvam, K. M. Vellasamy, and J. Vadivelu, "Simultaneous enhanced antibacterial and osteoblast cytocompatibility performance of Ti6Al7Nb implant by nano-silver/graphene oxide decorated mixed oxide nanotube composite," *Surface and Coatings Technology*, Vol. 360, pp. 181–195, 2019.

176. Marie, P. J., "Human Endosteal Osteoblastic Cells: Relationship with Bone Formation," *Calcified Tissue International*, Vol. 56, pp. S13–S16, 2015.

177. Heras-Bautista, C. O., N. Mikhael, J. Lam, V. Shinde, A. Katsen-Globa, S. Dieluweit, M. Molcanyi, V. Uvarov, P. Jütten, R. G. Sahito, F. Mederos-Henry, A. Piechot, K. Brockmeier, J. Hescheler, A. Sachinidis, and K. Pfannkuche, "Cardiomyocytes facing fibrotic conditions re-express extracellular matrix transcripts," *Acta Biomaterialia*, Vol. 89, pp. 180–192, 2019.

178. Heras-Bautista, C. O., A. Katsen-Globa, N. E. Schloerer, S. Dieluweit, O. M. Abd El Aziz, G. Peinkofer, W. A. Attia, M. Khalil, K. Brockmeier, J. Hescheler, and K. Pfannkuche, "The influence of physiological matrix conditions on permanent culture of induced pluripotent stem cell-derived cardiomyocytes," *Biomaterials*, Vol. 35, pp. 7374–7385, 2014.

179. Ateş, G. B., A. Ak, B. Garipcan, and M. Gülsoy, "Methylene blue mediated photobiomodulation on human osteoblast cells," *Lasers in Medical Science*, Vol. 32, pp. 1847–1855, 2017.

180. Al Shehadat, S., M. O. Gorduysus, S. S. A. Hamid, N. A. Abdullah, A. R. Samsudin, and A. Ahmad, "Optimization of scanning electron microscope technique for amniotic membrane investigation: A preliminary study," *European Journal of Dentistry*, Vol. 12, pp. 574–578, 2018.

181. Ivanyuk, D., G. Budash, Y. Zheng, J. A. Gaspar, U. Chaudhari, A. Fatima, S. Bahmanpour, V. K. Grin, A. G. Popandopulo, A. Sachinidis, J. Hescheler, and T. Šarić, "Ascorbic acid-induced cardiac differentiation of murine pluripotent stem cells: Transcriptional profiling and effect of a small molecule synergist of Wnt/β-catenin signaling pathway," *Cellular Physiology and Biochemistry*, Vol. 36, no. 2, pp. 810–830, 2015.

182. Özgün, A., A. Marote, L. A. Behie, A. Salgado, and B. Garipcan, "Extremely low frequency magnetic field induces human neuronal differentiation through NMDA receptor activation," *Journal of Neural Transmission*, Vol. 126, pp. 1281–1290, 2019.

183. Lyra-Leite, D. M., A. M. Andres, N. Cho, A. P. Petersen, N. R. Ariyasinghe, S. S. Kim, R. A. Gottlieb, and M. L. McCain, "Matrix-guided control of mitochondrial function in cardiac myocytes," *Acta Biomaterialia*, Vol. 97, pp. 281–295, 2019.

184. Acres, R. G., A. V. Ellis, J. Alvino, C. E. Lenahan, D. A. Khodakov, G. F. Metha, and G. G. Andersson, "Molecular structure of 3-aminopropyltriethoxysilane layers formed on silanol-terminated silicon surfaces," *Journal of Physical Chemistry C*, Vol. 116, pp. 6289–6297, 2012.

185. Zhao, Y., J. Wen, Y. Ge, X. Zhang, H. Shi, K. Yang, X. Gao, S. Shi, and Y. Gong, "Fabrication of stable biomimetic coating on PDMS surface: Cooperativity of multivalent interactions," *Applied Surface Science*, Vol. 469, pp. 720–730, 2019.

186. Puerto, M. A., T. M. Costa, J. A. Jornada, and N. M. Balzaretti, "Pyrolisys of α-aminoacids under high-pressure investigated by XPS, Raman and infrared spectroscopy," *Materials Chemistry and Physics*, Vol. 211, pp. 107–116, 2018.

187. Stevens, J. S., A. C. De Luca, M. Pelendritis, G. Terenghi, S. Downes, and S. L. Schroeder, "Quantitative analysis of complex amino acids and RGD peptides by X-ray photoelectron spectroscopy (XPS)," *Surface and Interface Analysis*, Vol. 45, pp. 1238–1246, 2013.

188. Hersch, N., B. Wolters, G. Dreissen, R. Springer, N. Kirchgessner, R. Merkel, and B. Hoffmann, "The constant beat: cardiomyocytes adapt their forces by equal contraction upon environmental stiffening," *Biology Open*, Vol. 2, no. 3, pp. 351–361, 2013.

189. Rodriguez, M. L., K. M. Beussman, K. S. Chun, M. S. Walzer, X. Yang, C. E. Murry, and N. J. Sniadecki, "Substrate Stiffness, Cell Anisotropy, and Cell-Cell Contact Contribute to Enhanced Structural and Calcium Handling Properties of Human Embryonic Stem Cell-Derived Cardiomyocytes," *ACS Biomaterials Science and Engineering*, Vol. 5, pp. 3876–3888, 2019.

190. Crocini, C., C. J. Walker, K. S. Anseth, and L. A. Leinwand, "Three-dimensional encapsulation of adult mouse cardiomyocytes in hydrogels with tunable stiffness," *Progress in Biophysics and Molecular Biology*, Vol. 154, pp. 71–79, 2020.

191. Eddington, D. T., J. P. Puccinelli, and D. J. Beebe, "Thermal aging and reduced hydrophobic recovery of polydimethylsiloxane," *Sensors and Actuators, B: Chemical*, Vol. 114, pp. 170–172, 2006.

192. Regehr, K. J., M. Domenech, J. T. Koepsel, K. C. Carver, S. J. Ellison-Zelski, W. L. Murphy, L. A. Schuler, E. T. Alarid, and D. J. Beebe, "Biological implications of polydimethylsiloxane-based microfluidic cell culture," *Lab on a Chip*, Vol. 9, pp. 2132–2139, 2009.

193. Kim, J., M. K. Chaudhury, and M. J. Owen, "Hydrophobic recovery of polydimethylsiloxane elastomer exposed to partial electrical discharge," *Journal of Colloid and Interface Science*, Vol. 226, pp. 231–236, 2000.

194. Lee, J. N., C. Park, and G. M. Whitesides, "Solvent Compatibility of Poly(dimethylsiloxane)-Based Microfluidic Devices," *Analytical Chemistry*, Vol. 75, pp. 6544–6554, 12 2003.

195. Lam, M. T., and M. T. Longaker, "Comparison of several attachment methods for human iPS, embryonic and adipose-derived stem cells for tissue engineering," *Journal of Tissue Engineering and Regenerative Medicine*, Vol. 6, pp. s80–86, 2012.

196. Hasan, A., V. Saxena, and L. M. Pandey, "Surface Functionalization of Ti6Al4V via Self-assembled Monolayers for Improved Protein Adsorption and Fibroblast Adhesion," *Langmuir*, Vol. 34, pp. 3494–3506, 2018.

197. Yang, L., L. Li, Q. Tu, L. Ren, Y. Zhang, X. Wang, Z. Zhang, W. Liu, L. Xin, and J. Wang, "Photocatalyzed surface modification of poly(dimethylsiloxane) with Polysaccharides and assay of their protein adsorption and cytocompatibility," in *Analytical Chemistry*, Vol. 82, pp. 6430–6439, 2010.

198. Kyaw, H. H., S. H. Al-Harthi, A. Sellai, and J. Dutta, "Self-organization of gold nanoparticles on silanated surfaces," *Beilstein Journal of Nanotechnology*, Vol. 6, pp. 2345–2353, 2015.

199. Akkan, C. K., D. Hür, L. Uzun, and B. Garipcan, "Amino acid conjugated self assembling molecules for enhancing surface wettability of fiber laser treated titanium surfaces," *Applied Surface Science*, Vol. 366, pp. 284–291, 2016.

200. Zhang, L., S. Zhang, Y. He, R. Yang, L. Ma, Y. Xia, and Z. He, "Histidine and histidine dimer as green inhibitors for carbon steel in 3wt% sodium chloride solution; Electrochemical, XPS and quantum chemical calculation studies," *International Journal of Electrochemical Science*, Vol. 13, pp. 2136–2153, 2018.

201. Valamehr, B., S. J. Jonas, J. Polleux, R. Qiao, S. Guo, E. H. Gschweng, B. Stiles, K. Kam, T. J. M. Luo, O. N. Witte, X. Liu, B. Dunn, and H. Wu, "Hydrophobic surfaces for enhanced differentiation of embryonic stem cell-derived embryoid bodies," *Proceedings of the National Academy of Sciences of the United States of America*, Vol. 105, pp. 14459–64, 2008.

202. McCain, M. L., and K. K. Parker, "Mechanotransduction: The role of mechanical stress, myocyte shape, and cytoskeletal architecture on cardiac function," *Pflugers Archiv European Journal of Physiology*, Vol. 462, pp. 89–104, 2011.

203. Paoletti, C., C. Divieto, and V. Chiono, "Impact of Biomaterials on Differentiation and Reprogramming Approaches for the Generation of Functional Cardiomyocytes," *Cells*, Vol. 7, p. 114, 2018.

204. Kowalski, W. J., F. Yuan, T. Nakane, H. Masumoto, M. Dwenger, F. Ye, J. P. Tinney, and B. B. Keller, "Quantification of Cardiomyocyte Alignment from Three-Dimensional (3D) Confocal Microscopy of Engineered Tissue," *Microscopy and Microanalysis*, Vol. 23, pp. 826–842, 2017.

205. Gaspar, R., A. Gorbe, J. Paloczi, Z. V. Varga, K. Gomori, P. Ferdinandy, and T. Csont, "P148Cardiac myocytes are protected by small leucine rich proteoglycans against simulated ischemia/reperfusion injury," *Cardiovascular Research*, Vol. 103, pp. S26–S26, 7 2014.

206. Dupuis, L. E., M. G. Berger, S. Feldman, L. Doucette, V. Fowlkes, S. Chakravarti, S. Thibaudeau, N. E. Alcala, A. D. Bradshaw, and C. B. Kern, "Lumican deficiency results in cardiomyocyte hypertrophy with altered collagen assembly," *Journal of Molecular and Cellular Cardiology*, Vol. 84, pp. 70–80, 2015.

207. Brody, M. J., and Y. Lee, "The role of leucine-rich repeat containing protein 10 (LRRC10) in dilated cardiomyopathy," *Frontiers in Physiology*, Vol. 7, p. 337, 2016.

208. Kitsara, M., O. Agbulut, D. Kontziampasis, Y. Chen, and P. Menasché, "Fibers for hearts: A critical review on electrospinning for cardiac tissue engineering," *Acta Biomaterialia*, Vol. 48, pp. 20–40, 2017.

209. Arshi, A., Y. Nakashima, H. Nakano, S. Eaimkhong, D. Evseenko, J. Reed, A. Z. Stieg, J. K. Gimzewski, and A. Nakano, "Rigid microenvironments promote cardiac differentiation of mouse and human embryonic stem cells," *Science and Technology of Advanced Materials*, Vol. 14, 2013.

210. Zong, X., H. Bien, C. Y. Chung, L. Yin, D. Fang, B. S. Hsiao, B. Chu, and E. Entcheva, "Electrospun fine-textured scaffolds for heart tissue constructs," *Biomaterials*, Vol. 26, pp. 5330–5338, 2005.

211. Mehrotra, S., S. K. Nandi, and B. B. Mandal, "Stacked silk-cell monolayers as a biomimetic three dimensional construct for cardiac tissue reconstruction," *Journal of Materials Chemistry B*, Vol. 5, pp. 6325–6338, 2017.

212. Ikonen, L., E. Kerkelä, G. Metselaar, M. C. Stuart, M. R. De Jong, and K. Aalto-Setälä, "2D and 3D self-assembling nanofiber hydrogels for cardiomyocyte culture," *BioMed Research International*, Vol. 2013, 2013.

213. Trantidou, T., E. J. Humphrey, C. Poulet, J. Gorelik, T. Prodromakis, and C. M. Terracciano, "Surface Chemistry and Microtopography of Parylene C Films Control the Morphology and Microtubule Density of Cardiac Myocytes," *Tissue Engineering - Part C: Methods*, Vol. 22, pp. 464–472, 2016.

214. Yue, Z., X. Liu, P. J. Molino, and G. G. Wallace, "Bio-functionalisation of polydimethylsiloxane with hyaluronic acid and hyaluronic acid - Collagen conjugate for neural interfacing," *Biomaterials*, Vol. 32, no. 21, pp. 4714–4724, 2011.

215. Sarvi, F., Z. Yue, K. Hourigan, M. C. Thompson, and P. P. Y. Chan, "Surface-functionalization of PDMS for potential micro-bioreactor and embryonic stem cell culture applications," *J. Mater. Chem. B*, Vol. 1, pp. 987–996, 1 2013.

216. Eghrari, A. O., S. A. Riazuddin, and J. D. Gottsch, "Chapter Two - Overview of the Cornea: Structure, Function, and Development," in *Molecular Biology of Eye Disease* (Hejtmancik, J. F., J. M. B. T. P. i. M. B. Nickerson, and T. Science, eds.), Vol. 134, pp. 7–23, Academic Press, 2015.

217. Hamilton, K. E., and D. C. Pye, "Young's modulus in normal corneas and the effect on applanation tonometry," *Optometry and Vision Science*, Vol. 85, pp. 445–50, 2008.

218. Last, J. A., S. J. Liliensiek, P. F. Nealey, and C. J. Murphy, "Determining the mechanical properties of human corneal basement membranes with atomic force microscopy," *Journal of Structural Biology*, Vol. 167, no. 1, pp. 19–24, 2009.

219. Cartwright, N. E., J. R. Tyrer, and J. Marshall, "Age-related differences in the elasticity of the human cornea," *Investigative Ophthalmology and Visual Science*, Vol. 52, no. 7, pp. 4324–4329, 2011.

220. Shih, P. J., C. J. Huang, T. H. Huang, H. C. Lin, J. Y. Yen, I. J. Wang, H. J. Cao, W. P. Shih, and C. A. Dai, "Estimation of the Corneal Young's Modulus in Vivo Based on a Fluid-Filled Spherical-Shell Model with Scheimpflug Imaging," *Journal of Ophthalmology*, Vol. 2017, 2017.

221. Marín-Pareja, N., E. Salvagni, J. Guillem-Marti, C. Aparicio, and M. P. Ginebra, "Collagen-functionalised titanium surfaces for biological sealing of dental implants: Effect of immobilisation process on fibroblasts response," *Colloids and Surfaces B: Biointerfaces*, Vol. 122, pp. 601–610, 2014.

222. Scarano, A., F. Lorusso, T. Orsini, M. Morra, G. Iviglia, and L. Valbonetti, "Biomimetic surfaces coated with covalently immobilized collagen type I: An x-ray photoelectron spectroscopy, atomic force microscopy, micro-CT and histomorphometrical study in rabbits," *International Journal of Molecular Sciences*, Vol. 20, p. 724, 2019.

223. Qian, Z., D. Ross, W. Jia, Q. Xing, and F. Zhao, "Bioactive polydimethylsiloxane surface for optimal human mesenchymal stem cell sheet culture," *Bioactive Materials*, Vol. 3, no. 2, pp. 167–173, 2018.

224. Parekh, M., S. Ferrari, C. Sheridan, S. Kaye, and S. Ahmad, "Concise Review: An Update on the Culture of Human Corneal Endothelial Cells for Transplantation," *Stem Cells Translational Medicine*, Vol. 5, pp. 258–264, 2016.

225. Nikkhah, M., F. Edalat, S. Manoucheri, and A. Khademhosseini, "Engineering microscale topographies to control the cell-substrate interface," *Biomaterials*, Vol. 33, pp. 5230–5246, 2012.

226. Mirbagheri, M., V. Adibnia, B. R. Hughes, S. D. Waldman, X. Banquy, and D. K. Hwang, "Advanced cell culture platforms: a growing quest for emulating natural tissues," *Materials Horizons*, Vol. 6, pp. 45–71, 2019.

227. Schulte, V. A., M. Díez, M. Möller, and M. C. Lensen, "Surface topography induces fibroblast adhesion on intrinsically nonadhesive poly(ethylene glycol) substrates," *Biomacromolecules*, Vol. 10, pp. 2795–2801, 2009.

228. Charest, J. L., M. T. Eliason, A. J. García, and W. P. King, "Combined microscale mechanical topography and chemical patterns on polymer cell culture substrates," *Biomaterials*, Vol. 27, pp. 2487–2494, 2006.

229. McMurray, R. J., N. Gadegaard, P. M. Tsimbouri, K. V. Burgess, L. E. McNamara, R. Tare, K. Murawski, E. Kingham, R. O. Oreffo, and M. J. Dalby, "Nanoscale surfaces for the long-term maintenance of mesenchymal stem cell phenotype and multipotency," *Nature Materials*, Vol. 10, pp. 637–644, 2011.

230. Liliensiek, S. J., S. Campbell, P. F. Nealey, and C. J. Murphy, "The scale of substratum topographic features modulates proliferation of corneal epithelial cells and corneal fibroblasts," *Journal of Biomedical Materials Research - Part A*, Vol. 79, pp. 185–192, 2006.

231. Eberwein, P., T. Steinberg, S. Schulz, D. Zimmermann, R. Accardi, D. Beck, T. Reinhard, and P. Tomakidi, "Expression of keratinocyte biomarkers is governed by environmental biomechanics," *European Journal of Cell Biology*, Vol. 90, pp. 1029–1040, 2011.

232. Teixeira, A. I., P. F. Nealey, and C. J. Murphy, "Responses of human keratocytes to micro- and nanostructured substrates," *Journal of Biomedical Materials Research - Part A*, Vol. 71, pp. 369–376, 2004.

233. Bhattacharjee, P., B. L. Cavanagh, and M. Ahearne, "Effect of substrate topography on the regulation of human corneal stromal cells," *Colloids and Surfaces B: Biointerfaces*, Vol. 190, 2020.

234. Koo, S., R. Muhammad, G. S. L. Peh, J. S. Mehta, and E. K. F. Yim, "Micro- and nanotopography with extracellular matrix coating modulate human corneal endothelial cell behavior," *Acta Biomaterialia*, Vol. 10, no. 5, pp. 1975–1984, 2014.

235. Abrams, G. A., S. S. Schaus, S. L. Goodman, P. F. Nealey, and C. J. Murphy, "Nanoscale topography of the corneal epithelial basement membrane and Descemet's membrane of the human," *Cornea*, Vol. 19, pp. 57–64, 2000.

236. Zavala, J., G. Ló Pez Jaime, C. R. Barrientos, and J. Valdez-Garcia, "Corneal endothelium: developmental strategies for regeneration," *Eye*, Vol. 27, pp. 579–588, 2013.

237. Chen, R., L. Li, L. Feng, Y. Luo, M. Xu, K. W. Leong, and R. Yao, "Biomaterial-assisted scalable cell production for cell therapy," *Biomaterials*, Vol. 230, 2020.

238. Morra, M., C. Cassinelli, G. Cascardo, P. Cahalan, L. Cahalan, M. Fini, and R. Giardino, "Surface engineering of titanium by collagen immobilization. Surface characterization and in vitro and in vivo studies," *Biomaterials*, Vol. 24, pp. 4639–4654, 2003.

239. Li, C., Y. Ding, S. Kuddannaya, Y. Zhang, and L. Yang, "Anti-bacterial properties of collagen-coated glass and polydimethylsiloxane substrates," *Journal of Materials Science*, Vol. 52, pp. 9963–9978, 2017.

240. Xue, P., Q. Li, Y. Li, L. Sun, L. Zhang, Z. Xu, and Y. Kang, "Surface modification of poly(dimethylsiloxane) with polydopamine and hyaluronic acid to enhance hemocompatibility for potential applications in medical implants or devices," *ACS Applied Materials and Interfaces*, Vol. 9, pp. 33632–33644, 2017.

241. Ponce Márquez, S., V. S. Martínez, W. McIntosh Ambrose, J. Wang, N. G. Gantxegui, O. Schein, and J. Elisseeff, "Decellularization of bovine corneas for tissue engineering applications," *Acta Biomaterialia*, Vol. 5, pp. 1839–1847, 2009.

242. Bonanno, J. A., "Molecular mechanisms underlying the corneal endothelial pump," *Experimental Eye Research*, Vol. 95, pp. 2–7, 2012.

243. Hsueh, Y. J., D. H. K. Ma, K. S. C. Ma, T. K. Wang, C. H. Chou, C. C. Lin, M. C. Huang, L. J. Luo, J. Y. Lai, and H. C. Chen, "Extracellular matrix protein coating of processed fish scales improves human corneal endothelial cell adhesion and proliferation," *Translational Vision Science and Technology*, Vol. 8, 2019.